PARAMETRIC ANALYSIS OF THE SHOCK RESPONSE OF A SYSTEM OF TWO SUBMERGED CO-AXIAL CYLINDRICAL SHELLS COUPLED BY THE INTER-SHELL FLUID

by

Chad Furey

Submitted in partial fulfilment of the requirements

for the degree of Master of Science

at

Dalhousie University

Halifax, Nova Scotia

December 2015

TABLE OF CONTENTS

LIST OF TABLES

LIST OF FIGURES

ABSTRACT

A semi-analytical methodology based on classical mathematical physics is used to simulate the shock response of a submerged system consisting of two co-axial cylindrical shells coupled with a fluid filling the inter-shell space. Both the fluid and structural dynamics of the interaction are addressed.

The stress-strain states and the hydrodynamic fields are evaluated through analysis of both stress in the shells and pressure fields in the inner hull coupling fluid and compared to previously investigated cases of both a submerged cylindrical shell with and without a rigid core.

The main contribution of the thesis is in quantifying the changes in both the stress-strain states and peak pressures evaluated in a parametric study. This is accomplished by varying the inner and outer shell thickness, coupling fluids, outer shell material, and sizes of the inner-hull radius effectively changing the inner-hull fluid space.

LIST OF ABBREVIATIONS AND SYMBOLS USED

a radius of the inner shell, $\hat{a} = ar_0^{-1}$

c_i sound speed in the inter-shell fluid, $\hat{c}_i = c_i c_e^{-1}$

c_e sound speed in the external fluid, $\hat{c}_e = 1$

c_1 sound speed in the material of the inner shell, $\hat{c}_1 = c_1 c_e^{-1}$

c_2 sound speed in the material of the outer shell, $\hat{c}_2 = c_2 c_e^{-1}$

E_1 Young modulus of the material of the inner shell, $\hat{E}_1 = E_1 \rho_e^{-1} c_e^{-2}$

E_2 Young modulus of the material of the outer shell, $\hat{E}_2 = E_2 \rho_e^{-1} c_e^{-2}$

h_1 thickness of the inner shell, $\hat{h}_1 = h_1 r_0^{-1}$

h_2 thickness of the outer shell, $\hat{h}_2 = h_2 r_0^{-1}$

I_n modified Bessel function of the first kind of order n

J_n Bessel function of the first kind of order n

K_n modified Bessel function of the second kind of order n

p_α peak incident pressure, $\hat{p}_\alpha = p_\alpha \rho_e^{-1} c_e^{-2}$

p_1^s total pressure on the surface of the inner shell, $\hat{p}_1^s = p_1^s \rho_e^{-1} c_e^{-2}$

p_2^s total pressure on the surface of the outer shell, $\hat{p}_2^s = p_2^s \rho_e^{-1} c_e^{-2}$

p_0 incident pressure, $\hat{p}_0 = p_0 \rho_e^{-1} c_e^{-2}$

p_d diffraction pressure, $\hat{p}_d = p_d \rho_e^{-1} c_e^{-2}$

p_r^e external radiation pressure, $\hat{p}_r^e = p_r^e \rho_e^{-1} c_e^{-2}$

p_r^i inter-shell radiation pressure, $\hat{p}_r^i = p_r^i \rho_e^{-1} c_e^{-2}$

r radial coordinate of the polar coordinate system, $r = \varrho r_0^{-1}$

r_0 radius of the outer shell, $\hat{r}_0 = 1$

R_0 radial distance to the source of the shock wave, $\hat{R}_0 = R_0 r_0^{-1}$

S_R shock wave stand-off, $\hat{S}_0 = S_0 r_0^{-1}$

t time, $t = \tau c_e r_0^{-1}$

v_1^* transverse displacement of the middle surface of the inner shell, $v_1 = v_1^* r_0^{-1}$

v_2^* transverse displacement of the middle surface of the outer shell, $v_2 = v_2^* r_0^{-1}$

w_1^* normal displacement of the middle surface of the inner shell, $w_1 = w_1^* r_0^{-1}$

w_2^* normal displacement of the middle surface of the outer shell, $w_2 = w_2^* r_0^{-1}$

Y_n Bessel function of the second kind of order n

θ angular coordinate of the polar coordinate system

λ exponential decay rate, $\hat{a} = a r_0^{-1}$

υ_1 Poisson's ratio of the material of the inner shell

υ_2 Poisson's ratio of the material of the outer shell

ξ_n^e external response functions

ξ_n^1 first inter-shell response functions

ξ_n^2 second inter-shell response functions

ρ_i density of the inter-shell fluid, $\hat{\rho}_i = \rho_0 \rho_e^{-1}$

ρ_e density of the external fluid, $\hat{\rho}_e = 1$

ρ_1 density of the material of the inner shell, $\hat{\rho}_1 = \rho_1 \rho_e^{-1}$

ρ_2 density of the material of the outer shell, $\hat{\rho}_2 = \rho_2 \rho_e^{-1}$

ϱ radial coordinate of the polar coordinate system, $r = \varrho r_0^{-1}$

$\sigma_{\theta\theta}^1$ transverse stress in the inner shell, $\hat{\sigma}_{\theta\theta}^1 = \sigma_{\theta\theta}^1 \rho_e^{-1} c_e^{-2}$

$\sigma_{\theta\theta}^2$ transverse stress in the outer shell, $\hat{\sigma}_{\theta\theta}^2 = \sigma_{\theta\theta}^2 \rho_e^{-1} c_e^{-2}$

τ time, $t = \tau c_e r_0^{-1}$

ϕ total fluid velocity potential, $\hat{\phi} = \phi c_e^{-1} r_0^{-1}$

ϕ_0 fluid velocity potential in the incident wave $\hat{\phi}_0 = \phi_0 c_e^{-1} r_0^{-1}$

ϕ_d fluid velocity potential in the diffracted wave, $\hat{\phi}_d = \phi_d c_e^{-1} r_0^{-1}$

ϕ_r^e fluid velocity potential in the external radiated wave, $\hat{\phi}_r^e = \phi_r^e c_e^{-1} r_0^{-1}$

ϕ_r^i fluid velocity potential in the inter-shell radiated wave, $\hat{\phi}_r^i = \phi_r^i c_e^{-1} r_0^{-1}$

$(*)_n \sin n\theta$ and $(*)_n \cos n\theta$ denote the harmonics of $(*)$. Unless stated otherwise, capitalized symbols denote the Laplace transforms of the corresponding functions. Other symbols are defined in the text.

ACKNOWLEDGMENTS

Special thanks would like to be given to the Defence Research and Development Canada (DRDC) for providing funding for the following research. Without their assistance this would not have been possible. Furthermore, a special thank you to Dr. Malcolm Smith of DRDC for his consultation and assistance on the following research as well.

CHAPTER 1: INTRODUCTION

Cylindrical shells subjected to shock waves have been of interest and studied in great detail since the late 1940s. The majority of research has involved investigating and understanding the physical phenomena that occur through all stages, from the immediate inception of the shock wave and its propagation through the fluid medium, to the shock waves primary interaction with the shell, to the resulting stress-strain states of the shell and their resultant acoustics. The acoustic field can usually be represented by two distinct components: diffracted waves which scatter off the shell and the waves generated in the fluid as a result of the response of the shell. A brief description of the phenomena being investigated should demonstrate the complexity that must be taken into account to develop realistic and useful mathematical models of the interactions in question.

It should come as no surprise that cylindrical shells are used in a wide variety of engineering structures on a global scale. Examples include nuclear power plants, offshore platforms, as well as seafaring and submersible vessels, all of which make use of fluid-interacting shell structures. Due to the importance of these examples' contributions to the protection, innovation in and economics of society, and the major threats that shock loads pose to the safety and longevity of structures in these fields, the research of shock wave interactions with shells has always been of considerable interest. Recent disasters such as the Exxon Valdez spill in 1989 off the coast of Alaska which polluted the Alaskan coast with approximately 257 000 barrels of oil (Holba, 2010) and the Deep Water Horizon disaster in the Gulf of Mexico which polluted the gulf and American shore lines with an estimated 5 million barrels of oil (Mayer et al., 2013) it can be seen that these types of disasters cause extensive damage to environments, possibilities of future oil exploration, production of refined petroleum and increased oil prices. A better understanding of how impact on such shell structures (ie, tanker hulls and underwater pipelines) occurs would allow companies to choose appropriate construction guidelines, which would include protective measures to avoid future risks.

Additional interests into these types of interactions involve noise reduction measures. The impact of shock waves and vibrations, which generate radiated acoustic fields, can vary from audible to inaudible ranges. In areas with heavy machinery different

types of materials can absorb or reflect these acoustic fields, and if acoustic waves focus at a local point the resulting noise levels can be as low as a mild distraction or have the capability of causing severe damage to one's ears. Understanding these situations can provide better personal protection and reduction in potential medical claims.

Specific materials and structural shapes are also known to have their own acoustic signatures, so the resulting reflected wave can indicate the shape, type and distance of a specific object. Reducing these levels of acoustic radiation contribute to the degree of stealth for many different types of vehicles and are an important area of research. Amongst all cylindrical shell systems of special importance are double hull arrangements, where an interior shell is coaxially located within an exterior shell, which can provide a more realistic approximation of real engineering problems. Such a design is commonly seen in pipelines and certain submarine designs. Despite the importance of the double hull design there is far less information available discussing how shock waves can compromise the integrity of these designs versus a single-shell model. Many of the above areas of research are directly applicable to the investigation of submarines. Reduction on noise can improve the stealth capabilities of submarines for military purposes and understanding how shock waves interact with the exterior and interior portions of the shell can contribute to improving structural reinforcement at vital areas that are more likely to be compromised. Submarines are very expensive vessels that contribute a large portion of the defense and strength of many world militaries. Understanding how explosions will impact these vessels could save billions of dollars in repairs, replacements and loss of life.

Research into shell-shock interaction is a challenge, both from the theoretical point of view, as well as an experimental one. At the most basic level there are two mediums which interact with and are affected by the shock wave, a fluid and a solid (the shell), both of which have significant differences in how they will interact with the shock wave. These interactions are not stationary and also occur on a very short time scale in which the major effects of concern may occur within the first few milliseconds of the interaction. To further complicate the problem, we could consider additional fluid inside the shell of identical or different properties, varying thicknesses for the shell itself, additional shells inside the primary shell which could each be of varying thickness and materials, varying the strength

and distance of the shock wave when it occurs and the geometry of the shock wave when first interacting with the shell structure. During shock wave interaction among the phenomena of interest are the radiated external hydrodynamic field, the diffracted hydrodynamic field, the internally radiated hydrodynamic field and the stress strain states of the structure. Other effects such as cavitation are possible results of interest as well. Because of this level of complexity, physical experiments become a time consuming and costly endeavor. Thus, mathematical modeling is often chosen to investigate the effects of changing one or more set of variables.

Mathematical modeling is the process of using discovered mathematics and computational technologies to simulate the interactions described above. Benefits to mathematical modeling include but are not limited to a substantial decrease in cost, time, materials, and the required amount of personnel. Results can be easily stored and analyzed in many different ways depending on what is being investigated. It is possible to generate multiple images showing how the shock wave is interacting with the shell, maximum and minimum pressures and possible locations of cavitation at different time intervals. This allows investigators to physically “see” the interaction as it occurs. However, just as there are drawbacks to physical experiments, there are also drawbacks to mathematical models. A proper mathematical model will first prove its accuracy by simulating benchmark experiments to within an acceptable range of accuracy, then the model can be used to simulate more complicated cases that one is interested in. It should be understood that neither approach is sufficient on its own but that they complement one another. Experiments are required to demonstrate the accuracy of the simulations and simulations are required to reduce costs and time while contributing to the future development and understanding of fluid-shell interactions.

The following literary review is a description of research that has been carried out. Initial research into shock wave-shell interaction was driven by the naval industries and focused primarily on the structural components of the interaction (Haywood, 1958). These studies used modal method of analysis to approximate the relationship between the fluid pressure of either a plane or circular shock wave and its interaction with an infinitely long uniform cylindrical shell to translate into the structural response of the shell itself (Peralta and Raynor, 1964). Integral transformations (both Laplace and Fourier

transforms) were used to analyze the response of a cylindrical shell containing a different fluid from that of its exterior through radial displacements but was limited to an early dimensionless time frame and only viewed the displacements and the pressure on the shell surface at the front of the shell. There was a conclusion that varying the inner fluid as well as the shell's thickness considerably changed the peak velocity of the shell. The large time behavior of a scattered field resulting from a shock wave interacting with either a soft and hard spherical obstacle was generated and considered using three different "pulse shocks" (Cohen and Donald, 1965). The results suggest the resulting scattered field is determined more by the shape of the impacted object as opposed to the shape of the original shock wave. In another study, separation and analysis was performed on three distinct individual wave phenomena that occur during shell-shock wave interaction, waves tangential to the surface and travelling along the exterior of the shell, refracted circumferential waves and internal waves tangential to the interior surface of the shell (Neubauer, 1968).

A method to simultaneously solve both governing fluid and structural equations was later developed for the case of an infinite cylindrical shell submerged in fluid and subjected to a shock wave (Geers, 1969). However, due to the extended time requirements results were kept to shorter time frames. Early papers demonstrate this new approach to simultaneously solve the governing equations and then compare results for displacement, velocity and strains to previously obtained computations of modal expansion to prove the validity of the simultaneous solution. This work was then expanded to evaluate the transient acoustic field generated by the shock wave interaction with an infinite elastic circular cylindrical shell along with the wave front analysis to separate the scattering problem into two distinct parts and compare it to the previously published works on rigid cylinders and cylindrical cavities (Geers, 1970). A three-dimensional investigation into the effect of a spherical shock wave's impact on infinite cylinders was then considered by; once again, solving the governing wave and shell equations by use of the Laplace-Fourier transforms (Huang and Wang, 1970). This approach provided numerical results and demonstrated how a spherical wave may generate differing phenomena and results as those generated by a plane shock wave.

With all the effort put into modeling of these interactions, it was still important to continuously provide experimental results. Tests were conducted to visualize the radiation of shear and compression waves as well as internal reflection of waves generated from the shock loading of submerged aluminum cylinders (Neubauer, 1970). These images were produced using Schlieren visualization and hydrophone measurements. Images show the development of a prominent wave for air and water filled cylindrical shells, the dependency on the thin-shell characteristics and its effect on transmitted compressional waves and subsequent conversion to a shear wave.

An investigation into the three-dimensional case of transient scattering of a spherical pressure pulse by an infinitely long rigid circular cylinder and the time histories of the pressure wave fields was investigated, with the same solution being possible for a long elastic cylinder as well (Huang, 1975). The solution which uses two different approaches of separation of variables with Laplace transformations was used to address the two-dimensional case, are expanded to address the three dimensional case. Three-dimensional diffraction was addressed and the combination of all solutions was used to generate a full time-history. Another possibility was to investigate more specific phenomena, such as the use of shadowgraphs and pressure measurements for the focusing of weak shock waves (Sturtevant and Kulkarny, 1976). In this specific case, plane shock waves impacted concave surfaces to act as reflectors that reflect the waves back towards a focusing point. Results resemble those suggested for focusing theory in fluids and discuss certain phenomena that occur at the focal point such as the development of complex wave fields which all resemble one another and the addition of the diffracted wave behind the initial one.

Use of the separation of variables continued to be deemed suitable to simultaneously solve the wave and structural equations, and the inverse Laplace transforms were determined indirectly by an integral equation method or differential-integral method (Huang, 1979). The study focused on the structural effects of the interaction primarily on the inner hulls translational motions. It was found that a thin outer shell relative to the inner shell has very little effect on the basic responses in motions of the inner shell when the double hull case is compared to that of the single hull scenario and that the outer shell served primarily to reduce “breathing” of the internal shell and

translational motion. This exact case was quickly expanded into an identical situation where instead of dealing with cylindrical objects the author examined two spherical shells where one is located in the centre of the other. The system is once again submerged into a fluid medium with a fluid layer separating both spheres, and the transient response of the system is analyzed similarly to the cylindrical shell case with separation of variables and the use of Volterra integrals to solve the Laplace transformations. Identical conclusions are drawn with regard to a thin outer sphere relative to the thickness of the inner sphere, which will have very little influence on the basic structural impacts on the inner sphere resulting from the shock wave impact to the point that the outer sphere is viewed as transparent for early time frames, and later on the outer sphere reduces "breathing" and translational motion of the inner sphere.

As previously mentioned, there are many components to the shock wave-fluid-structure interactions. Specifically looked into areas, such as the non-linear phenomena of the reflections and effects of shock waves through specific types of fluid medium were the studies where the shock wave was treated as a plane surface of increased pressure not a surface with a decreasing pressure head (Hornung, 1987). The study analyzes the relations of the upstream and downstream states from the pressure wave and looks into the standard case of shock waves reflecting from a plane surface with varying states of flow and Mach numbers. This discussion continues into detail discussing what happens at physical corner boundaries and reflections from different surface types, and how one might make improper conclusions and to be aware of such possibilities for future analysis. In (Yang et al., 1987) computations for shock waves acting on a circular cylinder highlight some of the concerns expressed in the previous article, and a wide variety of Mach numbers are used once the two-dimensional inviscid compressible Euler equation of gas dynamics is solved through second order hybrid upwind method. The results are compared to previously discussed Scheirin images and that the model has high accuracy. There is a note that certain models do not match experimental ones because of the limitations of Euler's method. In (Summerfeld and Muller, 1988) extension of reflection analysis was done to investigate the non-linear relation of a plane and spherical shock wave that is reflected from a concave/ellipsoidal surface to focus the reflecting wave and compare the computational results to experimental shadowgraphs.

In the early nineties research for more details about specific aspects of shell shock interaction were possible due to advancement in experimental tools such as near field acoustical holography, Laser Doppler velocimetry, and accelerometers (Williams, 1988). These tools enabled one to produce substantially more data, often enough to produce complete mapping of accelerations and displacements generating large amounts of data for various vibrational characteristics.

More advanced research shifted from looking at the structural effects of the shell-shock interactions to the analysis of the hydrodynamic fields generated as a result of the interaction (Hasegawa, 1993). The frequency dependence of the pressure fields was investigated, and the study used a theoretical approach to analyze cylindrical and spherical shells subjected to a shock wave, with varying thicknesses of the shells where the hollow cavities were either filled with air or water. The resultant fields for elastic hollow shells were viewed as “more interesting” than previous results for solid cylinders and spheres and the acoustic pressures were different for different interior fluids. More research was done to analyze the transient response of elastic cylinders subjected to a plane wave with emphasis towards the improving model techniques to reduce computation times (Zhang, 1993). Double Fourier transforms were used to study the radial excitation of shell displacements and analyze the energy transfer of a shock loaded cylindrical pipe (Brevary and Fuller, 1994). This was accomplished with the assumption that the system behavior separates all the individual components of each waves characteristics, so that when combined, gives the solution for total displacement of the shell, and leads to better understanding of noise propagations through piping systems. Further research contributed experimental and computational results investigating shock waves and resultant hydrodynamic fields from parabolic reflectors (Izumi et al., 1994). There was then an investigation into the potential shielding effects of an outer shell on an inner shell for two concentric submerged cylindrical shells coupled by an entrained fluid (Yoshikawa et al., 1994). To solve the double hull problem with an infinite shell scenario, the wave equation and boundary conditions at the fluid-shell interfaces were used. (Yoshikawa et al., 1994) also carried out experimental tests with generalized near-field acoustical holography (GENAH), which provided experimental vibration characteristics. It was determined that the shielding affect of the outer shell is insufficient, the double hull

arrangements radiates at low level frequencies as well as high frequency due to the vibrations of one shell interacting with the other across the fluid barrier and the amplitudes of forced vibration in a single shell arrangements can be split between both shells of a double hull arrangement effectively reducing the total radiated sound. However, the double hull arrangement was found to generate a greater amplitude than the single shell case. Other works have looked at varying the radius of the shell structure with respect to time with generalized approximations (Pavlov, 1995). The energy exchange between the exterior fluid, the elastic cylindrical shell and the internal fluid was also investigated by using a double Fourier integration (Brevart and Fuller, 1996).

A preliminary set of underwater explosion benchmarks that were available and declassified at the time were compiled in hopes of initiating UNDEX community discussions on validation techniques for experimental and analytical studies (Mair, 1996). Summaries of the usefulness of one, two, and three-dimensional cases were provided as well as the drawbacks present in the obtained information. Emphasis is placed on the need for greater replication of tests because of the greater importance experiments can have for determining useful knowledge once the validity of the experiments is ensured. Sufficient summaries of multiple modeling methods and hydrocodes are provided as well as examples of validated codes that have generated faulty tests for their own specific reason. The importance to test all codes with as many validation techniques as possible is stressed in order to reduce the possibilities of flaws in analytical and experimental methods. Reflections were again analyzed for circular reflectors impacted by spherical shock waves (Sun and Takayama, 1996). Non-stationary loaded cylindrical shells were addressed using the Navier-Stokes equation and compared to similar results obtained from Eulers method with the use of adaptive grid methods for various Mach numbers (Ofengeim and Drikakis, 1997). This was later used to generate contour plots and pressure histories to analyze different blast wave durations and their affect when impacted on a submerged cylindrical shell (Schedin et al, 1997). Varying results were obtained from comparing viscous and inviscid fluids. These comparisons revealed that the length of the blast duration significantly affects the flow over the cylinder. Double-pulsed interferometry has been used to investigate the reflection and focusing of shock waves generated inside elliptically curved chambers with varying heights and

quantitatively analyzed to better understand the convergence of reflected pressure waves (Drikakis et al, 1997). Investigations were later expanded to address a two-layered infinite cylindrical shell (Lam et al, 1997). Structural dynamics were determined by finite element method for the fluid-structure interactions, and varying thicknesses of the shell were modeled. The effect of varying shell thicknesses on the structural dynamics was then compared to previously established models. Continued research into non-linear free and forced vibrations with Donnell's shallow-shell theory and Galerkin method allowed investigation into moderately strong vibrations (Amabili et al, 1998).

The effect of shock waves on the center section of a two-dimensional surface ship's hull, assumed a single shell, was analyzed, as well as investigations into the formation and effects of cavitation at the hull surface through use of the UAS-NASTRAN-CFA method (Shin and Santiago, 1998). This method makes use of the Doubly-Asymptotic Approach to model fluid-shell interactions (NASTRAN) and the CFA code to model the cavitation based on displacement potential. Additional investigations into floating single shell vessels at a free surface, with shock waves generated directly beneath the structure in an infinite depth basin are investigated with focus on bulk and hull cavitation (Van et al, 1998). Non-linear finite-element method allowing visualization and analysis in two dimensions with the possibility of extensions into three dimensions was used.

Experimental analysis and shadowgraphs have been used to analyze and observe pseudo-Rayleigh waves, which have been documented on flat surface plates, subjected to shock waves but were not observed during the interaction with cylindrical shells due to their rapid decay (Ahyi et al., 1998). Other wave phenomena include shell and fluid borne circumferential waves and the repulsion of the dispersion curves on a submerged cylindrical shell submerged in and filled by identical and different fluids (Bao et al, 1999). Experimental techniques have generated accurate high-speed visualizations of the acoustic scattering of impulsive geometrical waves by a glass sphere in water at high frequencies and correlated with experimental pressure readings taken (Latard et al., 1999). The curvature of the impact wave, from plane to spherical, as well as differing decay rates, are investigated with the Fourier solution for the response of the shell structure (Spraque and Geers, 1999). Smoothing techniques for finite element methods

were developed to improve calculations for quadrilateral grids in the analysis of shock reflections and channel flows (Sun, 1999).

Additional summaries were generated for review of hydrocodes for simulations of underwater shock responses to explosions. These give a description of predominantly used simulation methods and what needs to be included and considered for proper simulations (Mair, 1999, a). This was also followed by an improved review of benchmarks designed to test models for the response of structures to underwater explosion previously seen (Mair, 1999, b).

Shock wave interaction was experimentally tested on cooling tubes of inertial confinement fusion reactors by use of accelerometers and shadowgraphy for imaging of the flow and shock diffraction patterns (Oakley et al., 1999). To establish a good benchmark model, small explosives were detonated inside an aluminum cylindrical shell of specific dimensions with distilled water inside; the explosions were small enough to prevent rupture of the cylinder (Sandusky et al., 1999). Velocities, displacements and strains were directly measured in the shell and then the same can was modeled using codes to see how accurately the computational models could reproduce the physical experiment to verify the accuracy of the computer models. Generalization of non-reflecting boundaries for convex boundary conditions were shown to significantly improve the computational efficiency of finite element method for acoustic scattering problems without a significant loss in accuracy, being more suitable for submersible vehicles that are not bounded by exact circular ends (Diellouli et al., 2000). Analysis of close-in explosions showed the effect of the initial shock wave generated from the explosions interacting with the shell as well as the contributed effect of the bubble formation and its collapse. This caused cavitation, which created a second loading on the surface of the shell. It is suggested that deformation of the shell lowers the flow field pressure, facilitates cavitation and reduces initial shock loading on the shell (Andrew et al., 2000).

Case studies of double-hull surface vessels making contact with varying surfaces, sharp rocks, running aground of flat surface beds ect, were considered and computational models were used to determine how these varying collision scenarios would impact the double hulls such as membrane stretching, shell ruptures, inception and spreading of cracks, and damage to supporting sections (Wang et al., 2000). These simulations were

successfully compared to test results and could be used for statistical analysis of structural performance. The wave propagation approach for coupled structural-acoustic analysis of a finite cylindrical shell is compared to a numerical boundary element method/finite element method and it is shown that the second method of analysis produces similarly accurate results with the benefit of being less computationally intensive. Additional information states that the fluid effect of the fluid on the shell is substantial and if one does not take this into consideration, large errors in the simulations may result (Zhang et al., 2001). The transient response of a submerged spherical shell impacted by a strong plane shock wave is analyzed with the coupled finite element method, and a doubly asymptotic approximation is used to produce time-histories of surface pressures, stresses on the shell as well as radial velocities; results show that a strong shock wave generates significantly different radial velocities (Liang, 2001). Benchmarks were established for modeling codes by measuring pressures, deformations and strain states of aluminum cylindrical shells subjected to an internal explosion (Chambers et al., 2001). Stabilization of BEM/FEM coupling methods was accomplished enabling simulations of a variety of situations for loading of multi-domain fluid-structure interactions such as double shell arrangements (Lie and Yu, 2002). A different factor investigated was how a plane shock wave would interact with a cylinder rotating on its axis (Sun et al., 2003). It was found that the side of the cylinder rotating “into” the shock wave would retard the transition of regular reflection to a Mach reflection but the side rotating with the shock wave would promote the transition.

The focusing of strong shock waves was investigated numerically for two- and three-dimensional cases in which Geometrical Shock Dynamics (GSD) method was used to simulate the reflection of a spherical shock wave generated at one focal point rebounding off the elliptical cavities at either end with different tests for varying eccentricities (Apazidis, 2003). Examination of the difference between non-homogeneous flow surrounding the shock wave and homogenous flow were considered. Large-scale experiments have been carried out off the coast of Korea in which underwater explosions were originated around different types of ships (Park et al., 2003). Tests were then able to estimate the safety zone of these ships in shock environments through

explosive testing that registered on the instrumentation aboard the ships but that would not create lasting damage.

Other benchmarks have been developed to evaluate the acoustic fields generated during shock-shell interactions. Semi-analytical solutions have been used to observe focusing of the internal radiated wave inside an elastic cylindrical shell, elastic wave propagation in the shell, its radiation into the fluid and the affect the inner acoustical field has on the stress-strain state of the shell (Iakovlev, 2006). The effect of varying the parameters of the shell such as the shell thickness, and the bending stiffness of the shell would have on the radiated acoustic fields was also studied. Possibility of cavitation at locations of significant negative pressures and how these may contribute to the internal acoustic field was discussed in (Iakovlev, 2007). Study (Iakovlev, 2009) addressed how fluids inside the shell with densities and sound speeds greater or less than that of the external fluid would generate acoustic fields and have their own peak pressures and strains at different locations. Investigation of the acoustic fields generated by the presence of a rigid co-axial core inside an elastic cylindrical shell separated by, and submerged into, an identical fluid and impacted by an underwater explosion is presented in (Iakovlev et al., 2010). Results show that cores with smaller radii interact in a similar manner to a cylindrical shell without a core, but as the core radius becomes larger it begins to have a significant impact on the acoustic fields generating higher frequency rebounds between the shell and the core, thus creating more complex acoustic fields.

The problem of acoustic scattering of rebounded pulses being detected by instruments attached to submerged vessels is addressed and methods are developed to use the fact that interference patterns often exhibit strong spatial, angular, and spectral dependence for particular geometries and therefore provide valuable information regarding the location of the object (Sorokin and Terentiev, 2006). Explosive effects of shock waves generated at varying close ranges were investigated to see how the shock wave, bubble pulse, bubble collapse and water jetting would still contribute to the total interaction at the shell-fluid barrier (Brett and Yiannakopolous, 2008). It was found through high-speed photography as well as sensors measuring the pressures, displacements and accelerations of the shell that the secondary bubble pulse caused minimum stress on shell equal to approximately half of the initial shock wave.

Additionally, the bubble collapse caused the greatest peak stress, about twice that of the shock wave, which contributed the most to plastic deformation of the shell structure. Additional experiments were carried out to observe the effects of shock loading on various cylindrical shells that were unstiffened and internally/externally stiffened with the detonation occurring at various standoff distances. The obtained experimental results were then reproduced using FEM model approaches to compare accuracy for modeling of the linear and non-linear states of interaction (Hung et al., 2009). Submarine analytical modeling of a finite cylinder capped at the ends with two bulkheads excited by external loading was simulated to observe the influence of the various complicating effects such as the bulkheads, ring-stiffeners and fluid loading on the structural and acoustic responses of the finite cylindrical shell. Results from the analytical models were compared to the FEM/BEM models (Caresta and Kessissoglou, 2009). A time-domain Kirchhoff model was used to simulate the reflecting properties of polygonal surfaces that are submerged in water (Lee and Seong, 2009). A new shock factor was considered as a means to better understand and describe the characteristics of the incident shock wave. It was believed that a better shock factor could describe the effects that a spherical blast wave could have on the cylinder that was thought to be missed in other shock factors (Yao et al., 2009).

As a general conclusion of this literature review, various types of computational and experimental methods have been employed in the study of both complex and simple geometries. The majority of studies appear to employ numerical modeling for analysis of shell-shock interactions, and it appears that the majority of work for specified cases uses finite element method to obtain detailed results, as is the case for many investigations into shock wave effects on ship hulls. However, additional methods such as converged analytical or semi-analytical solutions can be used as comparison for other numerical codes; these analytical solutions serve as benchmarks for future codes to ensure their reliabilities (Mair, 1999a). All of these methods have been used to demonstrate the wave propagation, acoustic fields or stress-strain states of cylindrical shells subjected to a shock wave.

This thesis will demonstrate the capabilities of mathematical modeling to simulate the interaction of an external shock wave impacting a co-axially arranged double hulled

cylindrical shell structure coupled by an inter-shell fluid. The main objective is to evaluate the maximum stress-strain values in both shells as well as the maximum and minimum pressures experienced on both the internal and external shells. Where and when these maximum and minimum values occur is also of concern so that one can better understand the complexity of the interactions that occur. Once the solution is obtained, a parametric study is then carried out to look at how the variables of concern vary in location, timing and magnitude. The system's parameters of concern are the shell materials, thicknesses of both the inner and outer shells and the properties of the fluids. Conclusions will then be drawn aiming at better understanding how the two shells will behave after impact of the shock wave and how the double-hull scenario structure differs from the single shell one, with the ultimate goal of making better design decisions to improve safety, reduce cost and optimize performance of submerged double–hull structures in the context of their shock response.

CHAPTER 2: MATHEMATICAL FORMULATION

The following mathematical formulation is referencing the paper written simultaneously with the production of this thesis (Iakovlev *et al.*, 2015).

Considering two circular cylindrical shells of radii a and r_0 with thicknesses h_1 and h_2, respectively, and assuming that $h_1/r_0 << 1$ and $h_2/r_0 << 1$, we can then use the linear theory of shells if we further assume that the deflections of the shell surface are small compared to its thickness. The transverse and normal displacements of the internal and external shells are v_1, v_2 and w_1, w_2 respectively, with positive normal displacements described as inward. Characteristics of the internal and external shells are densities ρ_1, ρ_2, sound speeds c_1, c_2, and Poisson ratios v_1, v_2, respectively. The interior shell is evacuated and coaxially arranged inside the exterior shell and the two shells are coupled by an internal fluid with a density ρ_i, and sound speed c_i. This entire system is then submerged into external fluid with density ρ_e, and sound speed c_e. Both the internal and external fluids are linearly compressible, irrotational and inviscid. The cylindrical system is subjected to an external spherical shock wave at a standoff distance R. Polar coordinates (ϱ, θ) based on the axis of the double-shelled co-axial system are employed. The internal space of the internal shell will be considered evacuated. Figure 2.1 shows the geometry of the problem.

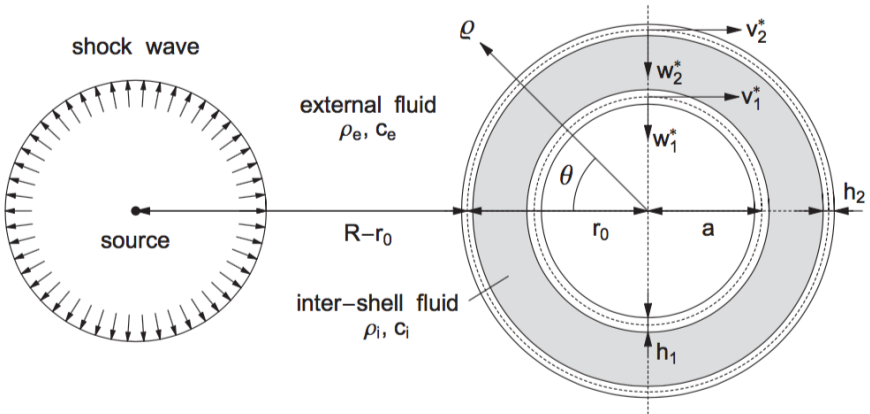

Figure 2.1. Geometry of problem

The fluids are governed by the wave equations,

$$\nabla^2\phi_i = \frac{1}{c_i^2}\frac{\partial^2\phi_i}{\partial\tau^2} \tag{1}$$

and

$$\nabla^2\phi_e = \frac{1}{c_e^2}\frac{\partial^2\phi_e}{\partial\tau^2} \tag{2}$$

where ϕ_i and ϕ_e are the respective internal and external fluid potential velocities and τ represents time.

Based on the Love-Kirchhoff hypothesis, the shell equations are, for the inner hull,

$$\frac{1}{r_1^2}\frac{\partial^2 v_1^*}{\partial\theta^2} - \frac{1}{r_1^2}\frac{\partial w_1^*}{\partial\theta} + k_1^2\left(\frac{1}{r_1^2}\frac{\partial^3 w_1^*}{\partial\theta^3} + \frac{1}{r_1^2}\frac{\partial^2 v_1^*}{\partial\theta^2}\right) = \frac{1}{c_1^2}\frac{\partial^2 v_1^*}{\partial\tau^2} \tag{3}$$

$$\frac{1}{r_1^2}w_1^* - \frac{1}{r_1^2}\frac{\partial v_1^*}{\partial\theta} + k_1^2\left(\frac{1}{r_1^2}\frac{\partial^4 w_1^*}{\partial\theta^4} + \frac{1}{r_1^2}\frac{\partial^3 v_1^*}{\partial\theta^3}\right) = \chi_1 p_s^1\frac{1}{c_1^2}\frac{\partial^2 w_1^*}{\partial\tau^2} \tag{4}$$

and for the outer hull,

$$\frac{1}{r_2^2}\frac{\partial^2 v_2^*}{\partial\theta^2} - \frac{1}{r_2^2}\frac{\partial w_2^*}{\partial\theta} + k_2^2\left(\frac{1}{r_2^2}\frac{\partial^3 w_2^*}{\partial\theta^3} + \frac{1}{r_2^2}\frac{\partial^2 v_2^*}{\partial\theta^2}\right) = \frac{1}{c_2^2}\frac{\partial^2 v_2^*}{\partial\tau^2} \tag{5}$$

$$\frac{1}{r_2^2}w_2^* - \frac{1}{r_2^2}\frac{\partial v_2^*}{\partial \theta} + k_2^2\left(\frac{1}{r_2^2}\frac{\partial^4 w_2^*}{\partial \theta^4} + \frac{1}{r_2^2}\frac{\partial^3 v_2^*}{\partial \theta^3}\right) = \chi_2 p_s^2 \frac{1}{c_2^2}\frac{\partial^2 w_2^*}{\partial \tau^2} \tag{6}$$

where, $k_1^2 = h_1^2/(12a^2)$, $k_2^2 = h_2^2/(12r_0^2)$, $\chi_1 = h_1\rho_1 c_1^2$, $\chi_2 = h_2\rho_2 c_2^2$, and p is the total acoustical pressure evaluated at each respective shells' surface. The total pressure p,

$$p_s^2 = p|_{\varrho=r_0} = (p_o + p_d + p_r^e - p_r^i)|_{\varrho=r_0} \tag{7}$$

and

$$p_s^1 = p|_{\varrho=a} = p_r^i|_{\varrho=a} \tag{8}$$

for the external and internal shells, respectively, where p_o is the incident pressure, p_d is the diffracted pressure, p_r^e is the external radiated pressure, and p_r^i is the internal radiated pressure.

The boundary conditions of the problem are the no-flow and dynamic conditions at the surface of each shell,

$$\frac{\partial \phi_r^i}{\partial \varrho}|_{\varrho=r_0} = -\frac{\partial w_2^*}{\partial \tau}, \qquad \frac{\partial \phi_r^i}{\partial \varrho}|_{\varrho=a} = -\frac{\partial w_1^*}{\partial \tau}, \tag{9}$$

$$\frac{\partial \phi_r^e}{\partial \varrho}|_{\varrho=r_0} = -\frac{\partial w_2^*}{\partial \tau}, \qquad \frac{\partial \phi_d}{\partial \varrho}|_{\varrho=r_0} = -\frac{\partial \phi_0}{\partial \varrho}|_{\varrho=r_0} \tag{10}$$

and the decay conditions at the infinity,

$$\phi_d \to 0 \text{ and } \phi_r^e \to 0 \text{ when } \varrho \to \infty \tag{11}$$

and the periodicity conditions θ-wise. All initial conditions are assumed to be zero.

The external shell is subjected to an external shockwave with a pressure p_0 and potential ϕ_0, which are given by,

$$p_0 = \frac{p_\propto S_R}{R^*} e^{-\left(\tau - c_e^{-1}(R^* - S_R)\right)\lambda^{-1}} H(\tau - c_e^{-1}(R^* - S_R)) \tag{12}$$

$$\phi_0 = -\frac{\lambda p_\alpha S_R}{\rho_e R^*} e^{-\left(\tau - c_e^{-1}(R^* - S_R)\right)\lambda^{-1}} H(\tau - c_e^{-1}(R^* - S_R)) \tag{13}$$

where,

$$R^* = \sqrt{R_0^2 + \varrho^2 - 2R_0\varrho cos\theta} \tag{14}$$

p_α is the pressure in front of the wave when it first impinges on the shell, λ is the rate of exponential decay, $S_R = R_0 - r_0$ is the standoff distance of the shockwave and H is the Heaviside unit step function. The transverse stresses in the shells are given by

$$\sigma_{\theta\theta}^1 = \frac{E_1}{1 - v_1^2}\left(\frac{1}{a}\frac{\partial v_1}{\partial \theta} - \frac{1}{a}w_1\right) \tag{15}$$

$$\sigma_{\theta\theta}^2 = \frac{E_2}{1 - v_2^2}\left(\frac{1}{r_0}\frac{\partial v_2}{\partial \theta} - \frac{1}{r_0}w_2\right) \tag{16}$$

We consider a dimensionless form of the problem with the normalization of all variables to $r_0, \rho_e,$ and c_e. Dimensionless variables are distinguished from their dimensional forms by a hat symbol, $\widehat{\ }$, above the variable with the exception of the time $t = \tau c_e r_0^{-1}$, the radial coordinate $r = \varrho r_0^{-1}$, and the normal and transverse displacements $w = w_* r_0^{-1}$ and $v = v_* r_0^{-1}$, respectively.

CHAPTER 3: SOLUTION METHODOLOGY

Throughout the next two sections, the methodology outlined in Iakovlev et al., 2015 will be followed.

3.1 FLUID DYNAMICS

Pressure components can be obtained by applying the Laplace transform to the dimensionless wave equations (1) and (2),

$$\frac{\partial^2\hat{\Phi}_e}{\partial r^2}+\frac{1}{r}\frac{\partial\hat{\Phi}_e}{\partial r}+\frac{1}{r^2}\frac{\partial^2\hat{\Phi}_e}{\partial\theta^2}-s^2\hat{\Phi}_e=0 \tag{17}$$

and

$$\frac{\partial^2\hat{\Phi}_i}{\partial r^2}+\frac{1}{r}\frac{\partial\hat{\Phi}_i}{\partial r}+\frac{1}{r^2}\frac{\partial^2\hat{\Phi}_i}{\partial\theta^2}-s^2\frac{c_e^2}{c_i^2}\hat{\Phi}_i=0 \tag{18}$$

where $\hat{\Phi}_e$ and $\hat{\Phi}_i$ are the dimensionless Laplace transforms of $\hat{\phi}_e$ and $\hat{\phi}_i$, respectively, and *s* is the transform variable. We then separate the spatial variables and provide the general solutions of (17) and (18) with the forms

$$\hat{\Phi}_n^e=F_n^eK_n(rs)\cos(n\theta),\ \ n=0,1,2\ldots. \tag{19}$$

and

$$\hat{\Phi}_n^i=\{F_n^iK_n(r\alpha s)+G_n^iI_n(r\alpha s)\}\cos(n\theta),\ \ n=0,1,2\ldots \tag{20}$$

respectively, where $\alpha=c_e/c_i$, I_n is the modified Bessel function of the first kind of order n, K_n is the modified Bessel function of the second kind of order n, and F_n^e, F_n^i and G_n^i are arbitrary functions of s.

Considering the matching series expansions for the normal incident velocity on the surface of the outer shell and the normal displacements of the middle surfaces of the shells,

$$\frac{\partial\hat{\phi}_0}{\partial r}|_{r=1}=\sum_{n=0}^{\infty}b_n(t)\cos n\theta \tag{21}$$

$$w_1 = \sum_{n=0}^{\infty} w_n^1(t) \cos n\theta \tag{22}$$

and

$$w_2 = \sum_{n=0}^{\infty} w_n^2(t) \cos n\theta \tag{23}$$

after application of all boundary conditions the Laplace transforms of the harmonics of the fluid velocity potential components are found to be

$$\widehat{\Phi}_n^d(r,s) = B_n(s)\Xi_n^e(r,s) \cos n\theta, \tag{24}$$

$$\widehat{\Phi}_n^{r,e}(r,s) = sW_n(s)\Xi_n^e(r,s) \cos n\theta, \tag{25}$$

and

$$\widehat{\Phi}_n^{r,i}(r,s) = \{sW_n^1(s)\Xi_n^1(r,\alpha s) - sW_n^2(s)\Xi_n^2(r,\alpha s)\} \cos n\theta, \tag{26}$$

where B_n, W_n^1, and W_n^2 are the Laplace transforms of b_n, w_n^1 and w_n^2, respectively, and Ξ_n^e, Ξ_n^1, and Ξ_n^1 are the Laplace transforms of the response functions of this problem, ξ_n^e, ξ_n^1, and ξ_n^2, respectively given by,

$$\Xi_n^e(r,s) = -\frac{K_n(rs)}{sK_n'(s)}, \tag{27}$$

$$\Xi_n^1(r,s) = \frac{I_n'(s)K_n(rs) - K_n'(s)I_n(rs)}{sI_n'\big((as)K_n'(\alpha s) - I_n'(s)K_n'(as)\big)}, \tag{28}$$

and

$$\Xi_n^2(r,s) = \frac{I_n'(as)K_n(rs) - K_n'(as)I_n(rs)}{s\big(I_n'(as)K_n'(s) - I_n'(s)K_n'(as)\big)}. \tag{29}$$

The response functions represent the response of the fluid to the motion of the shells and/or scattering by the outer shell (Iakovlev, 2006, 2008b; Iakovlev et al., 2010). They do not depend on the parameters of the fluid or those of the shell, and are determined exclusively by the geometry of the system. As a result, approaches based on the use of the response functions are very attractive for practical implementation due to their high computational efficiency. The response functions ξ_n^e and ξ_n^2 have been extensively addressed in earlier work (the former in Iakovlev, 2008b, and the latter in

Iakovlev et al., 2010, where a shell containing a rigid core was considered, a scenario that is geometrically identical to the present case), and we do not repeat the respective derivations here. For discussion of the function ξ_n^1 see (Iakovlev et al., 2015).

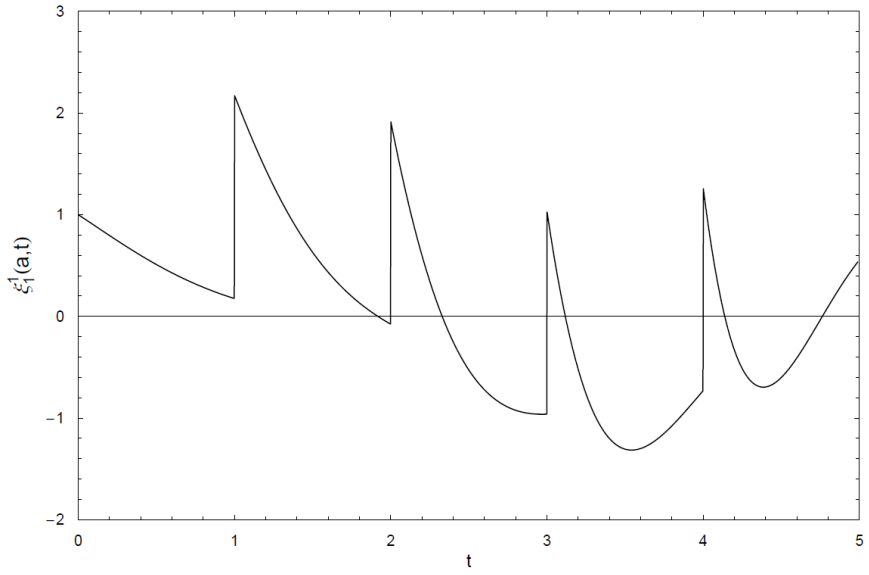

Figure 3.1. Response function $\xi_1^1(a,t)$

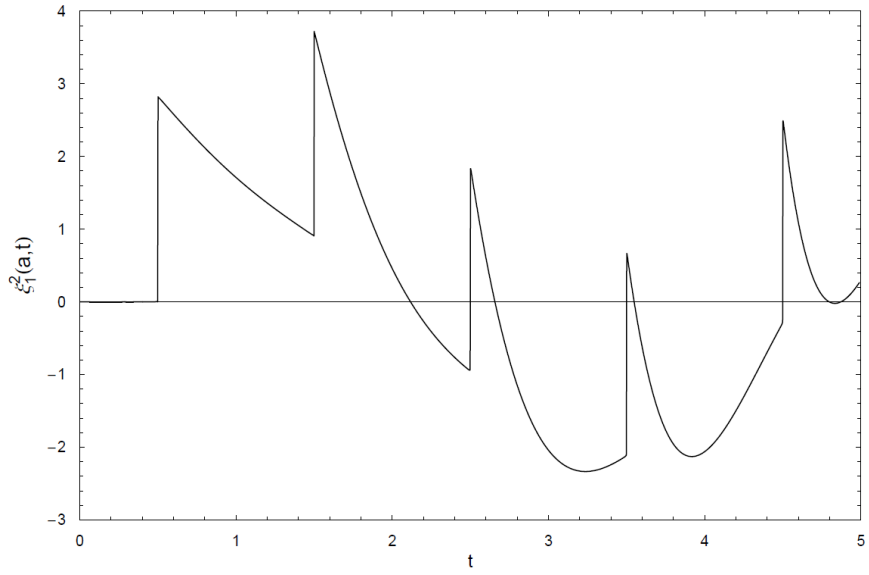

Figure 3.2. Response function $\xi_1^2(a,t)$

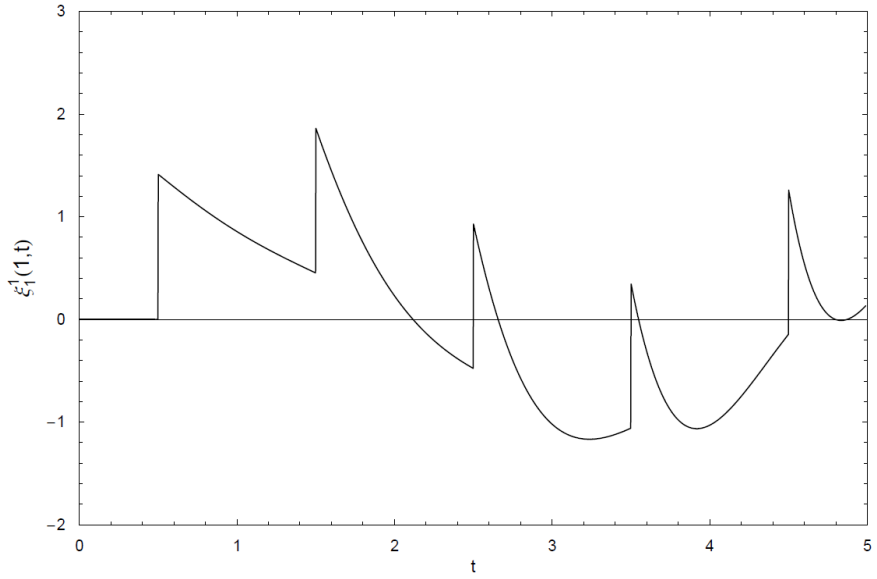

Figure 3.3. Response function $\xi_1^1(1,t)$

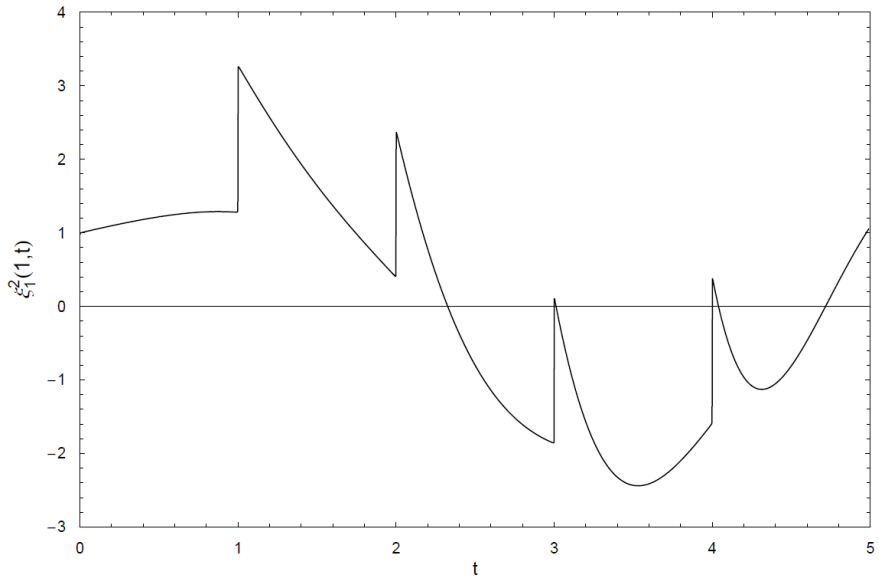

Figure 3.4. Response function $\xi_1^2(1,t)$

Taking into account the assumptions of the model we use here, for the dimensionless pressure $\hat{p}$ and the fluid velocity potential $\hat{\phi}$ we have

$$\hat{p} = -\frac{\partial \hat{\phi}}{\partial t}, \tag{30}$$

This allows us, after applying certain theorems pertaining to the Laplace transform to

(24), (25), and (26), to obtain the pressure components as

$$\hat{p}_d = \sum_{n=0}^{\infty} \hat{p}_n^d \cos n\theta, \tag{31}$$

$$\hat{p}_r^e = \sum_{n=0}^{\infty} \hat{p}_n^{r,e} \cos n\theta, \tag{32}$$

$$\hat{p}_r^i = \sum_{n=0}^{\infty} \hat{p}_n^{r,i} \cos n\theta, \tag{33}$$

where,

$$\hat{p}_n^d = -\frac{1}{\sqrt{r}} b_n(t) - \int_0^t b_n(\eta) \frac{d\xi_n^e}{d\eta}(r, t-\eta) d\eta, \tag{34}$$

$$\hat{p}_n^{r,e} = -\int_0^t \frac{d^2 w_n^2(\eta)}{d\eta^2} \xi_n^e(r, t-\eta) d\eta, \tag{35}$$

$$\hat{p}_n^{r,i} = -\frac{\rho_i c_i}{\rho_e c_e} \int_0^t \frac{d^2 w_n^1(\eta)}{d\eta^2} \xi_n^1\left(r, \frac{c_i}{c_e}(\mathrm{t}-\eta)\right) d\eta + \frac{\rho_i c_i}{\rho_e c_e} \int_0^t \frac{d^2 w_n^2(\eta)}{d\eta^2} \xi_n^2\left(r, \frac{c_i}{c_e}(t-\eta)\right) d\eta. \tag{36}$$

3.2 STRUCTURAL DYNAMICS

We consider the matching series expansion for the displacements,

$$v_1 = \sum_{n=0}^{\infty} v_n^1 \sin n\theta, \tag{37}$$

$$w_1 = \sum_{n=0}^{\infty} w_n^1 \cos n\theta, \tag{38}$$

$$v_2 = \sum_{n=0}^{\infty} v_n^2 \sin n\theta, \tag{39}$$

and

$$w_2 = \sum_{n=0}^{\infty} w_n^2 \cos n\theta, \tag{40}$$

and then rewrite the dimensionless shell equations in terms of the harmonics $v_n^1 \sin n\theta$, $v_n^2 \sin n\theta$, $w_n^1 \cos n\theta$ and $w_n^2 \cos n\theta$. For each n, we obtain an integro-differential system for $v_n^1, v_n^2, w_n^1 \; and \; w_n^2$,

$$\gamma_1^2 \frac{d^2 v_n^1}{dt^2} + c_1^{11} v_n^1 + c_1^{12} w_n^1 = 0, \tag{41}$$

$$\gamma_1^2 \tfrac{d^2 w_n^1}{dt^2} + c_1^{21} v_n^1 + c_1^{22} w_n^1 = \chi_1 \left\{ -\tfrac{\rho_i c_i}{\rho_e c_e} \int_0^t \tfrac{d^2 w_n^1(\eta)}{d\eta^2} \xi_n^1 \left(a, \tfrac{c_i}{c_e}(t-\eta) \right) d\eta + \tfrac{\rho_i c_i}{\rho_e c_e} \int_0^t \tfrac{d^2 w_n^2(\eta)}{d\eta^2} \xi_n^2 \left(a, \tfrac{c_i}{c_e}(t-\eta) \right) d\eta \right\}, \tag{42}$$

$$\gamma_2^2 \frac{d^2 v_n^2}{dt^2} + c_2^{11} v_n^2 + c_2^{12} w_n^2 = 0, \tag{43}$$

and

$$\gamma_2^2 \tfrac{d^2 w_n^2}{dt^2} + c_2^{21} v_n^2 + c_2^{22} w_n^2 = \chi_2 \left\{ p_n^0 + p_n^d - \int_0^t \tfrac{d^2 w_n^2(\eta)}{d\eta^2} \xi_n^e \big(1, (t-\eta)\big) d\eta + \tfrac{\rho_i c_i}{\rho_e c_e} \int_0^t \tfrac{d^2 w_n^1(\eta)}{d\eta^2} \xi_n^1 \left(1, \tfrac{c_i}{c_e}(t-\eta) \right) d\eta - \tfrac{\rho_i c_i}{\rho_e c_e} \int_0^t \tfrac{d^2 w_n^2(\eta)}{d\eta^2} \xi_n^2 \left(1, \tfrac{c_i}{c_e}(t-\eta) \right) d\eta \right\}, \tag{44}$$

where,

$$c_1^{11} = n^2 + k_1^2 n^2, \qquad c_1^{12} = c_1^{21} = -n - k_1^2 n^3, \qquad c_1^{22} = 1 + k_1^2 n^4 \tag{45}$$

$$c_2^{11} = n^2 + k_2^2 n^2, \qquad c_2^{12} = c_2^{21} = -n - k_2^2 n^3, \quad c_2^{22} = 1 + k_1^2 n^4, \tag{46}$$

and

$$\gamma_1 = a\frac{c_e}{c_s^1}, \qquad \gamma_2 = \frac{c_e}{c_s^2}, \tag{47}$$

$$\chi_1 = a^2\left(\frac{r_0\rho_e(c_e)^2}{h_1^2\rho_1(c_1)^2}\right), \qquad \chi_2 = \left(\frac{r_0\rho_e(c_e)^2}{h_2^2\rho_2(c_2)^2}\right), \tag{48}$$

$$k_1^2 = \frac{h_1^2}{12a^2}, \quad k_1^2 = \frac{h_2^2}{12r_0^2}, \tag{49}$$

complemented by the zero-value initial conditions for, v_n^1, w_n^1, v_n^2, w_n^2 and their first derivatives (for brevity, the index 'n' is omitted in the notations for the c-coefficients.)

The systems were approached numerically using finite differences, and a simple explicit finite-difference scheme was used where the integrals were approximated using the trapezoidal rule, and the derivatives were approximated using central differences. The systems in question are ordinary, thus the computational costs were not an issue, and the step size could be decreased without any difficulty until convergence was reached for all cases of interest. The resulting finite-difference schemes were obtained as

$$v_1^{i+1} = 2v_1^i - v_1^{i-1} + \frac{h^2}{\gamma_1^2}\left(-c_1^{11}v_1^i - c_1^{12}w_1^i\right) \tag{50}$$

$$w_1^{i+1} = 2w_1^i - w_1^{i-1} - \frac{h^2}{\gamma_1^2}\left(\chi_1\left\{\gamma_0 hJ_{1a}^i - \gamma_0 hJ_{2a}^i\right\} + c_1^{21}v_1^i - c_1^{22}w_1^i\right) \tag{51}$$

and

$$v_2^{i+1} = 2v_2^i - v_2^{i-1} + \frac{h^2}{\gamma_2^2}\left(-c_2^{11}v_2^i - c_2^{12}w_2^i\right) \tag{52}$$

$$w_2^{i+1} = 2w_2^i - w_2^{i-1} - \Omega\left(\chi_2\left\{-p_0^i + hJ_e^i - \gamma_0 hJ_{11}^i + \gamma_0 hJ_{21}^i\right\} + c_2^{21}v_2^i + c_2^{22}w_2^i\right), \tag{53}$$

where h is the time step,

$$\gamma_0 = \frac{\rho_i c_i}{\rho_e \rho_e}, \qquad \Omega = \frac{2h^2}{(2\gamma_2^2 + h\chi_2)}, \tag{54}$$

$$J_{1a}^i = \sum_{j=1}^{i-1} \frac{w_1^{j+1} - 2w_1^j + w_1^{j-1}}{h^2} \xi_{1a}^{i-j}, \tag{55}$$

$$J_{2a}^i = \sum_{j=1}^{i-1} \frac{w_2^{j+1} - 2w_2^j + w_2^{j-1}}{h^2} \xi_{2a}^{i-j}, \tag{56}$$

$$J_{11}^i = \sum_{j=1}^{i-1} \frac{w_1^{j+1} - 2w_1^j + w_1^{j-1}}{h^2} \xi_{11}^{i-j}, \tag{57}$$

$$J_{21}^i = \sum_{j=1}^{i-1} \frac{w_2^{j+1} - 2w_2^j + w_2^{j-1}}{h^2} \xi_{21}^{i-j}, \tag{58}$$

$$J_e^i = \sum_{j=1}^{i-1} \frac{w_2^{j+1} - 2w_2^j + w_2^{j-1}}{h^2} \xi_e^{i-j}, \tag{59}$$

and $v_1^i, w_1^i, v_2^i, w_2^i, p_n^i\ \xi_{1a}^i, \xi_{2a}^i, \xi_{11}^i, \xi_{21}^i$ and ξ_e^i are the nodal values of $v_n^1(t), w_n^1(t), v_n^2(t), w_n^2(t), p_n^0(t) + p_n^d(t), \xi_n^1\left(a, \frac{c_i}{c_e}t\right), \xi_n^2\left(a, \frac{c_i}{c_e}t\right), \xi_n^1\left(1, \frac{c_i}{c_e}t\right), \xi_n^2\left(1, \frac{c_i}{c_e}t\right)$, and $\xi_e^i(1,t)$, respectively.

Previous work regarding convergence of the finite difference schemes was used to establish the appropriate time step to ensure convergence (Iakovlev, 2008b). When the shell thicknesses are similar, the time step of 0.001 is sufficient for all other parameter ranges of interest. However, when the outer shell is much thinner than the inner shell, the convergence was observed to worsen, so another doubling of the time step (h=0.0005) was evaluate for this case and determined it did ensure convergence even for the most dramatic differences considered (h_1/h_2 = 10, Iakovlev et al, 2015).

The convergence of the series for the displacements and pressure components has been analyzed as well, and it was established that 150 harmonics were sufficient to

accurately simulate and realistically visualize (Iakovlev, 2008b) all quantities addressed here except for the diffraction pressure which required 300 harmonics. It should be made aware that the benefit of such a solution in terms of the implementation of its application in code is what makes this approach so appealing. Due to the “simplicity” of the approach the ability to reduce processing time allows us to generate greater amounts of data in less time than other methods can provide. This is truly beneficial for applications in preliminary design ideas because one could quickly, relatively speaking, determine in which direction the design process should proceed saving both time and money early on in the development process. In summary of the processing time required; it took 221 seconds to compute all structural harmonics for a single set of system parameters, as compared to 11 seconds it would take for a single submerged fluid-filled shell, with all computations being carried out on an Intel i7 3.40 GHz CPU. The hydrodynamic fields and simulated inter-shell and external fields required 2.45 and 2.08 hours, respectively, to create. These appealing features became very important for the parametric study discussed later in the thesis.

CHAPTER 4: RESULTS AND DISCUSSIONS

4.1 HYDRODYNAMIC FIELDS

For initial investigations of the solution we consider the interior shell with radius a = 0.50 m and exterior shell with a radius of r_o = 1.00 m, with thicknesses h_1 = h_2 = 0.01m, made of steel c_1 = c_2 = 5000 kg/m^3, ρ_1 = ρ_2 = 7800 kg/m^3, and ν_1 = ν_2 = 0.3, submerged in water, c_e = 1400 m/s and ρ_e = 1000 kg/m^3, and with water filling the inter-shell space, c_i = 1400 m/s and ρ_i = 1000 kg/m^3. The incident loading is assumed to be a shock wave originated at the distance of five radii of the outer shell from the axis of the shells (i.e., the standoff of S_r = $4r_0$), with the rate of exponential decay λ = 0.0001314 s and the pressure in the front at the moment of the initial contact p_α = 250 kPa.

For this system, we visualize the hydrodynamic fields and address how the pressure waves are behaving and to better understand the dynamics of the stress-strain states (Iakovlev 2006, 2007), which are considered the most vital aspect of the interaction. Therefore, figure 4.1 shows a sequence of pressure field images that are taken at times that best represent the overall dynamics of the interactions. To better ensure optimal appearances, each image has been scaled separately, with the blacks corresponding to the lowest pressure and white to the highest; respective pressure ranges are noted in the figure caption. Units are expressed in the dimensionless form for the snapshots in order to compare the difference in magnitude between the highest and lowest pressures seen in each snapshot; The unit of time is also viewed in dimensionless form.

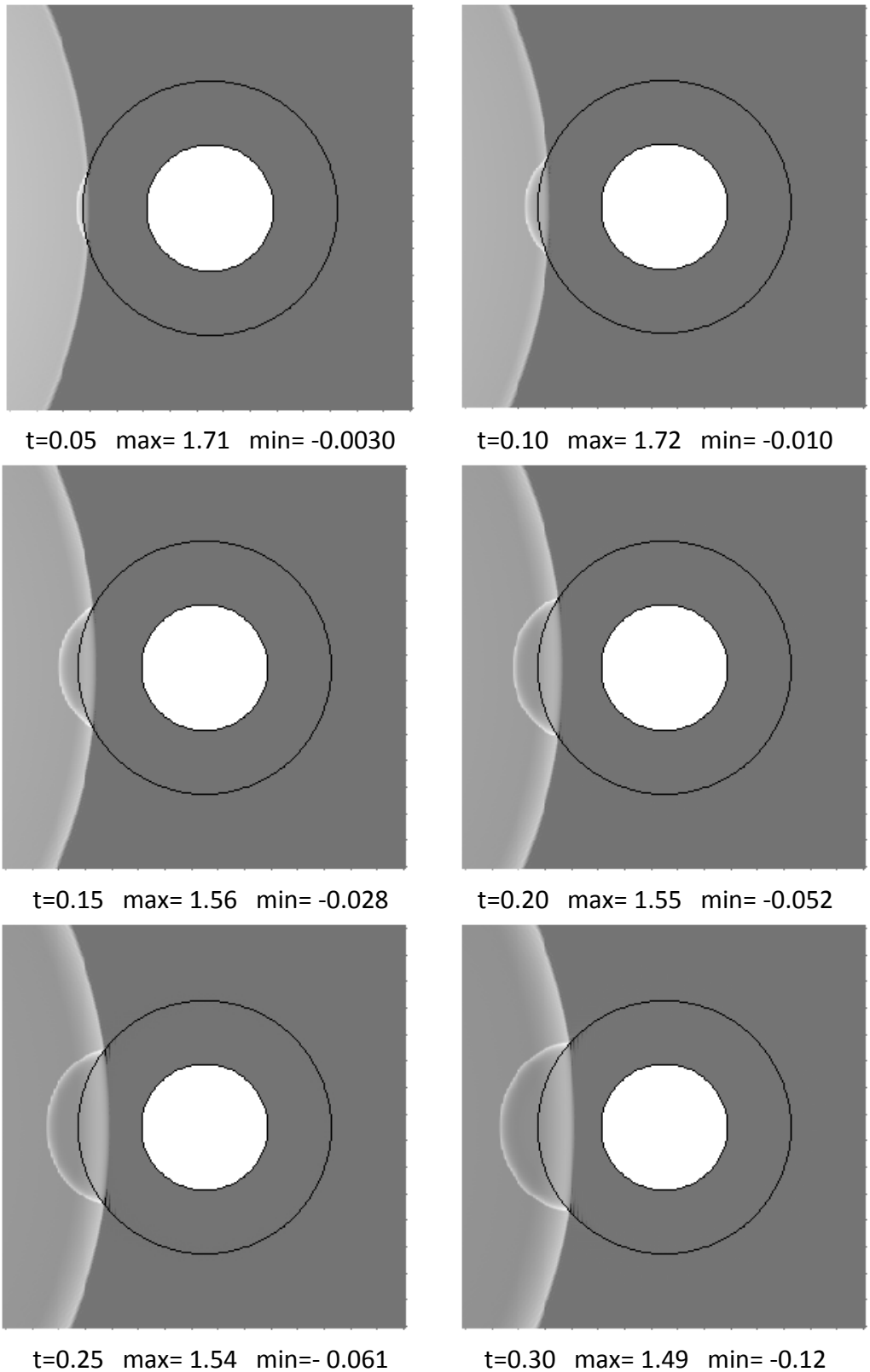

Figure 4.1. Two-dimensional Snapshots of the hydrodynamic fields.

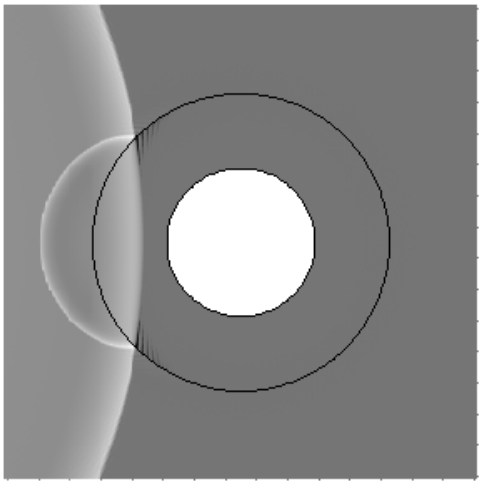

t=0.35 max= 1.43 min= -0.12

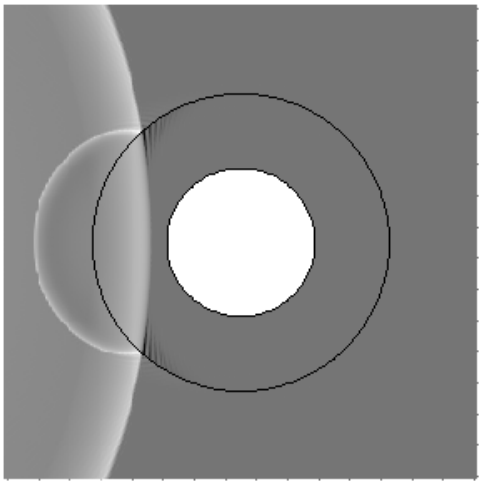

t=0.40 max= 1.39 min=- 0.15

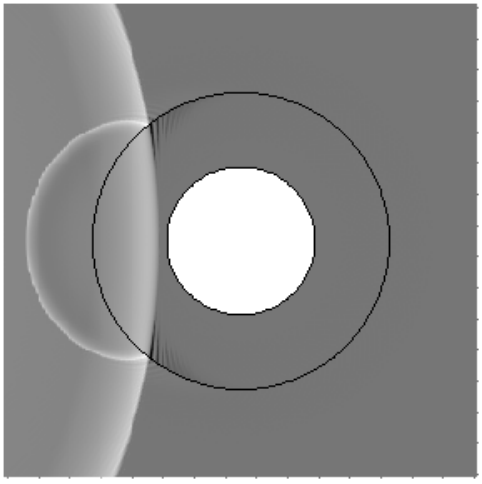

t=0.45 max= 1.36 min=- 0.16

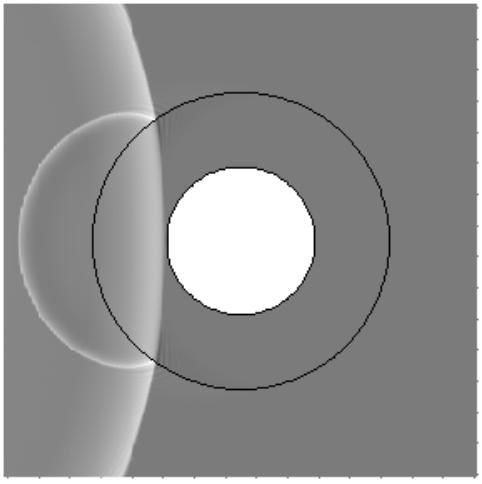

t=0.50 max= 1.24 min=- 0.62

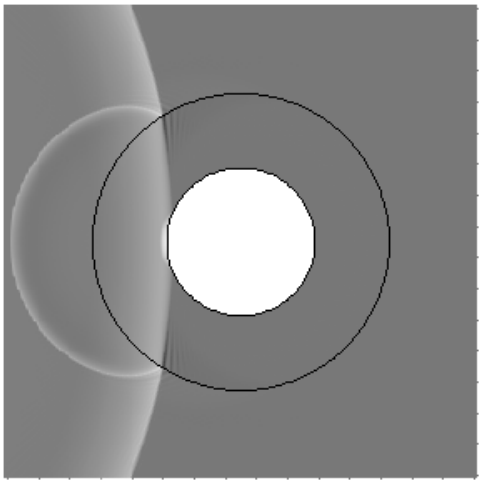

t=0.55 max= 1.80 min=- 0.42

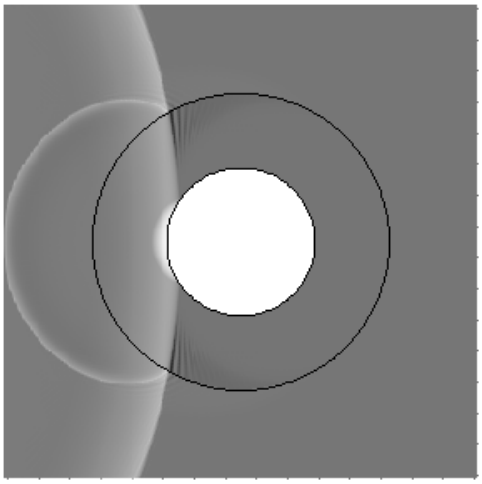

t=0.60 max= 1.92 min=- 0.28

Fig. 4.1 Continued

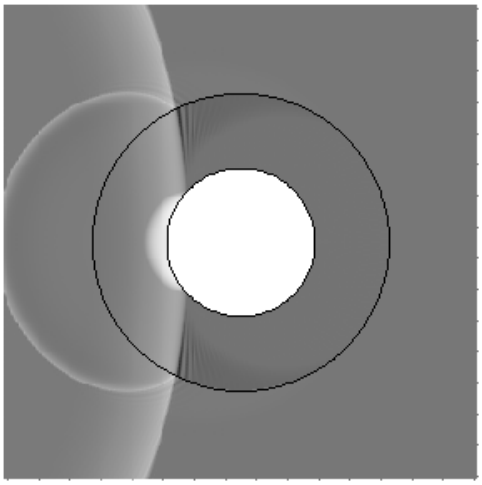

t=0.65 max= 1.86 min=- 0.33

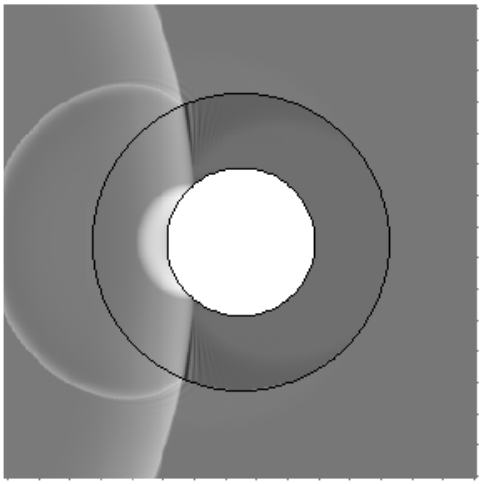

t=0.70 max= 1.74 min= -0.36

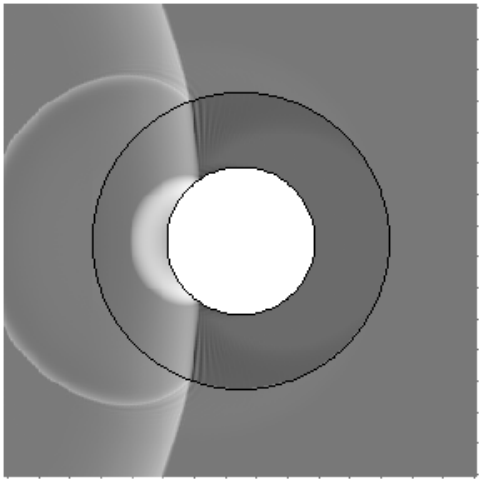

t=0.75 max= 1.60 min= -0.42

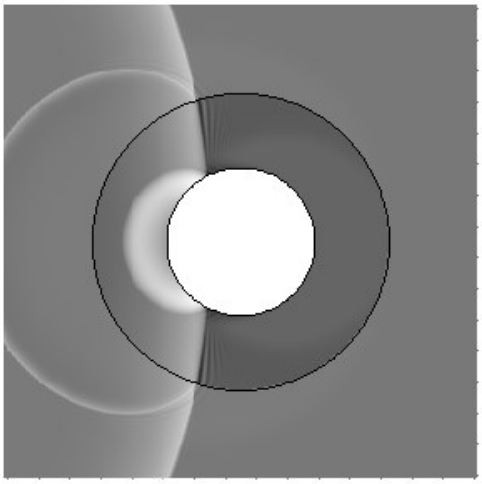

t=0.80 max= 1.48 min=- 0.42

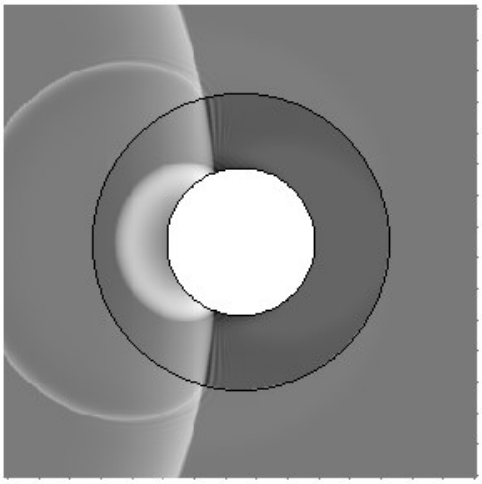

t=0.85 max= 1.39 min=- 0.49

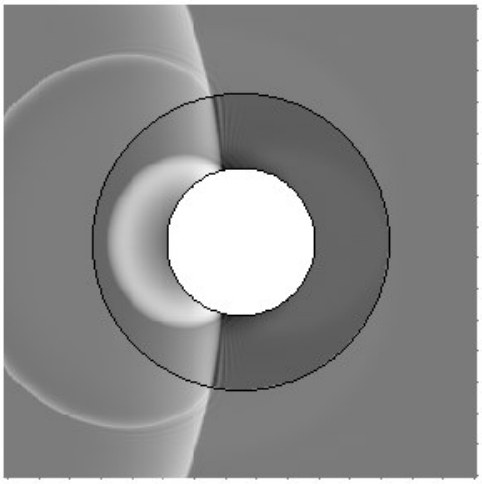

t=0.90 max= 1.27 min= -0.55

Fig. 4.1 continued.

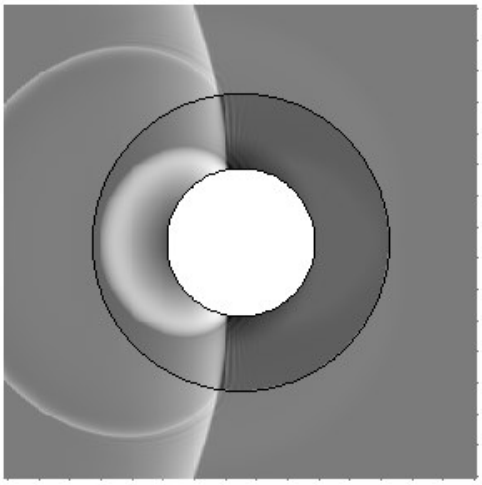

t=0.95 max= 1.19 min= -0.59

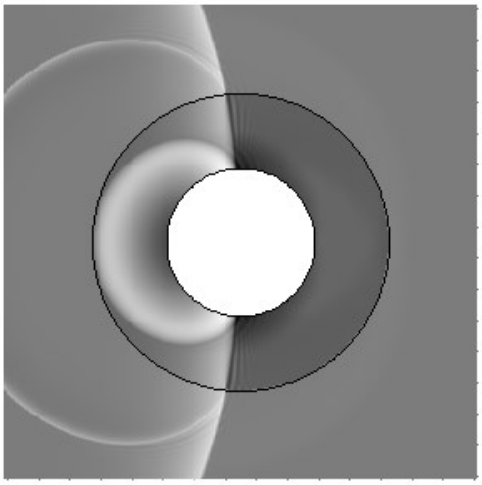

t=1.00 max= 1.11 min=- 0.60

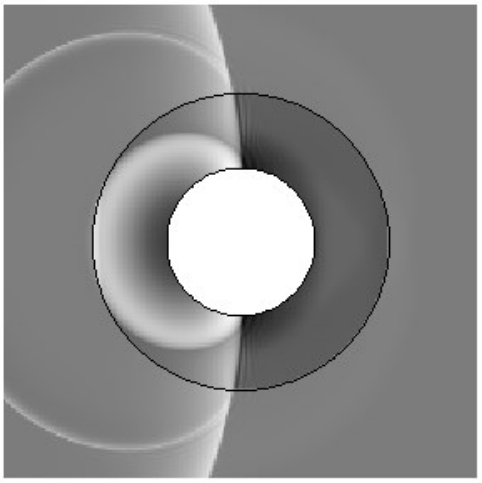

t=1.05 max= 1.03 min= -0.57

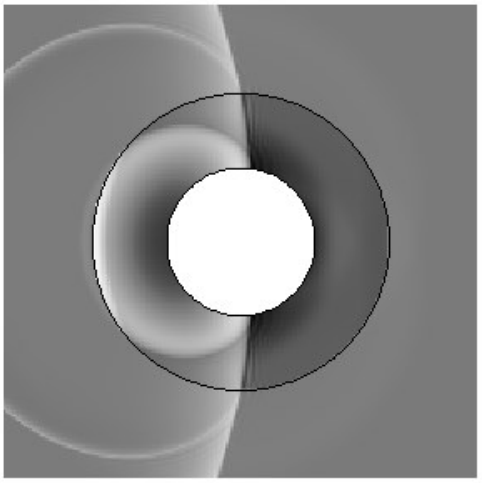

t=1.10 max= 1.28 min=- 0.54

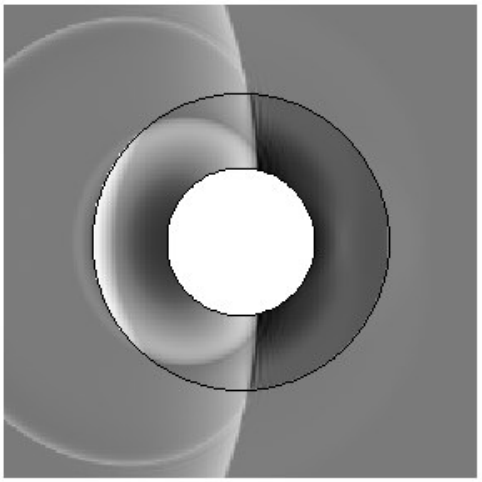

t=1.15 max= 1.34 min=- 0.50

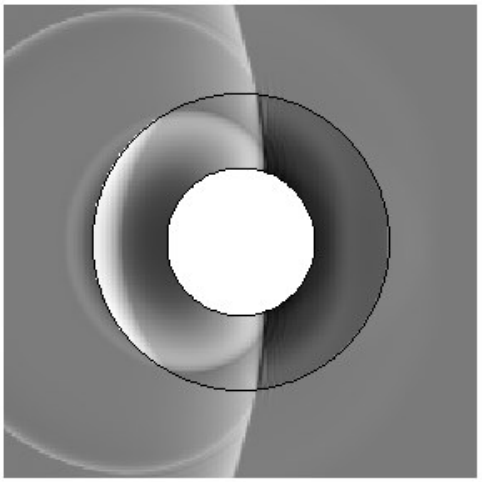

t=1.20 max= 1.24 min=- 0.52

Fig. 4.1 Continued

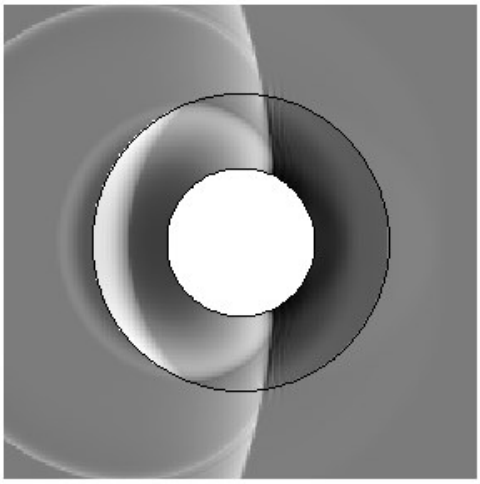

t=1.25 max= 1.12 min=- 0.50

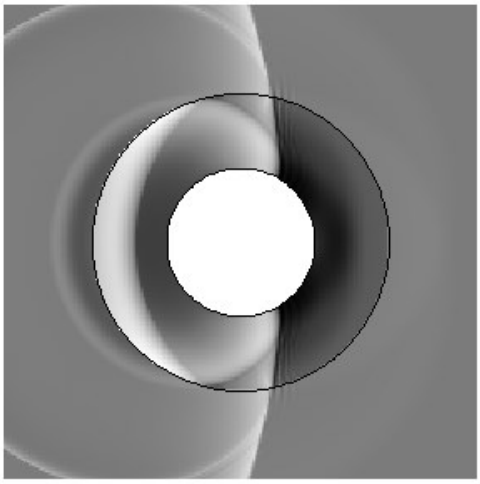

t=1.30 max= 1.00 min= -0.47

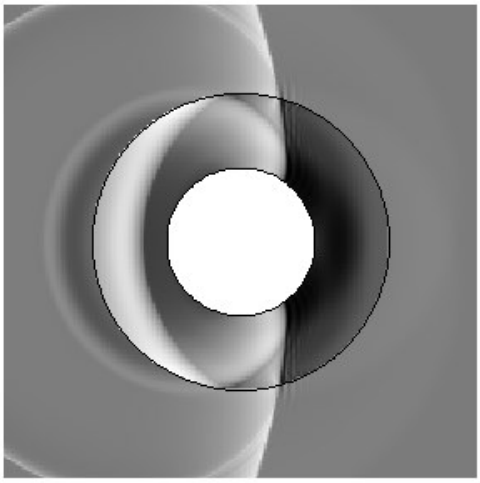

t=1.35 max= 0.89 min= -0.44

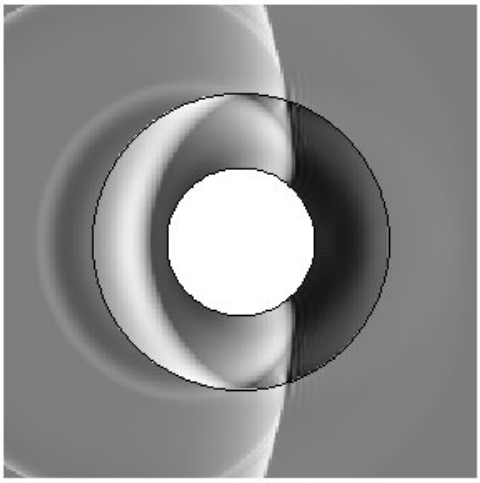

t=1.40 max= 0.80 min=- 0.48

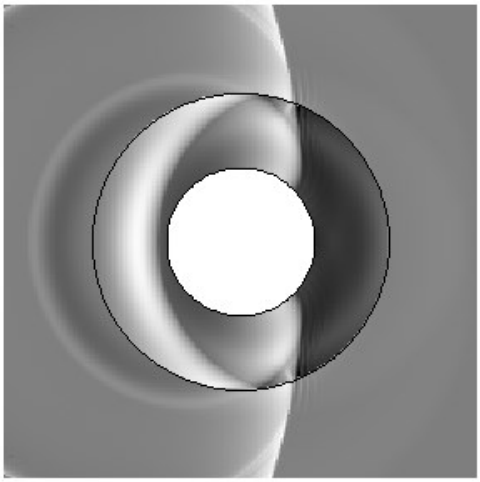

t=1.45 max= 0.76 min= -0.59

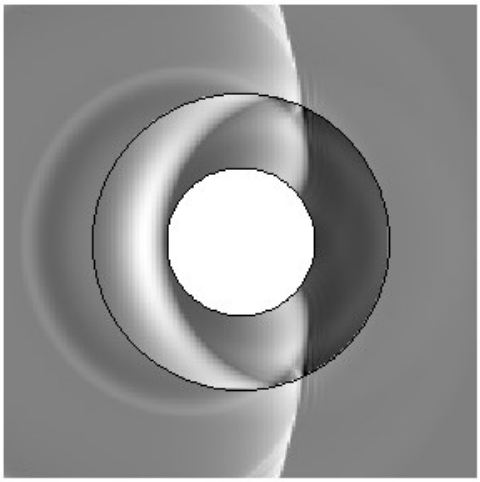

t=1.50 max= 0.77 min= -0.72

Fig. 4.1 Continued

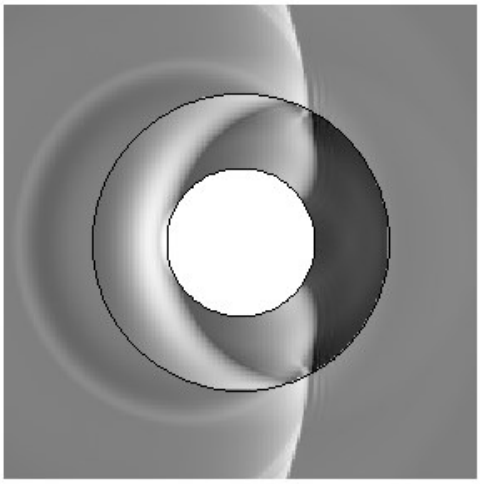

t=1.55 max= 0.84 min=- 0.69

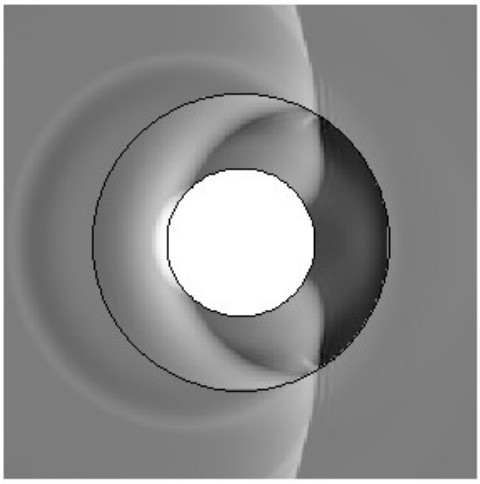

t=1.60 max= 1.46 min= -0.75

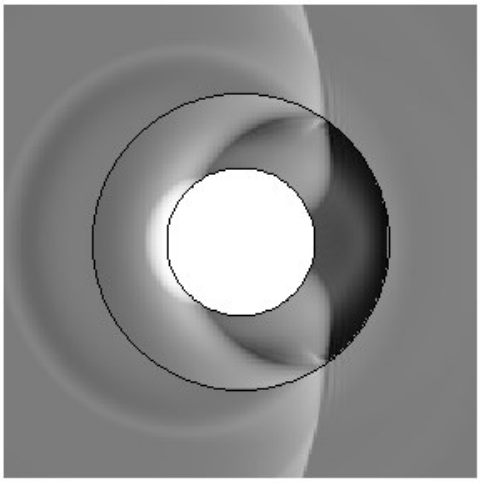

t=1.65 max= 1.47 min=- 0.74

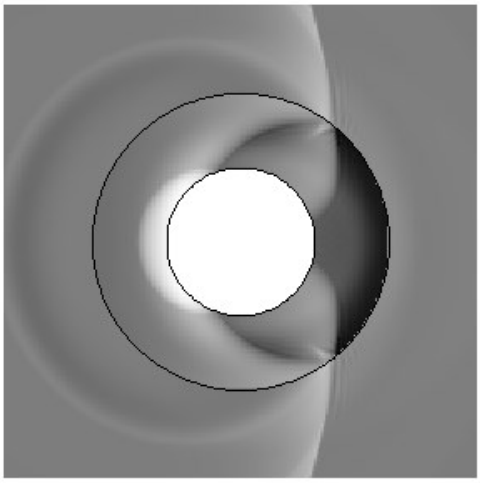

t=1.70 max= 1.46 min=- 0.85

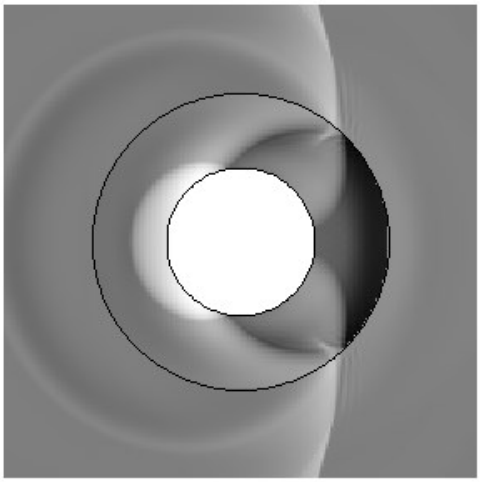

t=1.75 max= 1.33 min=- 0.87

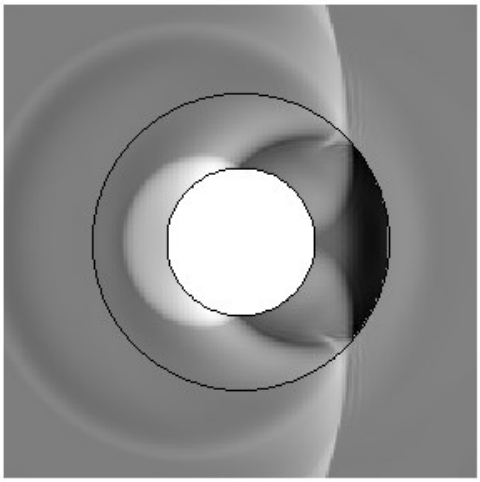

t=1.80 max= 1.23 min= -0.81

Fig. 4.1 Continued

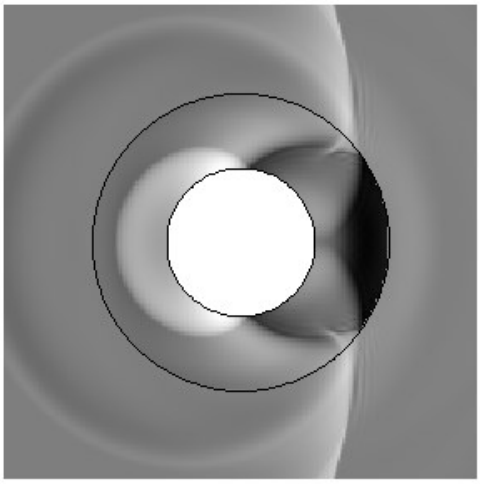

t=1.85 max= 1.11 min=- 0.76

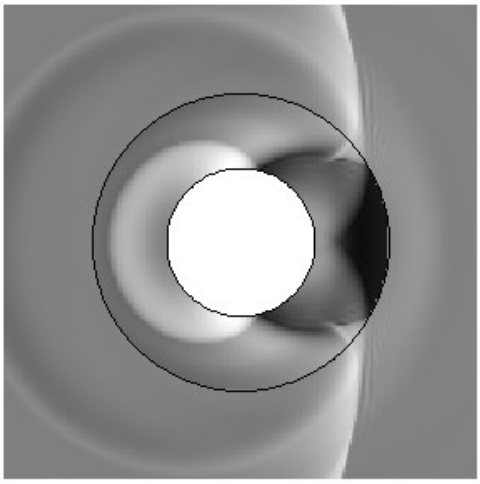

t=1.90 max= 0.91 min= -0.79

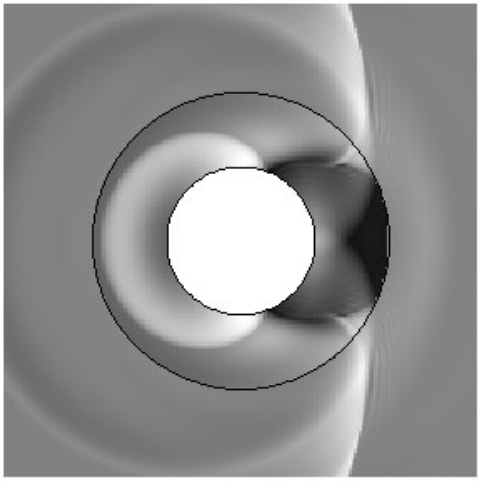

t=1.95 max= 0.78 min= -0.79

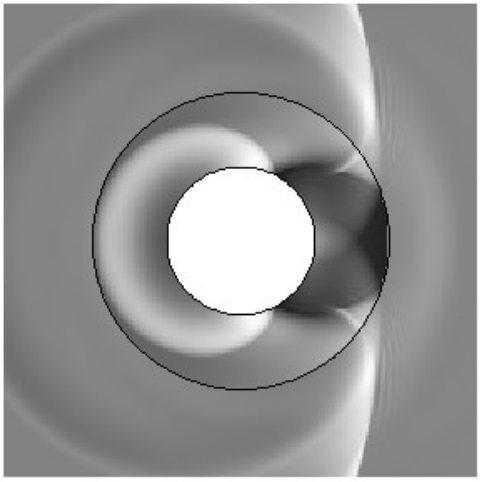

t=2.00 max= 0.71 min= -0.91

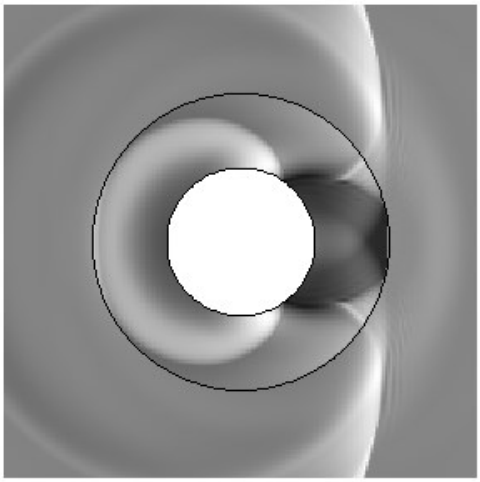

t=2.05 max= 0.69 min=- 0.94

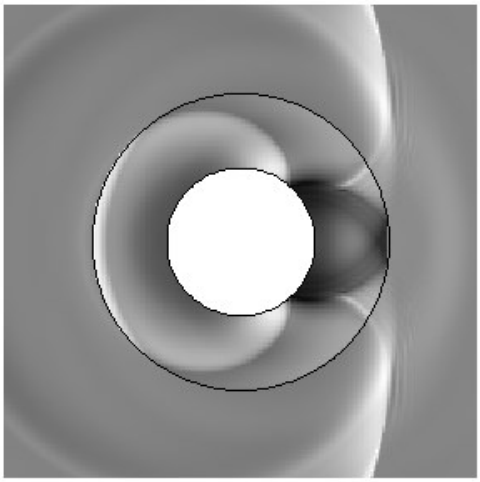

t=2.10 max=0.70 min=- 0.96

Fig. 4.1 Continued

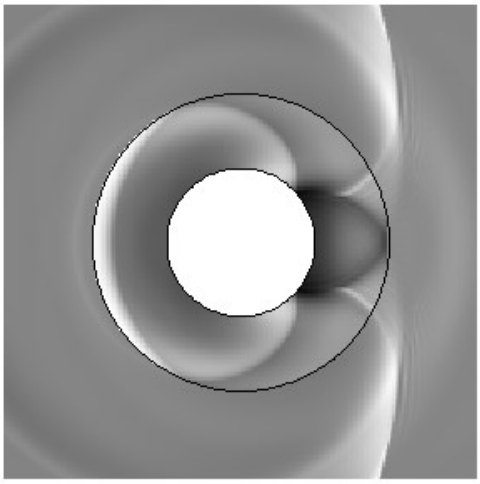

t=2.15 max= 0.70 min=- 1.11

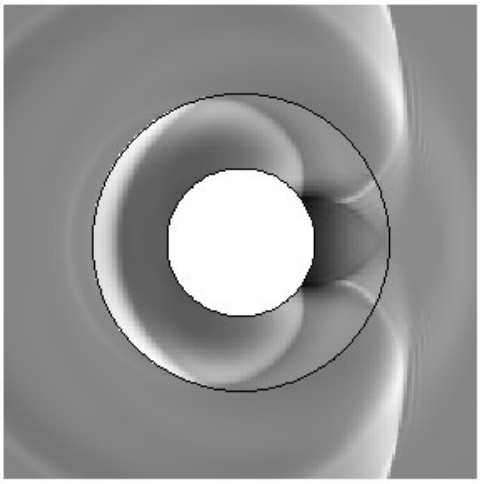

t=2.20 max= 0.71 min= -1.14

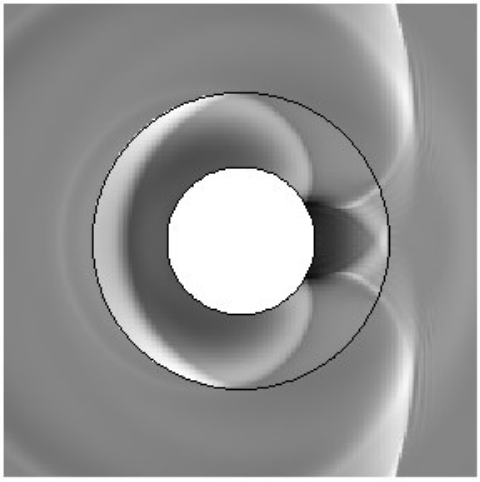

t=2.25 max= 0.70 min= -1.03

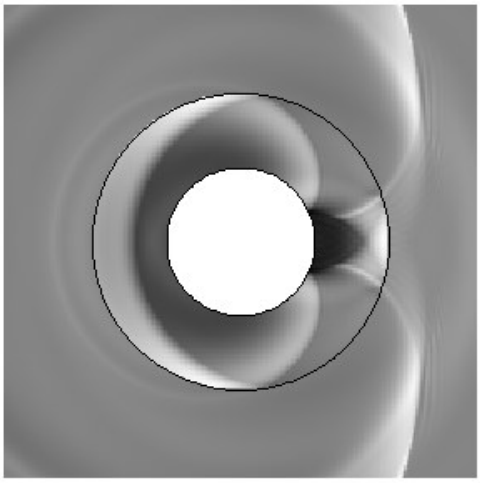

t=2.30 max= 0.69 min=-0.90

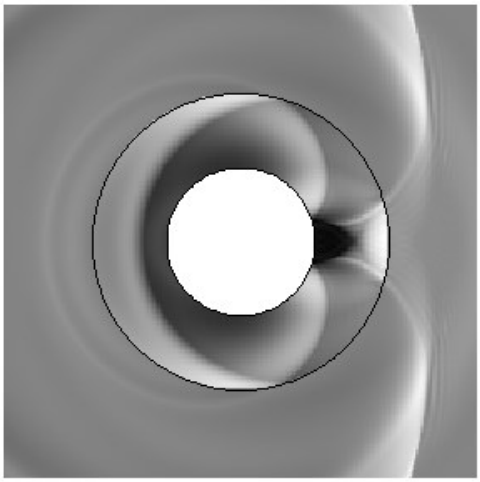

t=2.35 max= 0.70 min= -0.76

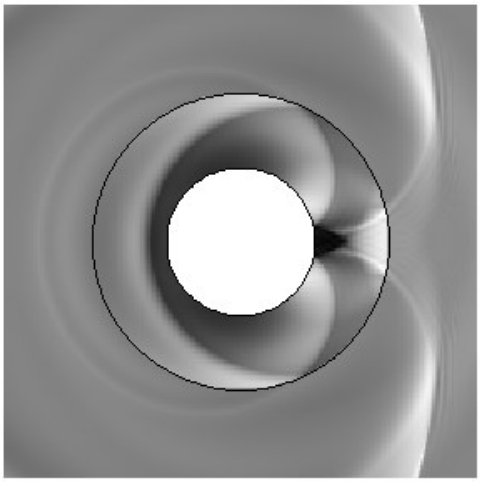

t=2.40 max= 0.68 min=-0.75

Fig. 4.1 Continued

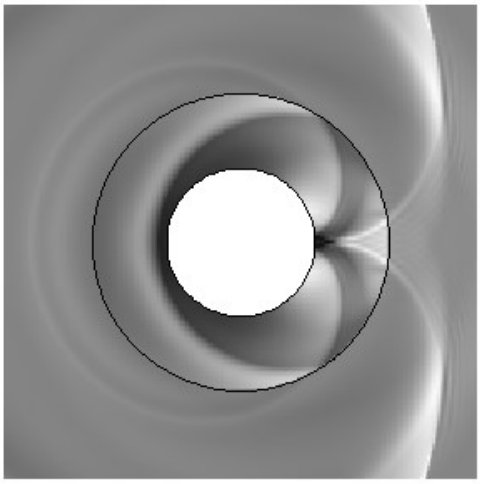

t=2.45 max= 0.64 min= -0.78

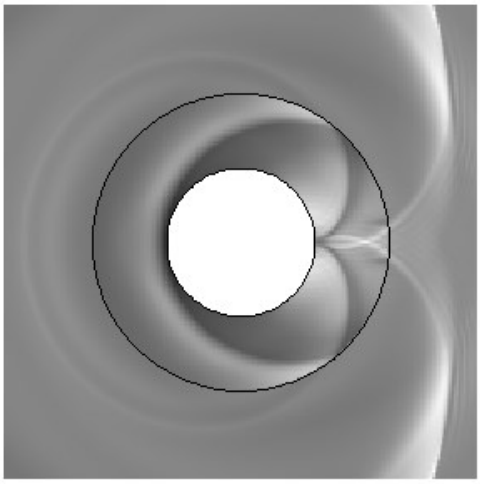

t=2.50 max= 0.66 min= -1.01

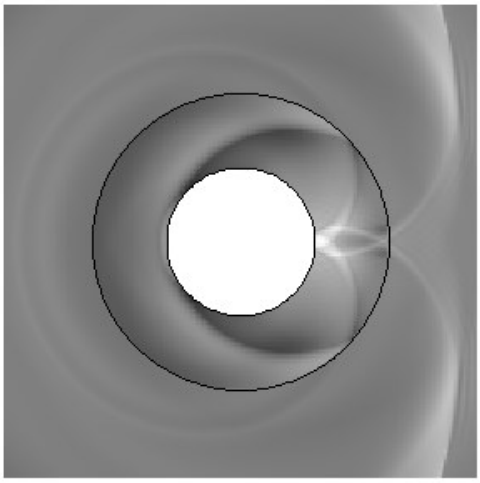

t=2.55 max= 1.14 min= -0.82

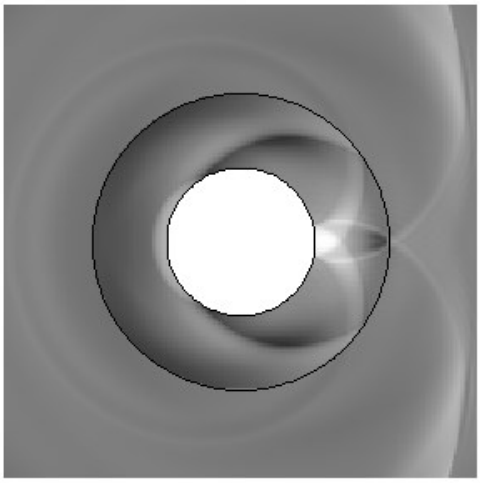

t=2.60 max= 1.41 min=- 0.65

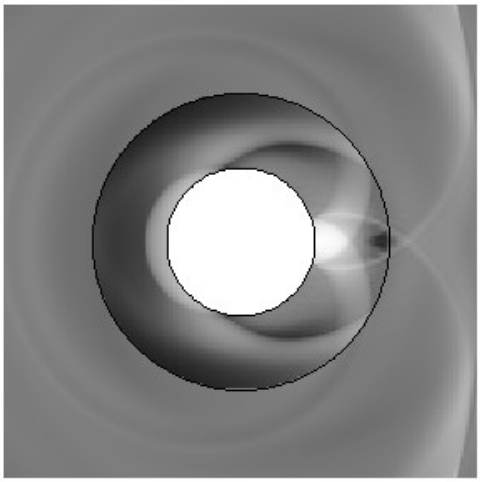

t=2.65 max= 1.45 min=- 0.50

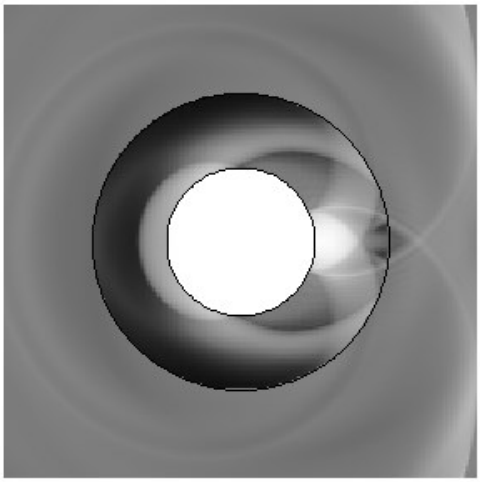

t=2.70 max= 1.35 min= -0.47

Fig. 4.1 Continued

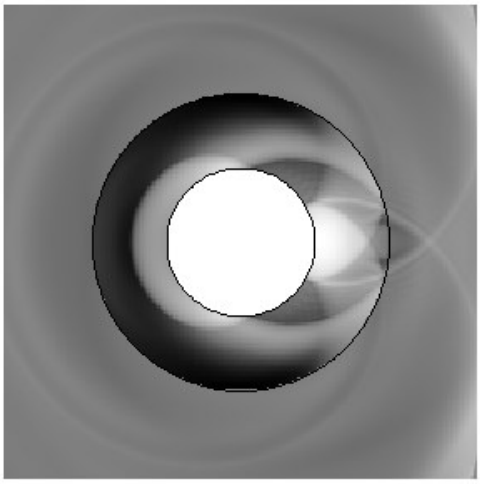

t=2.75 max= 1.15 min=- 0.48

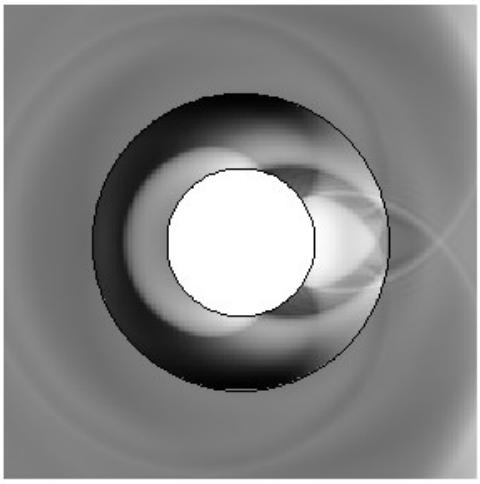

t=2.80 max= 0.97 min= -0.52

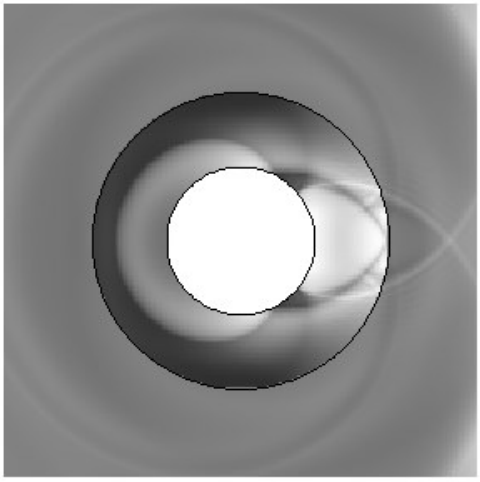

t=2.85 max= 0.79 min=- 0.79

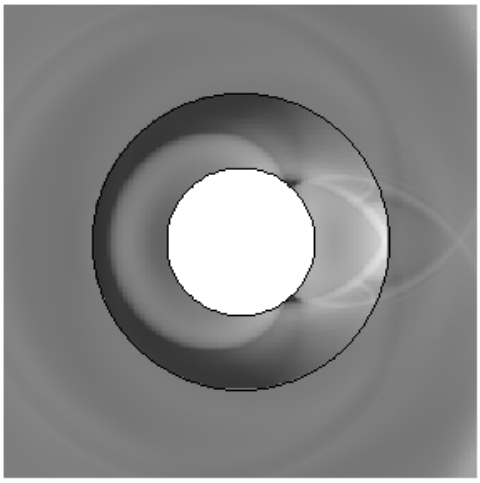

t=2.90 max= 1.42 min=- 0.82

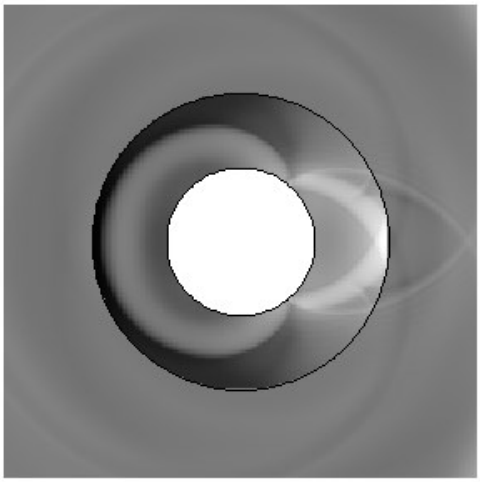

t=2.95 max= 1.48 min=- 0.62

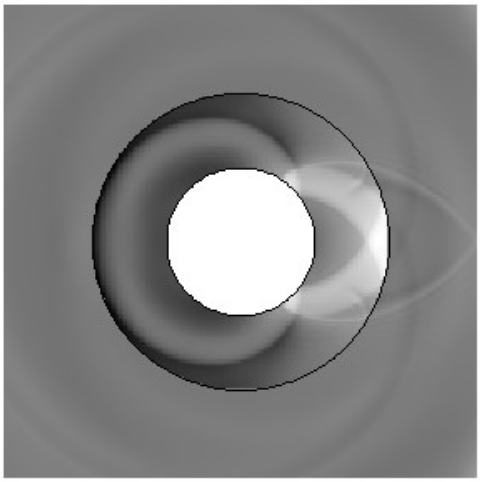

t=3.00 max= 1.36 min=- 0.67

Fig. 4.1 Continued

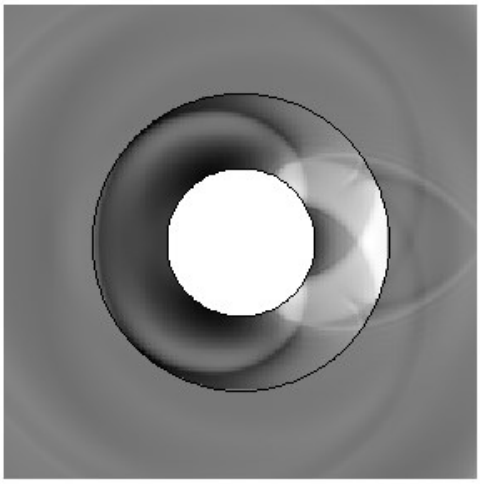

t=3.05 max= 1.21 min=- 0.52

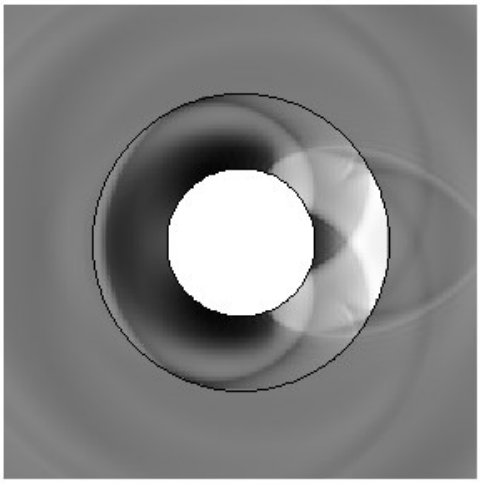

t=3.10 max= 1.09 min=- 0.58

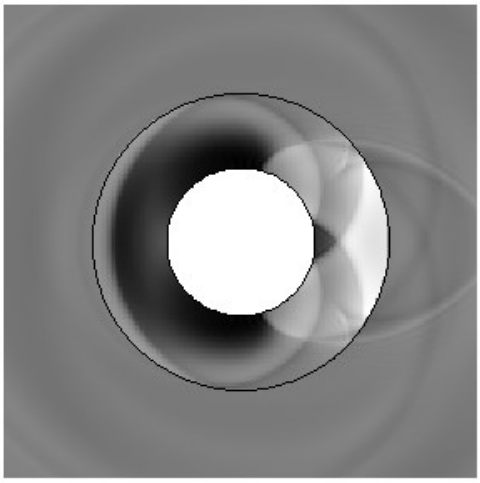

t=3.15 max= 1.06 min=- 0.64

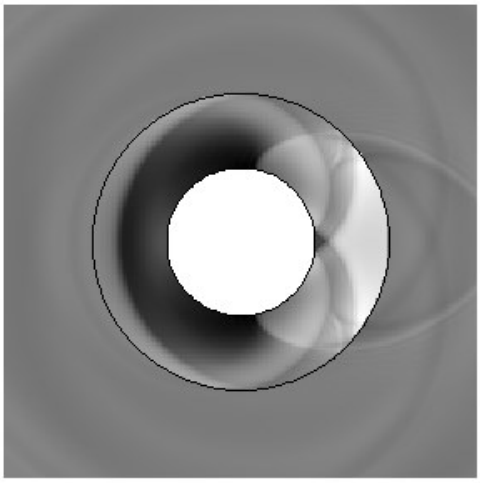

t=3.20 max= 1.04 min=- 0.76

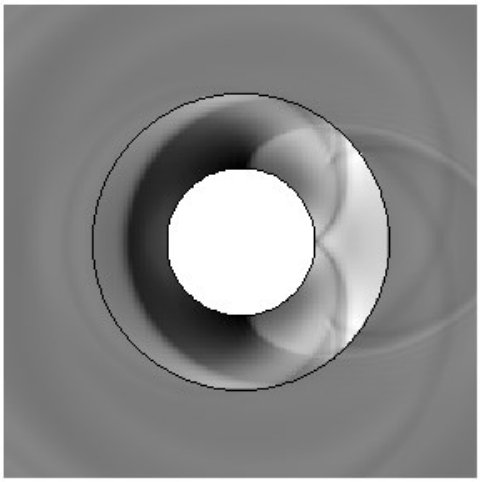

t=3.25 max= 0.99 min= -0.80

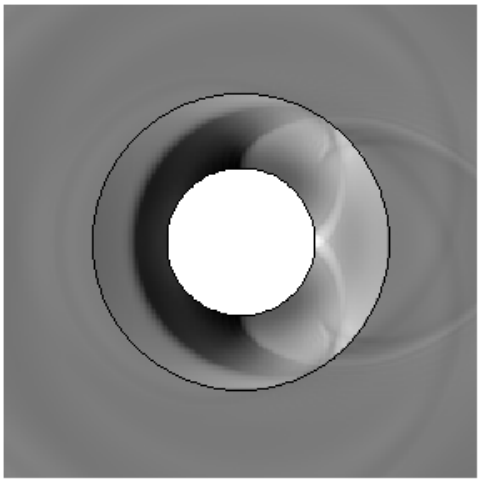

t=3.30 max= 1.48 min=- 0.78

Fig. 4.1 Continued

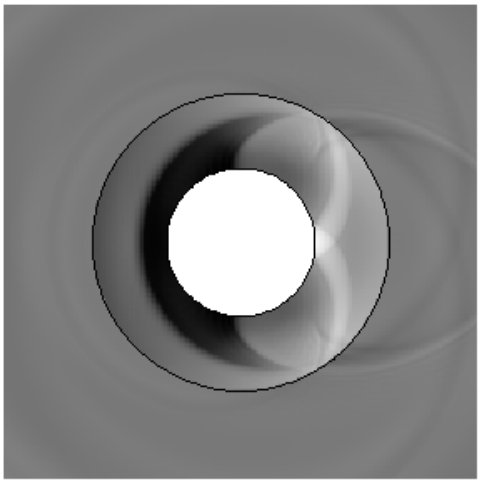

t=3.35 max= 1.60 min=- 0.70

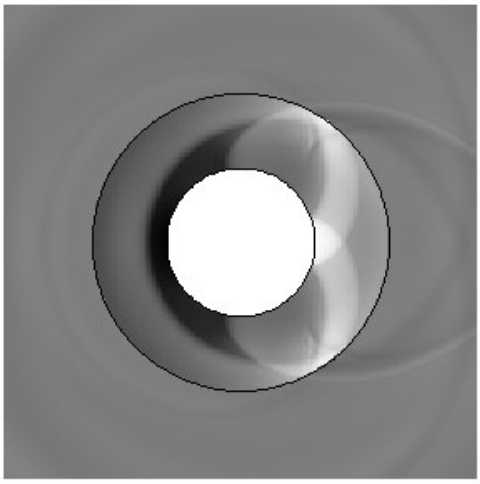

t=3.40 max= 1.23 min=- 0.86

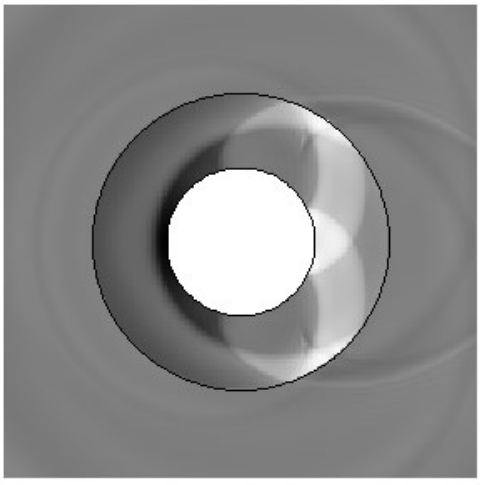

t=3.45 max= 1.07 min=- 1.02

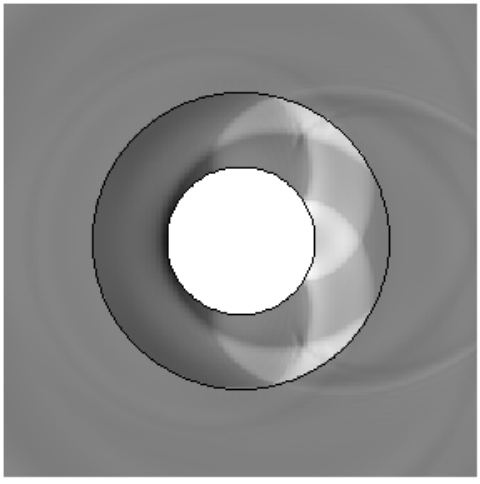

t=3.50 max= 1.07 min=- 1.35

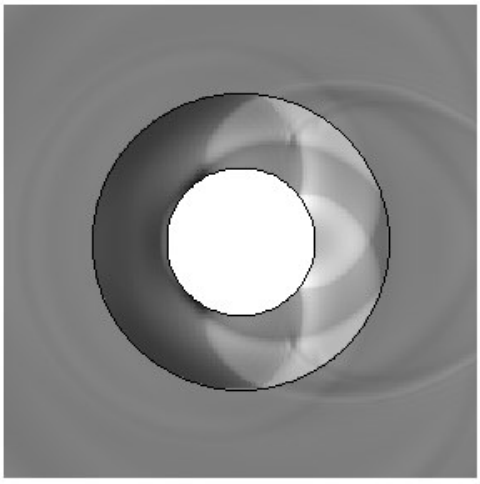

t=3.55 max= 1.09 min=- 0.92

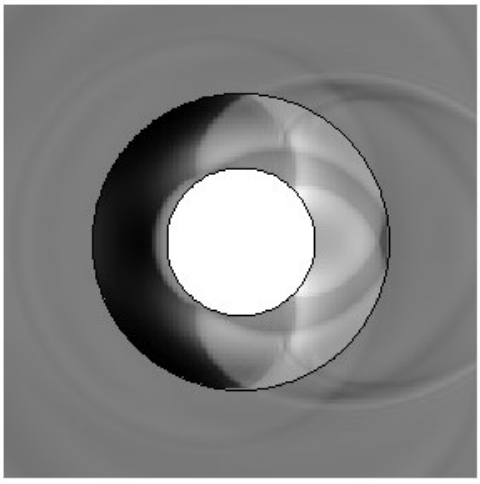

t=3.60 max= 1.19 min=- 0.54

Fig. 4.1 Continued

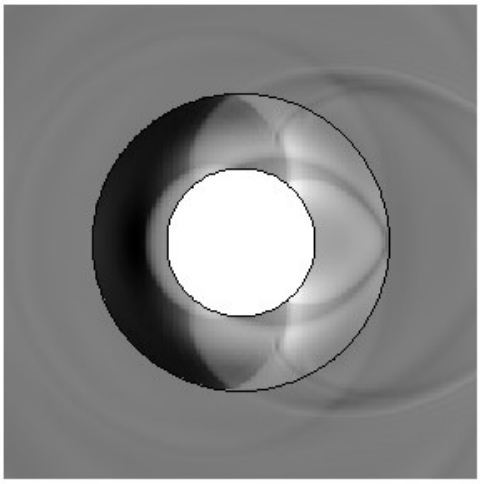

t=3.65 max= 1.22 min= -0.63

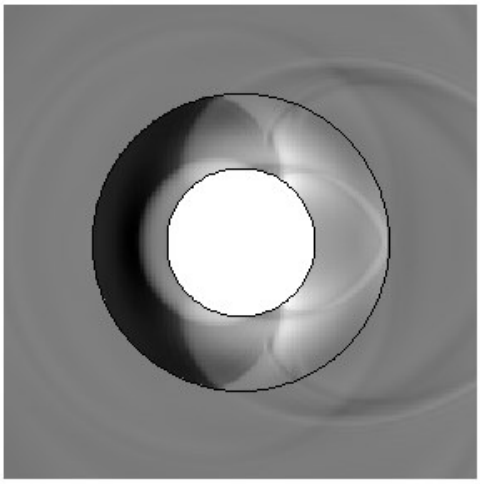

t=3.70 max= 1.22 min=- 0.69

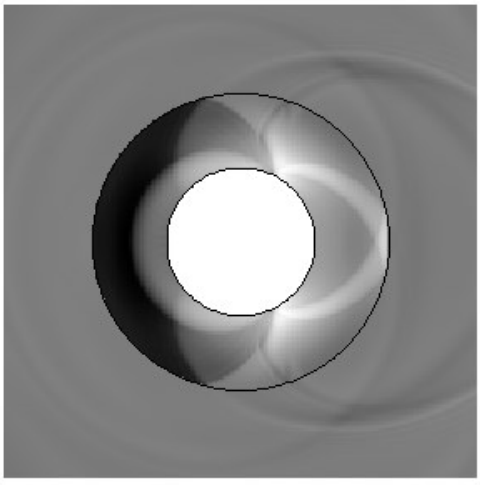

t=3.75 max= 1.18 min= -0.70

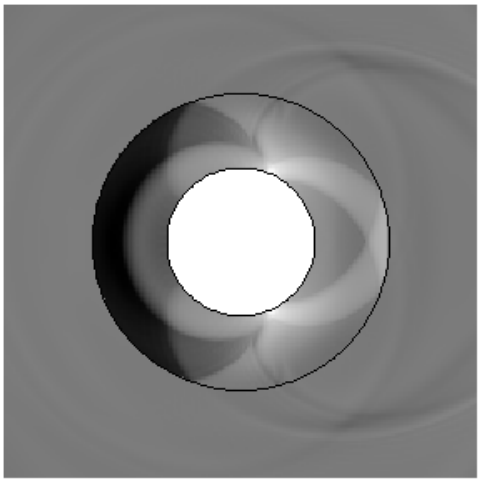

t=3.80 max= 1.74 min=- 0.71

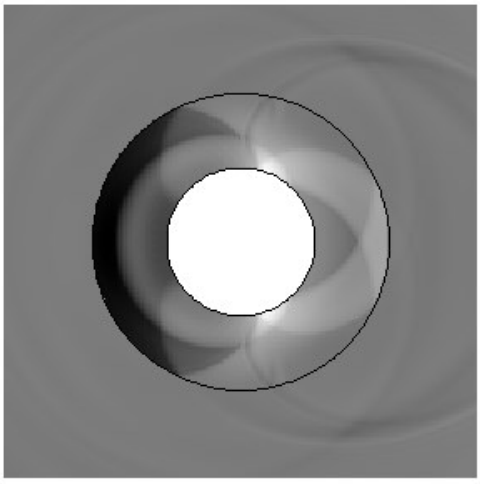

t=3.85 max= 1.76 min= -0.77

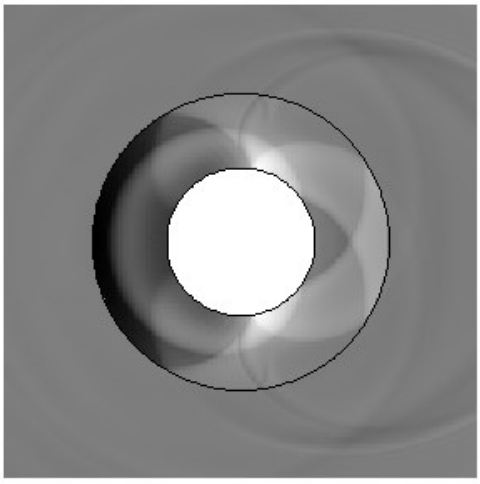

t=3.90 max= 1.36 min=- 0.84

Fig. 4.1 Continued

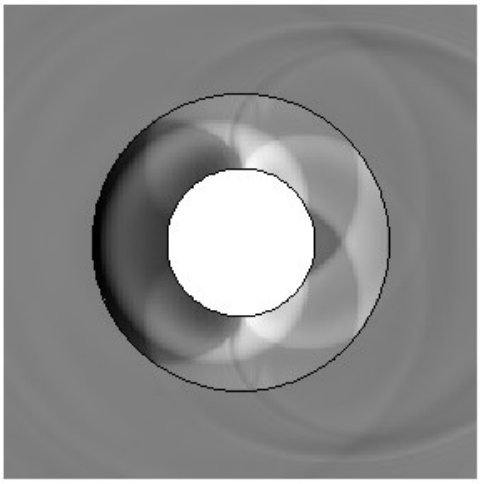

t=3.95 max= 1.01 min=- 0.92

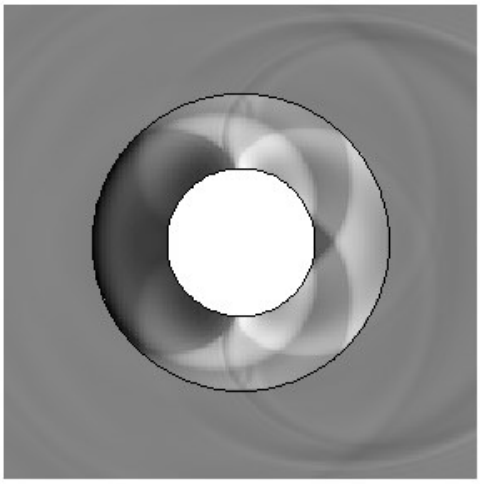

t=4.00 max= 0.78 min=- 0.93

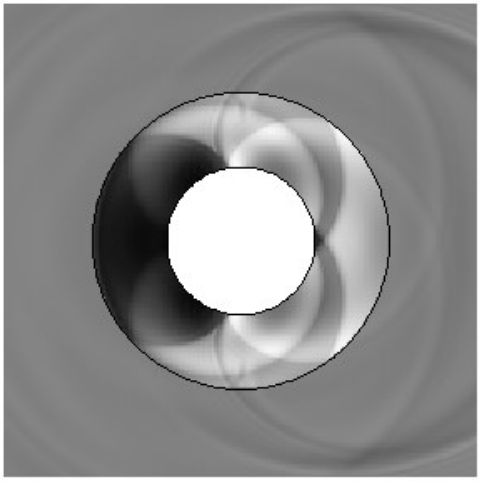

t=4.05 max= 0.60 min=- 0.62

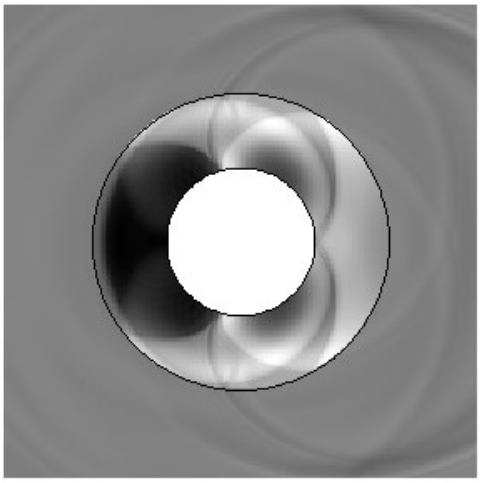

t=4.10 max= 0.61 min= -0.65

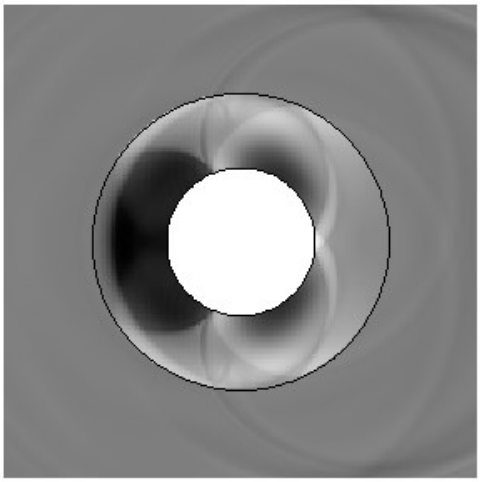

t=4.15 max= 1.02 min= -0.73

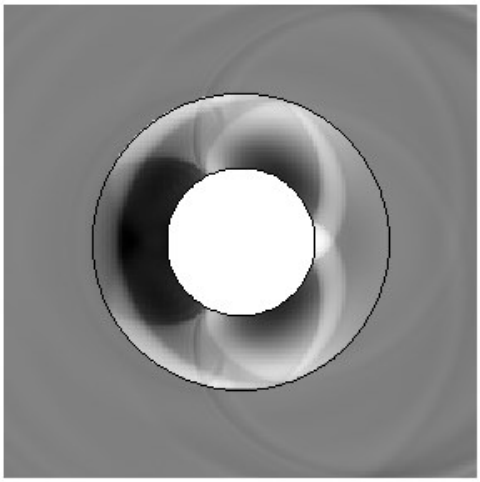

t=4.20 max= 0.85 min= -0.78

Fig. 4.1 Continued

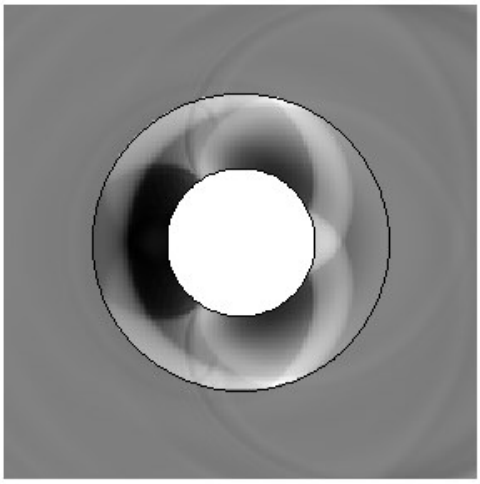

t=4.25 max= 0.98 min=- 0.75

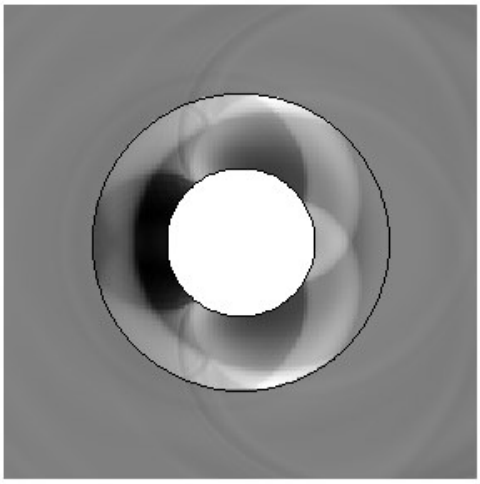

t=4.30 max= 0.94 min=- 0.80

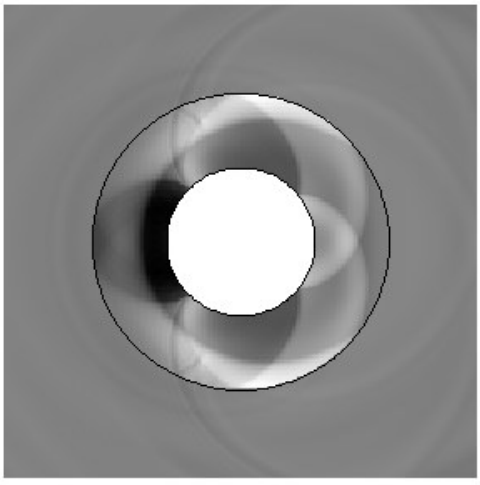

t=4.35 max= 0.73 min=- 0.85

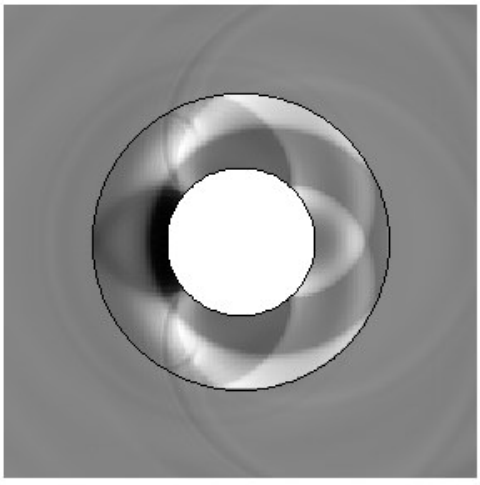

t=4.40 max= 0.56 min= -0.89

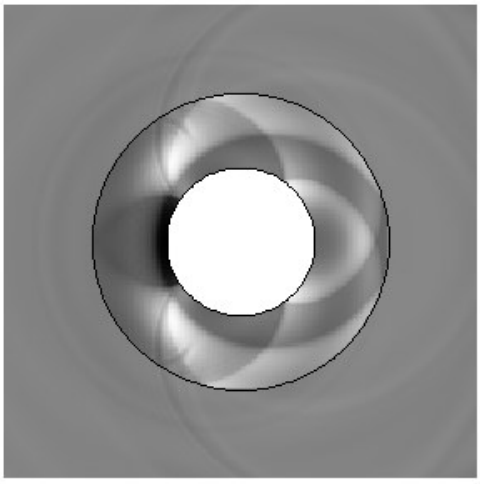

t=4.45 max= 0.60 min=- 0.94

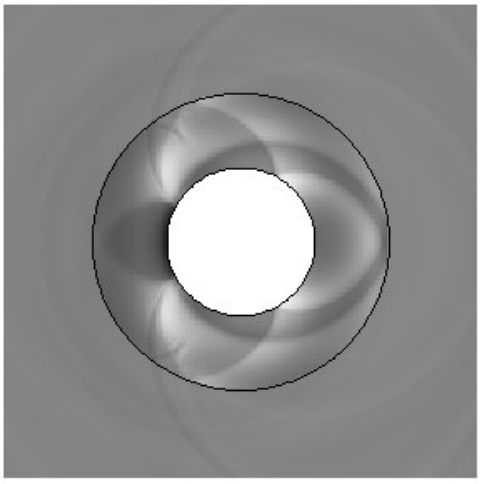

t=4.50 max= 0.69 min=- 1.20

Fig. 4.1 Continued

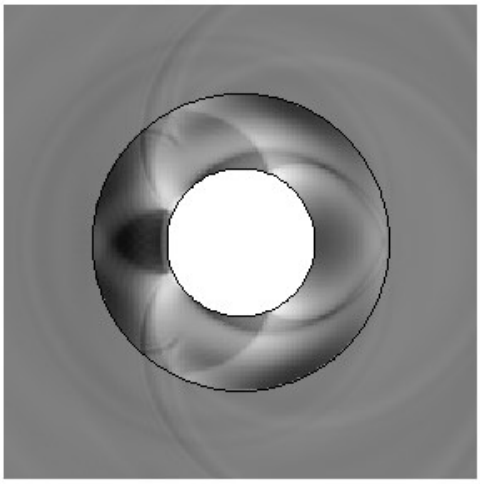

t=4.55 max= 0.75 min=- 0.49

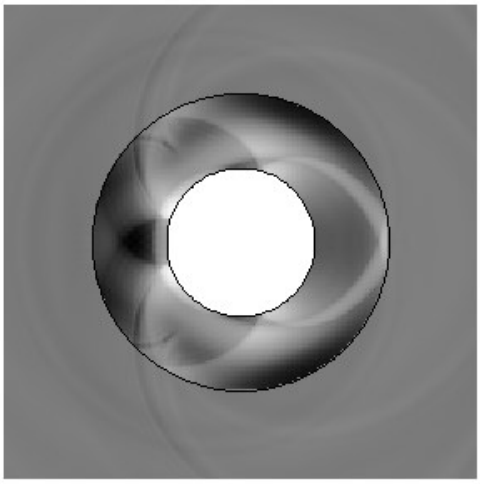

t=4.60 max= 1.05 min=- 0.47

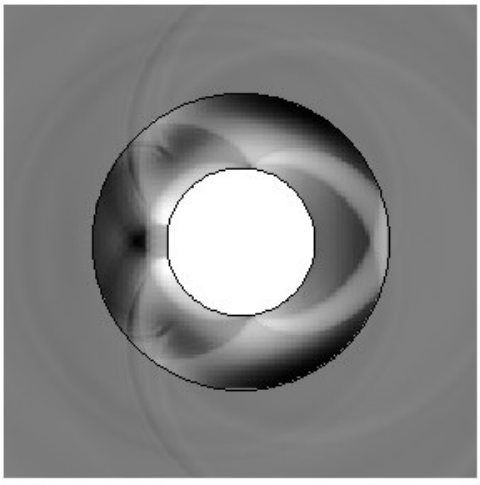

t=4.65 max= 1.06 min=- 0.46

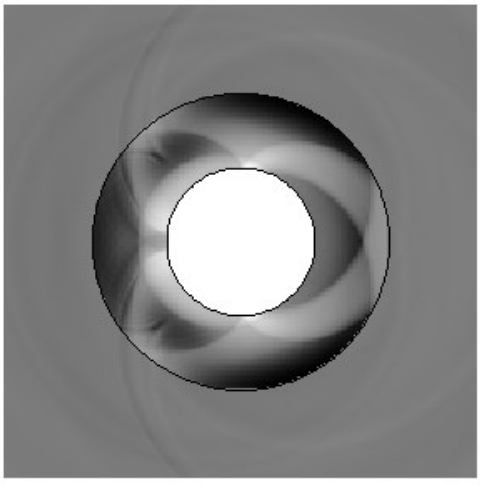

t=4.70 max= 1.22 min=- 0.47

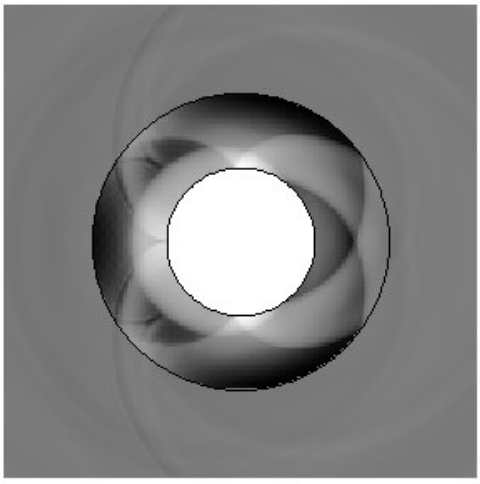

t=4.75 max= 1.19 min=- 0.43

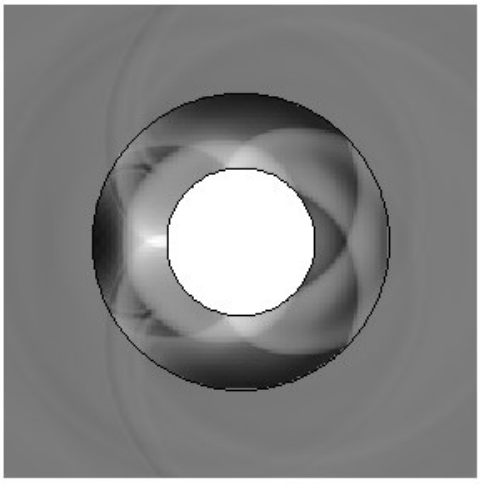

t=4.80 max= 1.34 min=- 0.46

Fig. 4.1 Continued

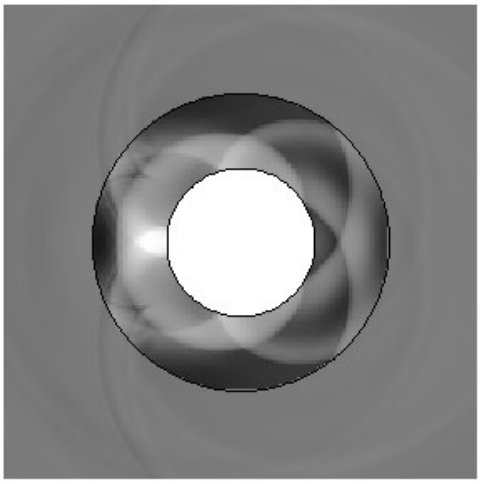

t=4.85 max= 1.17 min=- 0.44

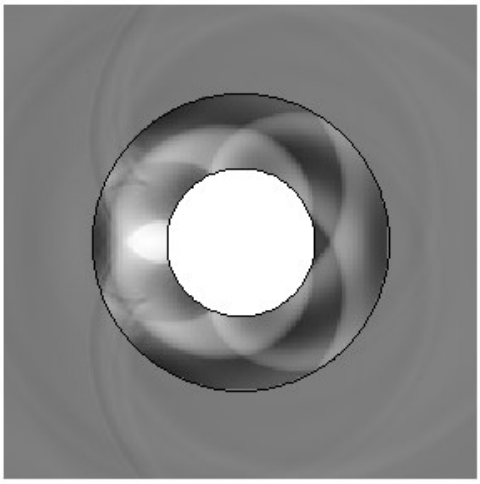

t=4.90 max= 0.94 min=- 0.55

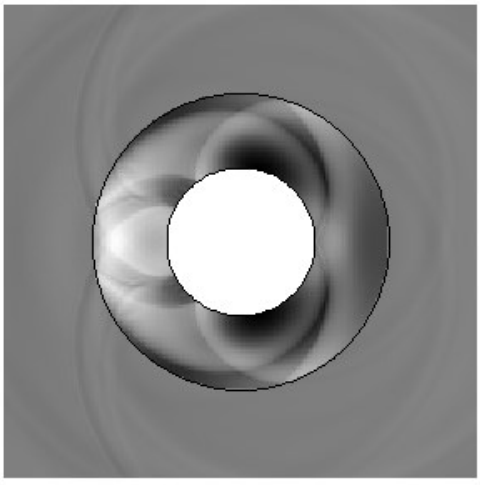

t=4.95 max= 0.77 min= -0.73

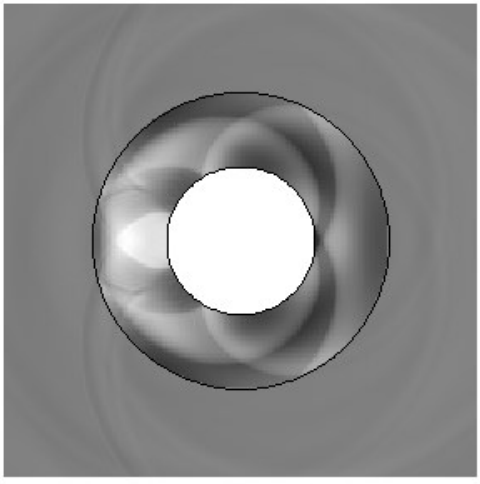

t=5.00 max= 0.76 min=- 0.54

Fig. 4.1 Continued

The most important features seen are the multiple reflections of the internal pressure wave originated in the very beginning of the interaction off the shell surfaces. Specifically, the reflections off the inside of the external shell as the wave travels upstream and its reflection off the outside of the internal shell as it travels downstream. Later, it will be seen that these reflections play an important role in the stress-strain states of both shells. Whenever this internal pressure wave reflects off the inner surface of the external shell, some energy is always lost to the external fluid domain, which is manifested by the appearance of a pressure wave leaving the system. The overall appearance of the

internal pressure field, as far as the first order effects are concerned, remain qualitatively similar to situations without an internal shell (Iakovlev, 2006 and 2007). It is when we consider the generation of second-order waves from the multitude of sources that the interaction becomes phenomenally more complex.

Concerning the second-order waves, the most important ones are those radiated into the inter-shell fluid by the stress waves propagating through both the external and internal shells (the single shell scenario was investigated in Iakovlev, 2006, 2007, and Iakovlev et al., 2013). With the importance of investigating these waves their graphical representation presents a complication of a technical nature. The magnitude of these are an order of magnitude less than that of the primary pressure waves resulting in very poor graphical representations of these second order wave properties. An efficient way to overcome these shortfalls, as demonstrated in Iakovlev 2009, and Iakovlev et al., 2013, is to “accentuate” certain components or consider close-ups of areas of focus. This is to ensure that these second-order, lower magnitude pressures, are not overshadowed by the larger magnitude pressure elsewhere. These measures do affect the overall realistic representation of the fields, but are worth it for a better representation of the specific areas of interest. Figure 4.2 shows two representative snapshots.

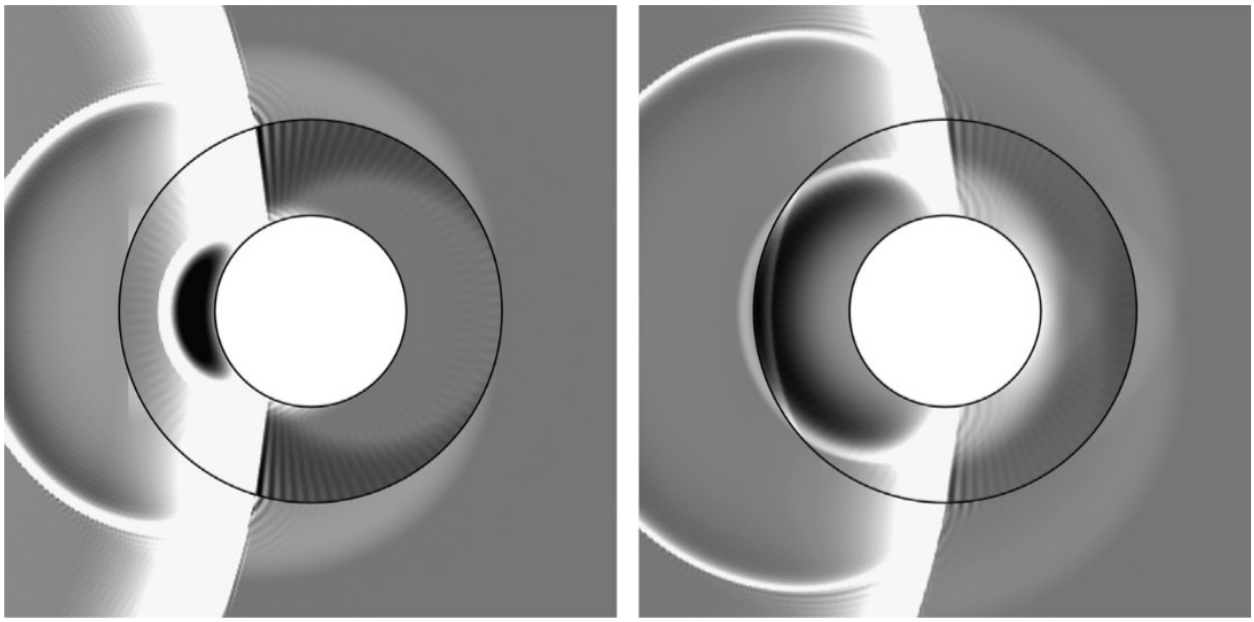

(a) (b)

Figure 4.2. Representative snapshots in which the developing shell-induced hydrodynamic components can be seen, two radiated by the outer shell into the inter-shell fluid and external fluid, (a), and the other radiated by the inner shell, creating one wave into the inter-shell fluid, (b).

As the interaction progresses, we can see that the hydrodynamic field becomes more complex due to the presence of the internal shell. The field resembles what was seen in Iakovlev *et al.,* 2010 with a rigid co-axial core but even more complex because of the second order waves radiated by the, now, non-rigid internal shell.

4.2 STRUCTURAL DYNAMICS

After discussing the hydrodynamic fields, we will now focus on the stress-strain states, the most important aspects of the analysis. Three different forms of visualization are used to highlight specific aspects of the stress-strain state. Such an approach has been shown in (Iakovlev, 2007) to be quite useful. First, time-history plots of the normal displacements are considered at the head and tail points, Figures 4.3 and 4.4, respectively. We can see from both graphs the time delay for the waves to reach the tail points of each shell, as well as the time delay for the shockwave to initially impact the interior shell. These time histories have a similar pattern to those seen for evacuated

shells (Iakovlev, 2008a, 2009; Iakovlev et al., 2013), but are now more complex due to the presence of multiple reflections of the pressure waves from both shells, a phenomenon discussed above. We see these affects in the outer shell displacements at the moments when the displacement is reduced slightly. One can visualize this, as the returning shockwave rebounding off the inner shell pushing the outer shall back towards its initial position when it returns to the head point of the outer shell. We can see similar affects in the inner shell with the second passage of the rebounding wave off the outer shell returning to the head point of the inner shell pushing further downstream.

Figure 4.5 shows the dynamics of the normal displacements in their 'natural' geometrical context, but significantly scaled up as the actual displacements are a small fraction of the thickness of the shell. One of the immediately apparent features is the simultaneous shift of both shells downstream, something that could be referred to as the 'rigid body' component of the motion. It is interesting to point out that the deviation of the distance between the shells from its initial value is always considerably lower than the maximum displacement of the shells themselves, which in turn are only a fraction of the thickness of the shells, an observation that is in agreement with the conclusion made by Huang (1979a) about the negligible loss of concentricity of the shells. It is of further interest that the external shell retains a convex external surface, although minimal, for the entirety of the interactions. Whereas, the internal shell develops a concave external surface at the head point beginning at t = 2.30, this could be due to the effects of the initial

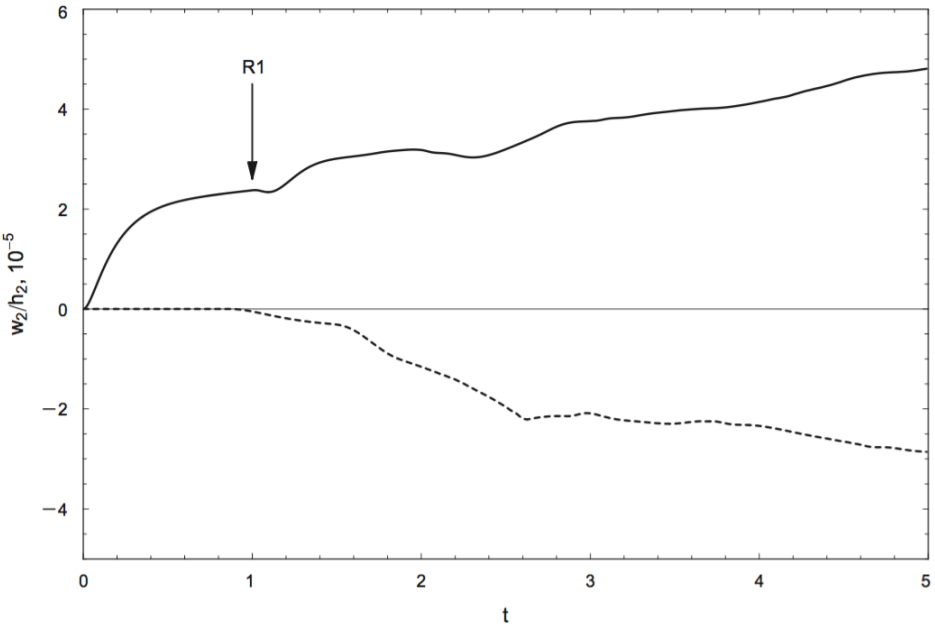

Figure 4.3. Normal displacement of outer shell where the solid and dashed lines represent the head and tail point respectively. 'R1' marks the arrival to the head point of the outer shell of the pressure wave reflected off the inner shell after its passage upstream.

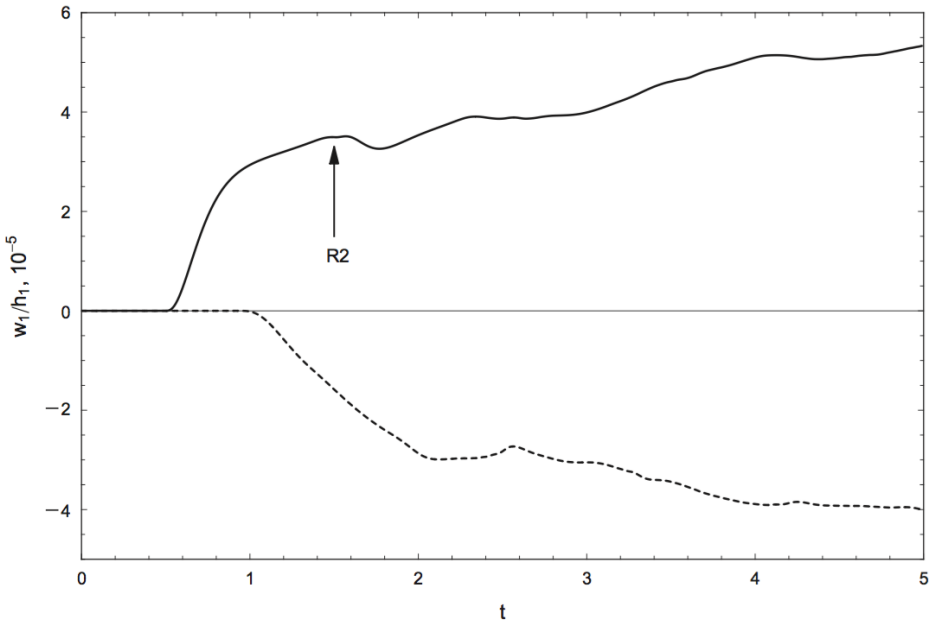

Figure 4.4. Normal displacement of inner shell where the solid and dashed lines represent the head and tail point respectively. 'R2' marks the arrival to the head point of the inner shell of the same wave after it completed its second passage downstream upon reflecting off the outer shell.

shockwave impacting the head point of the internal shell. This could be further amplified from the fact that the internal shell is evacuated and therefore there would be no fluid to reduce this deformation or allow a returning shockwave inside the internal shell to reduce this deformation.

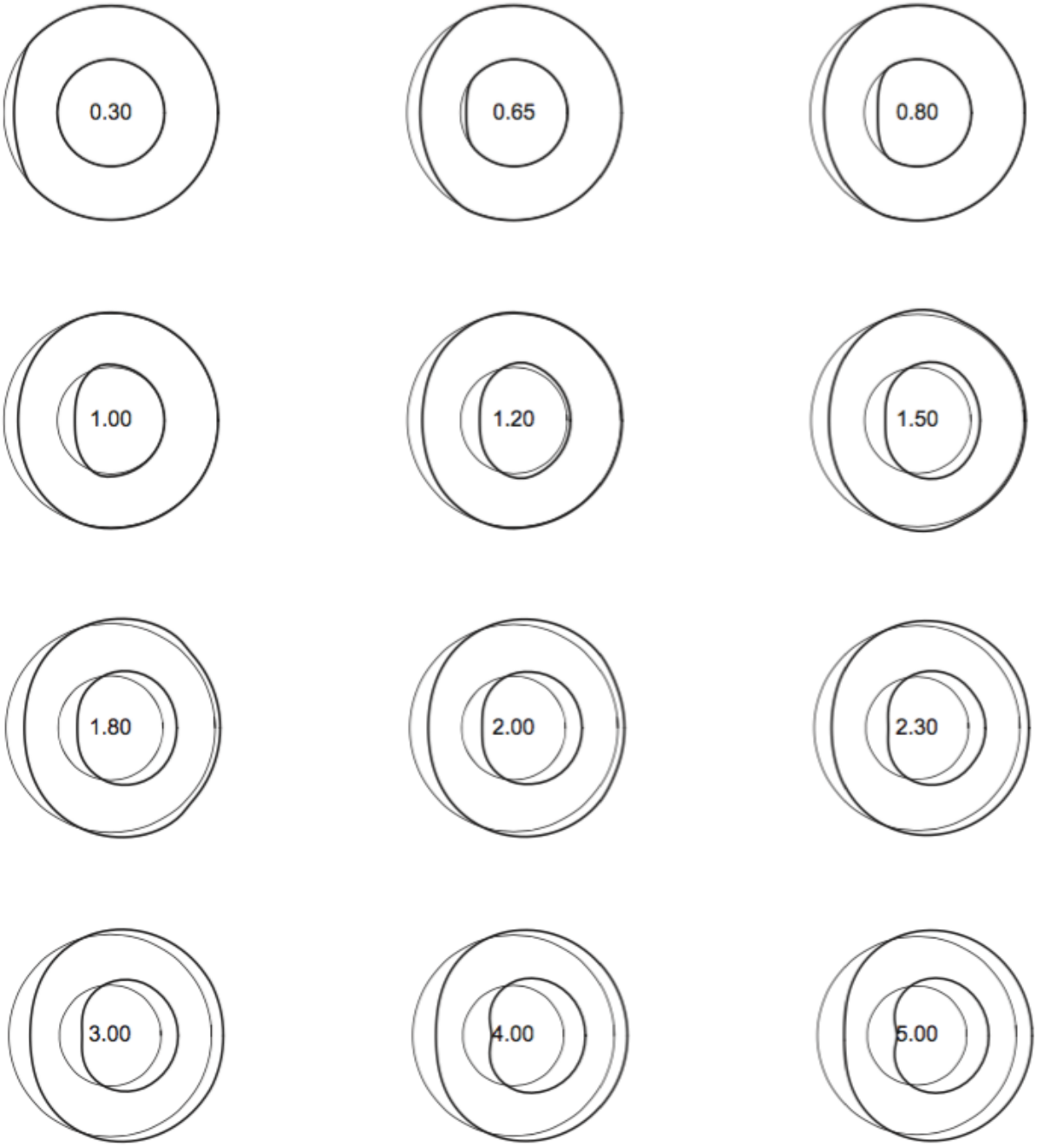

Figure 4.5. Dynamics of the normal displacements in their 'natural' geometrical context relative to the initial positions of the shells.

The most interesting analysis are the time history plots representing the stress in both shells. Figures 4.6 and 4.7 represent the inner shell and outer shell respectively. Two immediate differences seen between the two shells are that there is a much higher frequency of the stress waves propagating in the inner shell, and a much more pronounced tensile stress seen in the outer shell. The former is a purely geometrical effect due to a smaller radius of the inner shell. The latter is due to the fact that the present system combines two 'ends of the spectrum' in that the outer shell behaves more like a submerged fluid-filled shell as seen in Iakovlev 2006, a system for which the tensile stress was found to play a very significant role and the inner shell behaves more like a submerged evacuated shell as seen in Iakovlev 2008a, where the peak tensile stress was found to be much lower than the peak compressive stress, an effect observed and discussed in Iakovlev et al. 2015.

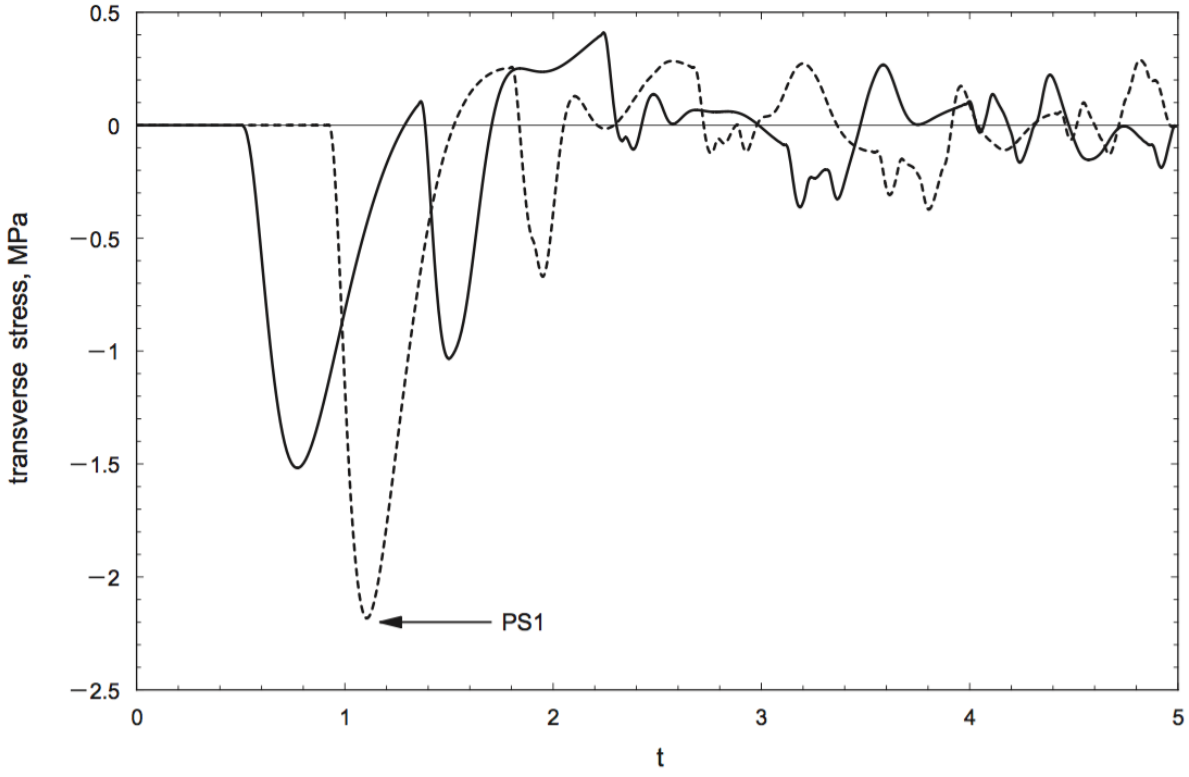

Figure 4.6. Transverse stress in inner shell where solid and dashed lines represent the head and tail points respectively. "PS1" is the superposition at the tail point of the shell.

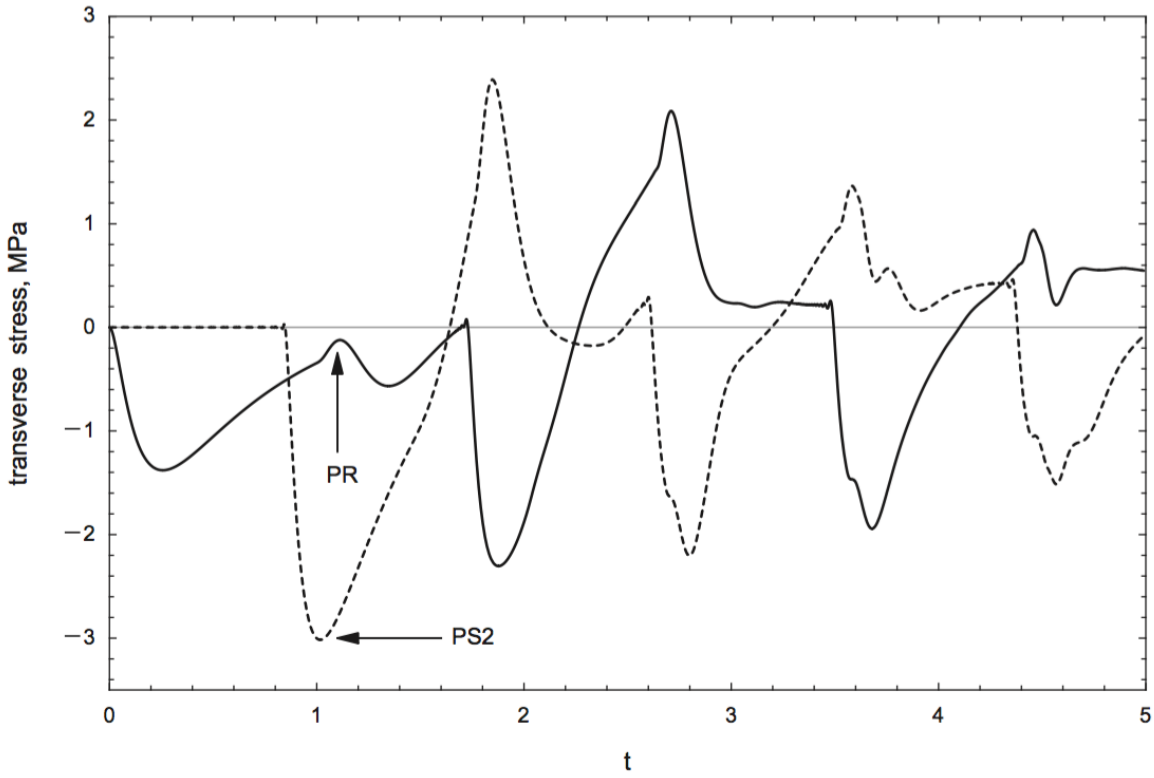

Figure 4.7. Transverse stresses of outer shell where solid and dashed lines represent the head and tail points respectively. "PS2" is the superposition at the tail point of the shell and "PR" is the impact on the outer shell from the returning pressure wave that rebounded off the inner shell.

There are many interesting features in both graphs; the wave repetition feature is the most apparent, especially in the outer shell where there is an obvious repetition of a waveform that is decreasing in amplitude at both the head and tail points. The minor differences at each waveform repetition is due to the effect of the hydrodynamic waves generated from the internal shell. As for the inner shell, the greater frequency of repetition has already been explained, and at approximately t=2.3 the appearance of repetition has disappeared, this is due primarily to the waves induced by the multiple hydrodynamic waves travelling in the inter-shell space, with the resulting wave pattern becoming increasingly complex as the interaction progresses.

Focusing on the head and tail points of the shells does not allow for a total analysis of the overall structural dynamics of the entire shells. To overcome this issue, a series of two-dimensional images representing the magnitude of the stresses experienced throughout both shells are provided in figure 4.8. The appearance is similar to the normal

displacement images but representing the compressive and tensile stress in the shells instead. The values are scaled for visual benefits with compressive stresses being represented as external to the shell and tensile stress as internal. Although, quantitatively, such plots are not very helpful when it comes to stress analysis, all the effects discussed earlier are particularly easy to see. Examples include the onset of the stress wave at t = 0.50 in the inner shell caused by the impact of the pressure wave on its first passage downstream, the similarity of the stress propagation in the inner and outer shells right after the initial impact, continued with the constructive superposition of the stress waves as they circumnavigate the shells, and the tensile stress caused by the wave effects in the inter-shell fluid, as mentioned in Iakovlev et al, 2015.

Figures 4.9 and 4.10 show time-space plots of the stress for the inner and outer shells respectively. The lower border corresponds to the head point of the shell and the upper border corresponds to the tail point, this technically only represents half the shell, but due to the symmetry, this is sufficient. The waves propagating with constant velocities appear in such plots as straight lines, and the halftones are scaled as to allow the most optimal appearance of both primary and secondary features of the respective stress fields.

One immediately apparent feature is the much higher frequency of the stress waves seen for the inner shell, an effect that we have already discussed. In all other respects, the plot for the inner shell qualitatively very much resembles that seen for a submerged evacuated shell but at a higher frequency. The secondary, much lower in magnitude, waves are also seen, all being the effects of the multiple reflections of the internal pressure wave travelling in the inter-shell space.

The outer shell is considerably different. At t = 1, a tensile stress wave is originated at the head point due to the direct impact of the upstream-propagating internal pressure wave after it reflects off the inner shell at t = 0.50. This stress wave then circumnavigates the shell and superimposes at the tail point shortly before t = 2, leading to the highest tensile stress in the system that is of the same order of magnitude as the highest compressive stress. It then circumnavigates the shell again and superimposes at the head point, leading to another tensile peak there. The presence of such a high-magnitude tensile stress constitutes the fundamental difference between the outer and inner shells,

and allows us to make an argument about the influence of the outer shell on the structural dynamics of the inner one being much less pronounced than vice versa.

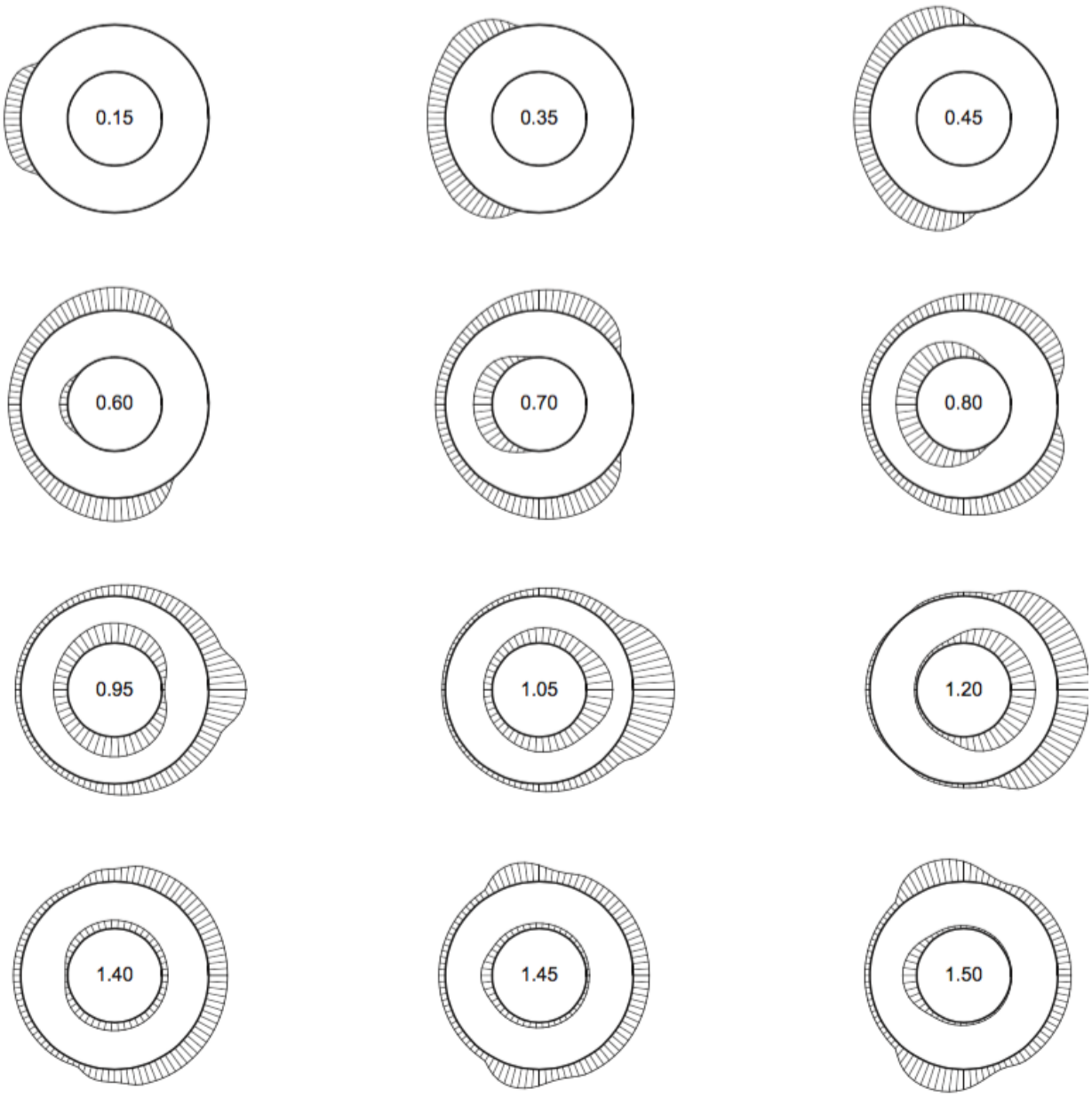

Figure 4.8. Series of two-dimensional images representing the stresses in the system.

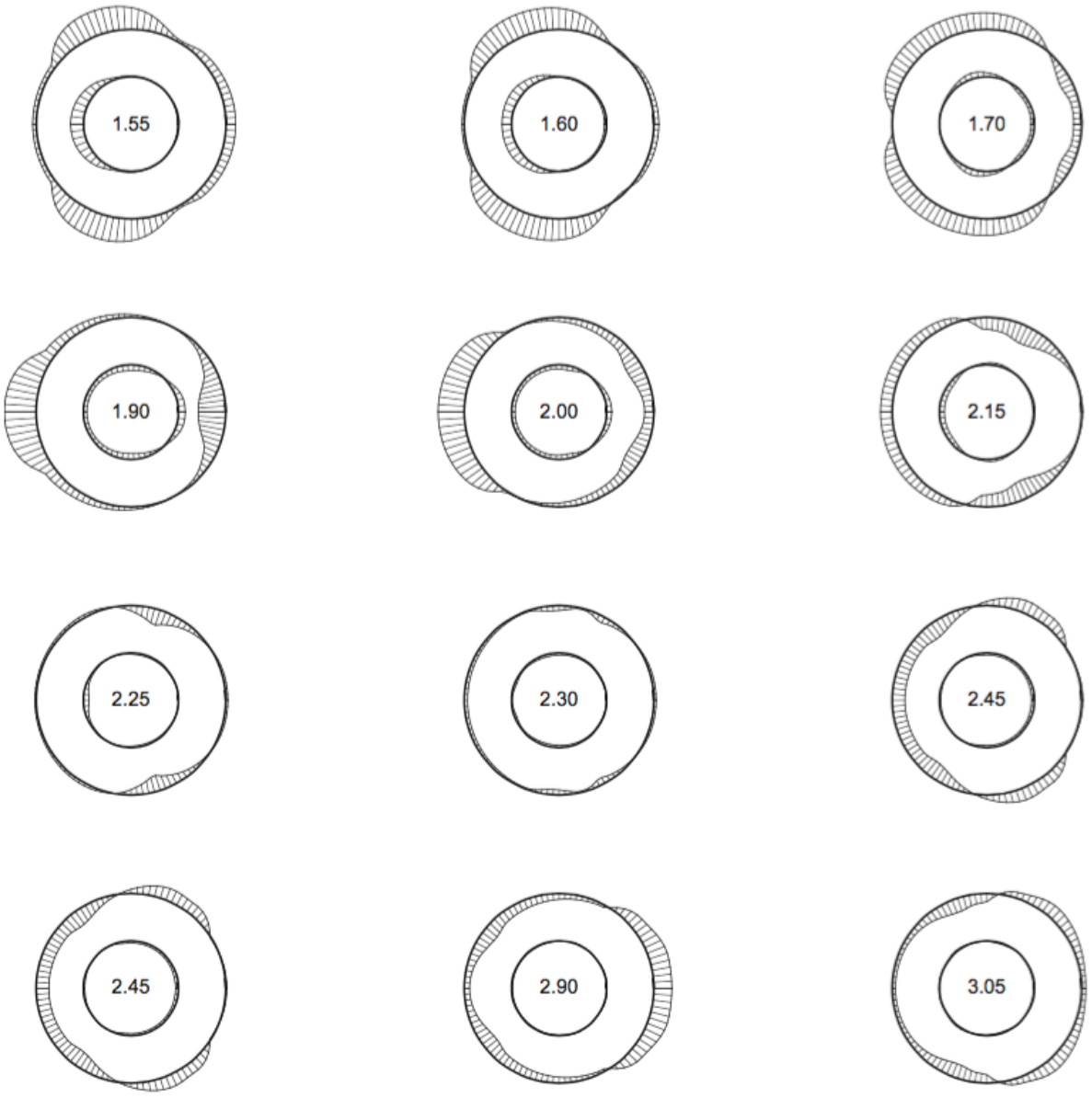

Figure 4.8. Continued.

Figure 4.8. Continued.

So far, we have considered both the fluid and structural dynamics of the interaction and simulated the hydrodynamic fields induced in the system during the considered shock loading. We have addressed the structural dynamics with the normal displacements of the shell and the stress state using three visualization techniques: the classical time-histories, the 'realistic geometry' snapshots, and the time-space plots that allow for a simultaneous analysis of all stages of the interaction. However, if one wanted to consider the structural integrity of a system the most important information would be to know when, where and to what magnitude the peak stress occurs in both shells. It is believed that this point is where the system is going to experience the greatest risk to structural integrity but it must be located within the results. The code used to run these models also includes a step to calculate and consider such results. Furthermore, not only can it provide this information for a given set of parameters, but

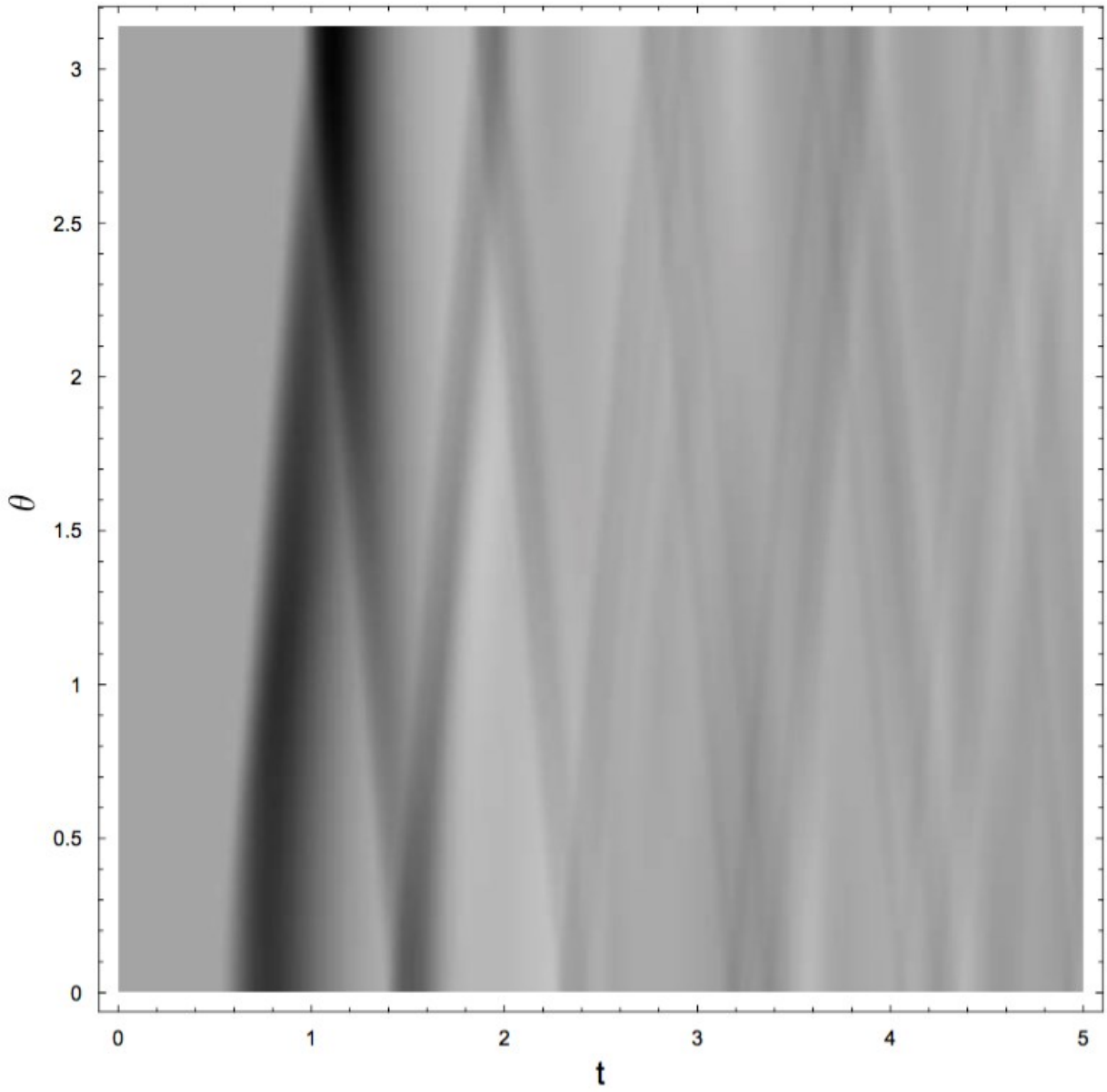

Figure 4.9. Time-space plot of the transverse stress in the inner shell.

also, the code has been designed to accommodate the variation in whatever parameters involved in the system are of interest. The following chapter will now focus on the parametric study carried out in order to determine the overall peak stress and pressure in the system, as well as their locations. The motivation for developing such a code was to facilitate the extensive parametric studies that are carried out at the pre-design stage and are aimed at the structural optimization of industrial systems, a task that appears to be becoming increasingly important today.

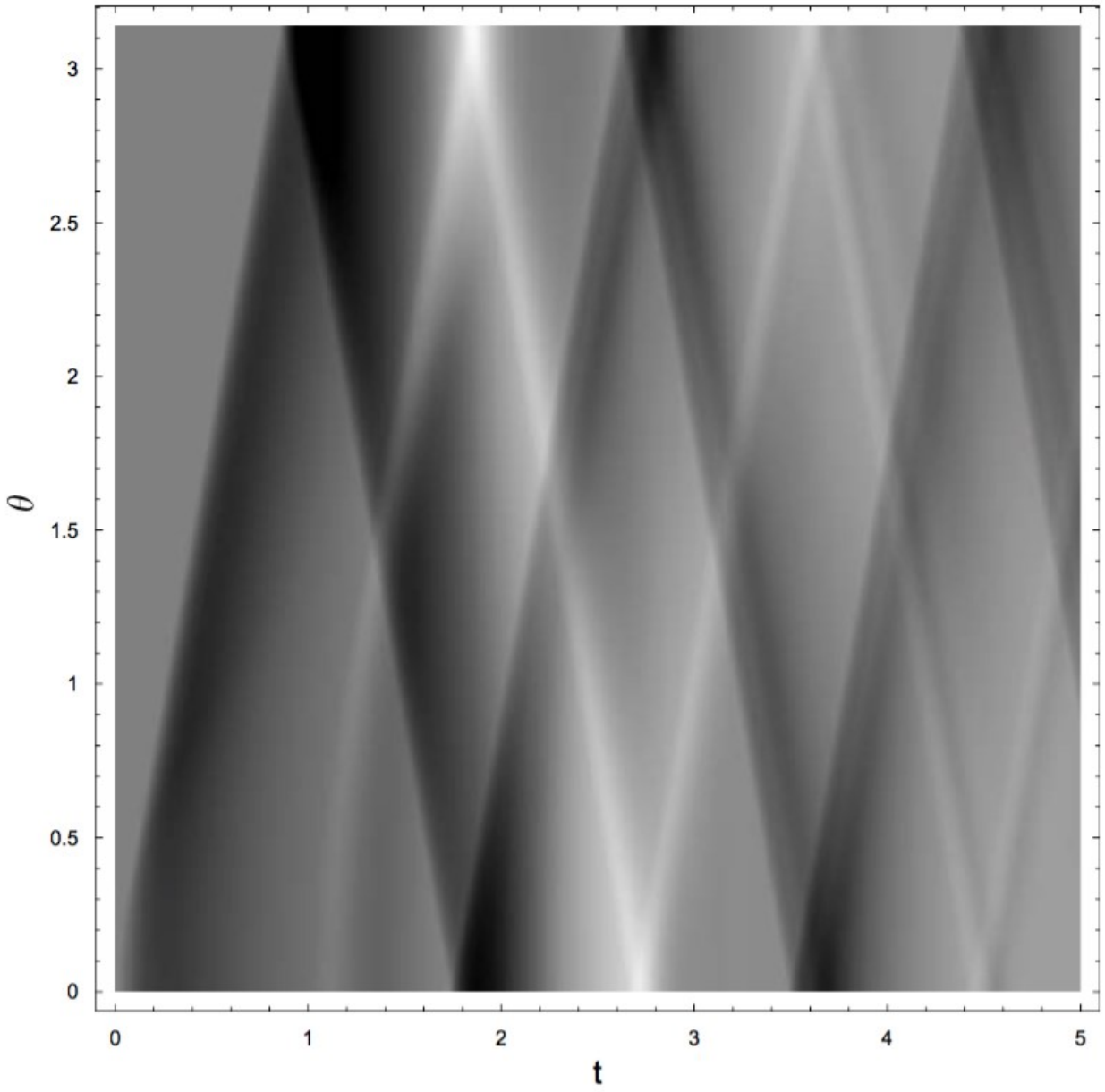

Figure 4.10. Time-space plot of the transverse stress in the outer shell.

CHAPTER 5: PARAMETRIC STUDY

5.1 PARAMETERS

The previous chapter demonstrated a qualitative and quantitative analysis of one specific scenario with a given set of parameters. This chapter will now provide a detailed comparison of a range of values for several parameters of interest, most notably being shell thicknesses, the ratio of the shell radii, the physical properties of the shell materials, and the physical properties of the inter-shell fluid. The code for the study has the user pre-set the physical properties of the fluid and shells' materials as well as the ratio of the shell radii and the range of shell thicknesses that are of interest. After everything has been completed, the code returns a three dimensional plot of the maximum stress experienced in each shell, the total normal displacement of each shell, as well as the maximum positive and negative pressures experienced on the surface of each shell for every set of shell thicknesses of interest. Additionally, the code provides the timing and location for all the previously mentioned results, excluding the total normal displacement, which is cumulative for the entire interaction. Each graph provides the value of interest along the Z-axis, the thickness of the inner shell along the X-axis, and the thickness of the outer shell along the Y-axis For this study Table 5.1 summarizes the parameters and their values that were considered and Table 5.2 details the physical properties of the necessary parameters.

Table 1. Summary of parameters considered in the study.

Parameters	Description of values	Values	Total Variables
Inner shell thickness, h_1	Percentage of the radius of the inner shell	0.2-1.0%, increasing in 0.1% intervals	9
Outer shell thickness, h_2	Percentage of the thickness of the inner shell	10-100%, increasing in 10% increments	10
Radius of inner shell	Ratio of inner shell to outer shell radii	0.5 and 0.9	2
Interhull fluid	Fluid between the inner and outer shells, properties determined by fluid of interest	Diesel Fuel Or Seawater	2
Outer shell material	Values are dependent on material properties	Composite Material Or Steel	2

Table 2. Physical Properties of Parameters

Substance	Density, kg/m^3	Acoustic Speed, m/s	Poisson Ratio
Steel	7800	5000	0.3
Composite	1800	3430	0.15
Water	1000	1400	-
Diesel Fuel	880	1250	-

One can easily appreciate the amount of data that would be produced once all of the various scenarios were considered. With just a small selection of 5 variables and predetermined ranges we have already created 720 unique scenarios and possible designs for the considered problem, with the potential for a much larger amount of possibilities.

5.2 STEEL INNER/STEEL OUTER/INTER-HULL WATER/RADIUS 50%

To introduce the parametric study, we will consider the initial case that was discussed in chapter 4 with varying inner and outer shell thicknesses, and then expand the parameters to the other values of interest after discussing some results in this initial consideration. We consider the interior shell with radius a = 0.50m and exterior shell with a radius of r_o = 1.00m, both made of steel c_1 = c_2 = 5000 kg/m^3, ρ_1 = ρ_2 = 7800 kg/m^3, and ν_1 = ν_2 = 0.3, submerged in water, c_e = 1400 m/s and ρ_e = 1000 kg/m^3, and with water filling the inter-shell space, c_i = 1400 m/s and ρ_i = 1000 kg/m^3. This loading is different from that discussed in chapter 4.

For a complete detailed consideration of all aspects of interest the following values are reported: The value, timing and location of the maximum stress in both the inner and outer shells (Figures 5.1, 5.2, 5.3 and figures 5.4, 5.5, and 5.6, respectively); the normal displacements of the inner and outer shells (Figures 5.7 and 5.8, respectively); value, timing and location of maximum pressure experienced on the surface of both the inner and outer shell surfaces (Figures 5.9, 5.10, 5.11 and figures 5.12, 5.13, and 5.14, respectively); and value, timing and location of the minimum pressure experienced on the surface of both the inner and outer shells (Figures 5.15, 5.16, 5.17 and figures 5.18, 5.19, and 5.20, respectively). The plots are arranged so the x-axis, y-axis and z-axis are the inner shell thickness, outer shell thickness and value of interest, respectively.

Concerning the maximum stresses in each shell, an important conclusion that can be drawn is how the changes in one shell affects the state of the other. The maximum stress in the inner shell is dramatically changed and influenced by the thickness of the inner shell itself, with maximum stresses at the thickest values being about half those experienced when the internal shell is thinnest, another way to see this is a 5 times increase in the internal shell thickness appears to have approximately a 50% decrease in the peak stress. The same cannot be said for the outer shell's thickness and how it influences the stress in the inner shell. We can see that as the outer shell increases in thickness, there is a very unsubstantial decrease in the stress in the inner shell. Similar to comparison of the inner shell thickness, a 10 times increase of thickness in the outer shell provides less than a 10% reduction in the peak internal shell stress.

The scenario is not the same when considering the stress in the outer shell: once again, the thickness of the shell itself does influence the peak stresses, but we can see that the thickness of the inner shell has a far greater influence on the stress of the outer shell than vice versa. This would be something that should be taken into consideration if the main purpose of the outer shell is to protect the integrity of the inner shell. As for the timing and location of peak stresses, it is apparent that they occur at either the tail point or the head point, as seen in the plots of location. An interesting feature is that the peak stress occurs at the head point later in the interaction than when it occurs at the tail point. An explanation for both the location and timing issues is that the peak stresses occur when the stress waves travelling around both sides of the shell superpose. The true first superposition at the head point does not actually occur until the stresses have completely circumnavigated the entire shell and returned to superpose at the head point. When this occurs, it does appear that the maximum values at both the head and tail points are similar in value and both points may be of interest during investigations later on in the development process.

With regards to the displacements, it is not surprising that the thinner shell had greater displacements, though still comparably minimal. We can also note that the inner shell displaces slightly more than the outer shell, this is believed to be due in part to the fact that the initial impact at the head point of the external shell maintains the concentricity of the system and displaces both the external and internal shell simultaneously, but once the shockwave enters the inter-hull space, it displaces the internal shell only. In summary, regarding the displacement, it appears that the inner shell is affected to a greater extent than the outer shell.

Having discussed the structural features, we will now turn our attentions back to the hydrodynamic pressure and its peak values at the surfaces of both the outer and inner shells. For the maximum values, it appears that the peak pressure experienced on both surfaces are more or less similar, this is not unexpected seeing as the pressure field is continuous and the pressure at one side of the inter-hull space will eventually reach the other side with very little loss in pressure resulting in similar values at both shells. Regarding the location of these pressures, it is of interest to note that the maximum values do not occur at the head or tail points in the shell. Instead, they occur at a specific “region”

somewhere along the surface of each shell. For the inner shell, the maximum pressures occur towards the head point of the shell whereas they occur towards the tail point for the outer shell. The fact the peak pressures occur at slightly different locations as the shell thicknesses change is expected, since the slight change in shell thickness will slightly advance or delay the propagation of the hydrodynamic fields causing a slight “shift” in location. What is fascinating, with regards to the maximum pressures, is how the outer shell now appears to have a much greater influence on the maximum pressures experienced by both shells. This is opposite of what was seen for the stresses occurring in each shell and should be taken into account when considering reducing the possibilities of large pressures in a double-hull system.

Finally, we turn our attention to the minimum pressure experienced at the surfaces of both shells. In terms of the minimum values, the minimum negative pressures only amount to approximately 20% of the peak positive pressures suggesting that protecting against peak positive pressures may be more of an importance. With regards to the inner shell, there does appear to be some influence of both shells on the minimum pressure. As both shells become thicker, there is a noticeable increase in the negative pressures, with the greater values also occurring at the tail point of the shell. The timing of the pressure is similar with most cases occurring in a similar region along the shell surfaces. This is another example of the “shift” created by the slight variations in the thicknesses of the shells. Turning our attention to the outer shell, the first thing we notice is that there is very little change in these minimum values. However, in terms of magnitude they all are close to the minimum value as the few minimum value cases seen on the inner shell. Another note of interest is that there are two distinct locations at where these minimum values occur. One being the head point of the shell, and the other being at a specific point towards the tail point. The timing of these values follow the exact same pattern, with all values at the head point occurring at the same time for each scenario, and likewise for when the minimum value is closer to the tail point.

Regarding sudden “shifts” in where and when maximum and minimum values occur, due to the complexity of the entire system, for purposeful conclusions we are only looking for moments of specific interest. These are the moments in time during the interaction where there is the most potential for harm. Throughout the entire system,

every point's value is in a constant state of change. Even though we locate one specific point of interest that does change for each scenario, every other point in our system is still experiencing constant changes in value as well. These values are all determined by the "sum" of every wave that is generated in the system and their specific values at each point in the system at each point in time. Due to the complexity of the system, there are multiple waves propagating constantly creating new waves, further adding to complications. Gradual changes in parameters cause gradual decreases and simultaneous increases at each point in time for every point in the system, so a sudden shift in location and time is indicative of when a new region has achieved the right superposition of waves to create the new maximum value. In some cases, there is no "shift" and the area of interest remains almost identical, with slight shifts accounted for by the slight change in the thickness parameters but at least for our current conditions there only appears to be two points where we see our maximum/minimum pressures. One final note regarding the timing of the peak pressure occurrences, it appears that the maximum pressures are occurring closer to the beginning of the system interaction whereas the minimum negative pressures seem to occur much later during the interaction.

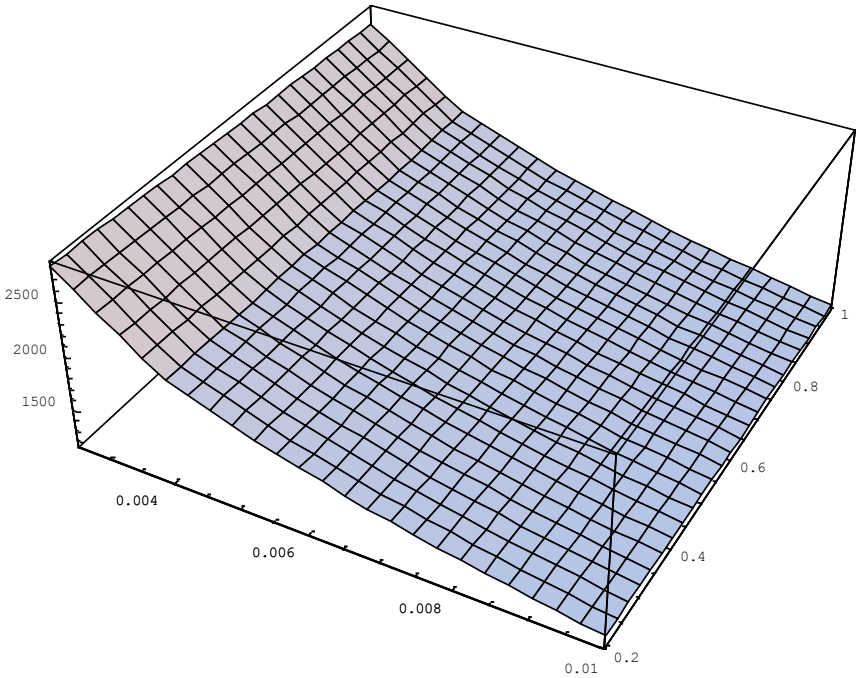

Figure 5.1. Maximum stress in inner shell (MPa).

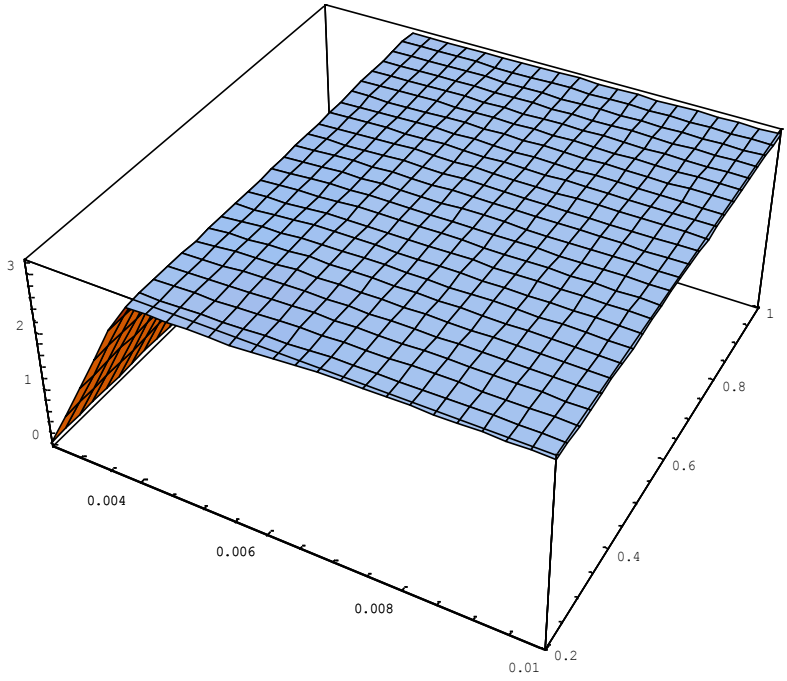

Figure 5.2. Location of maximum stress in inner shell (radians).

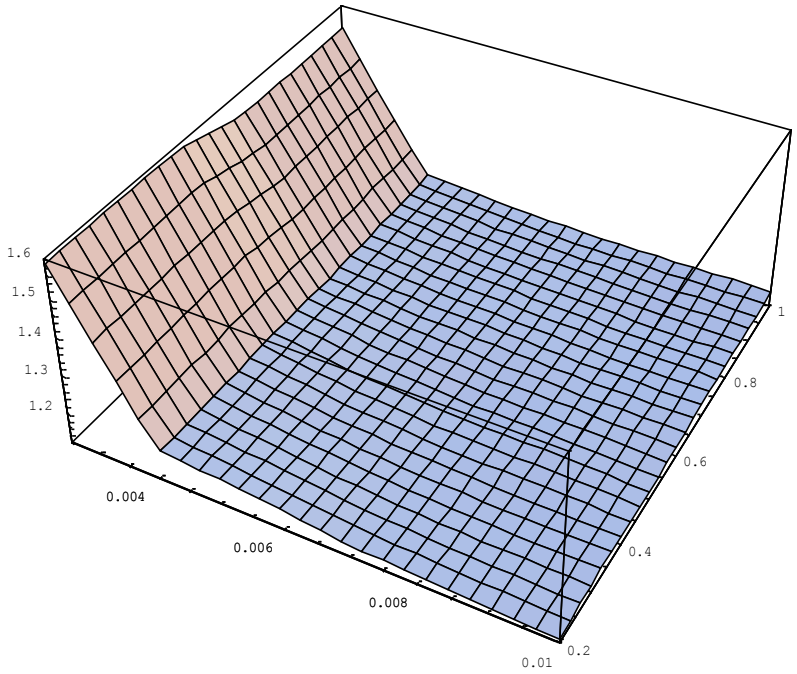

Figure 5.3. Timing of maximum stress in inner shell (dimensionless time).

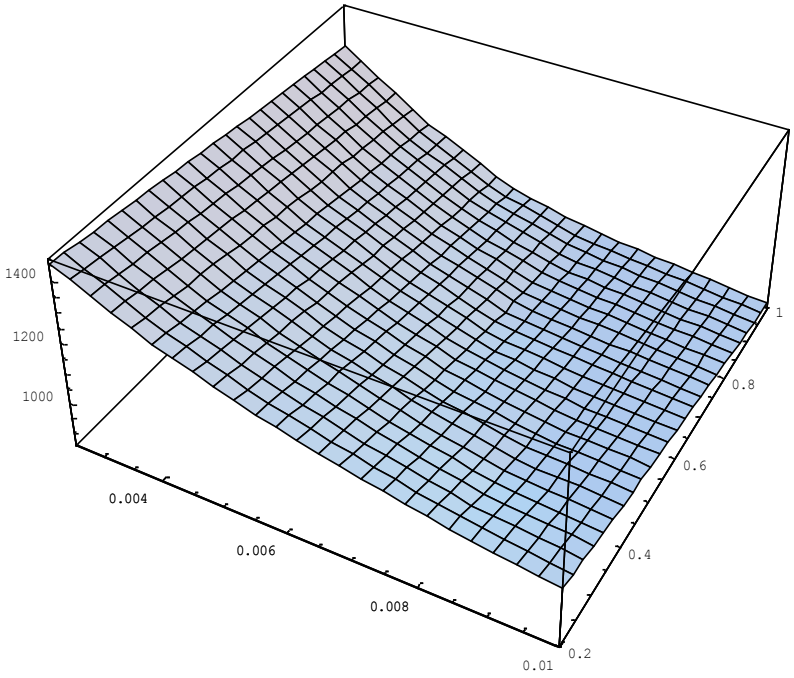

Figure 5.4. Maximum stress in outer shell (MPa).

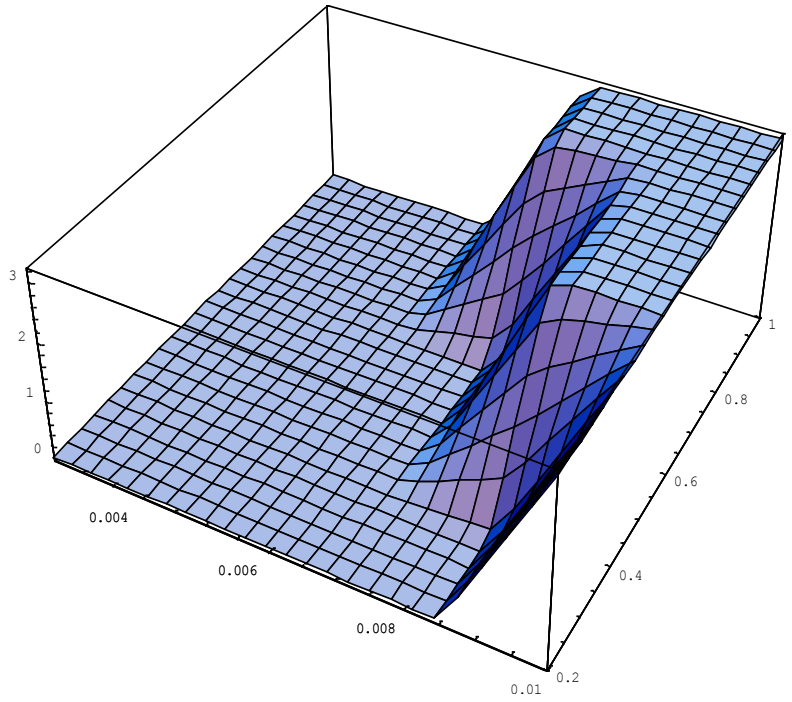

Figure 5.5. Location of maximum stress in outer shell (radians).

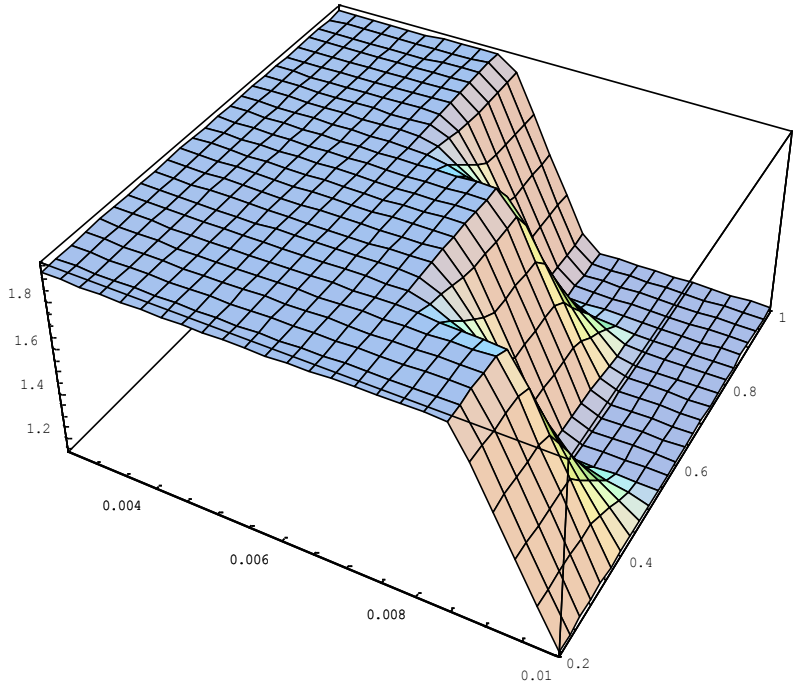

Figure 5.6. Timing of maximum stress in outer shell (dimensionless time).

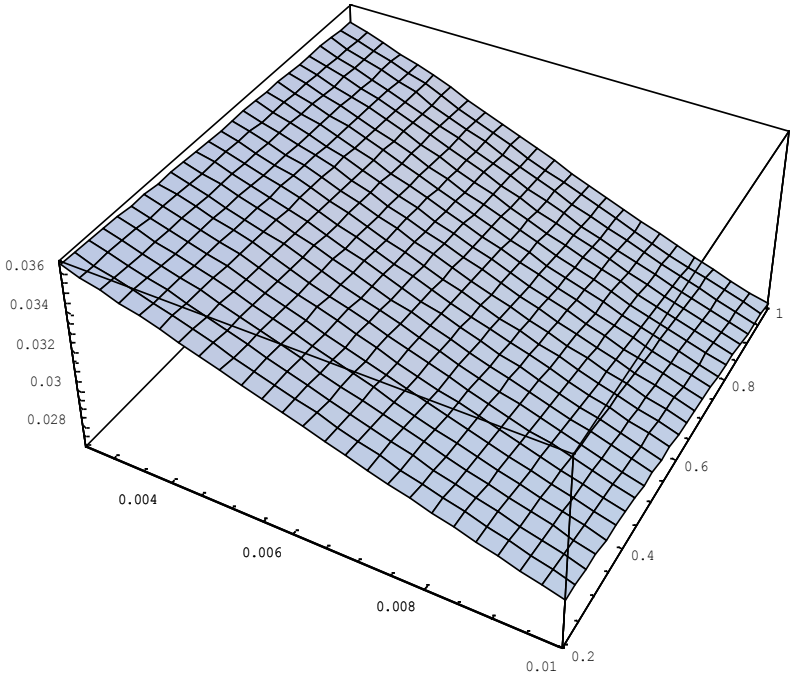

Figure 5.7. Maximum normal displacement in inner shell (normalised to r_0).

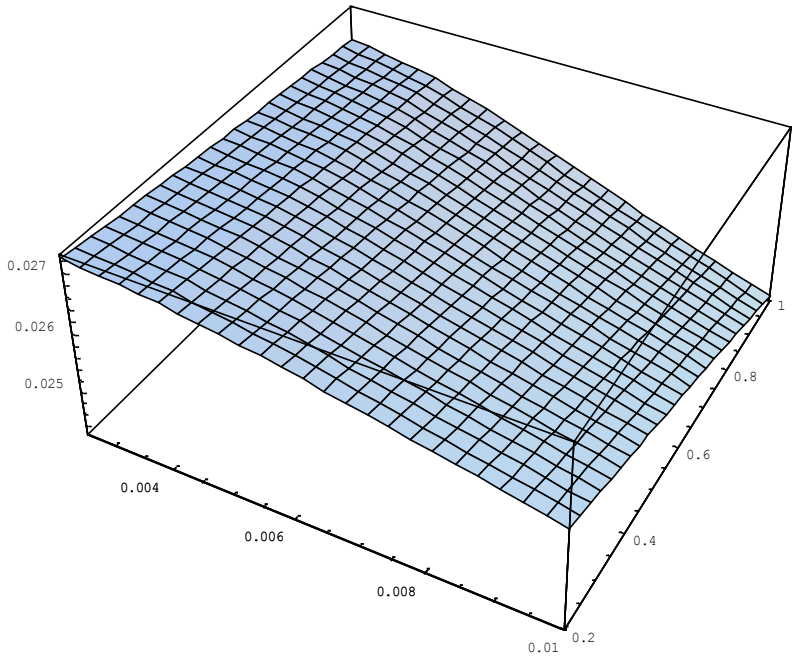

Figure 5.8. Maximum normal displacement in outer shell (normalised to r_0).

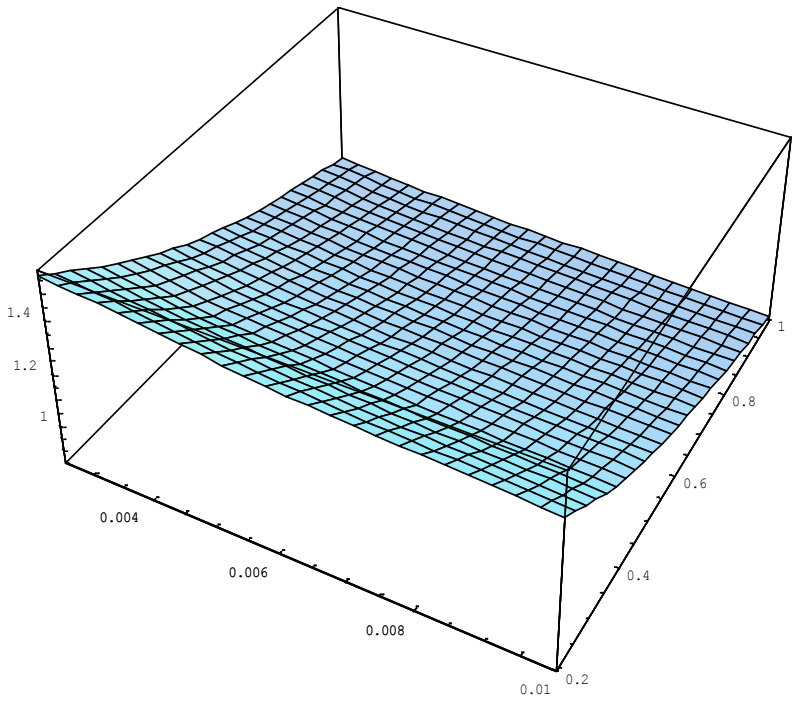

Figure 5.9. Maximum pressure on surface of inner shell (MPa).

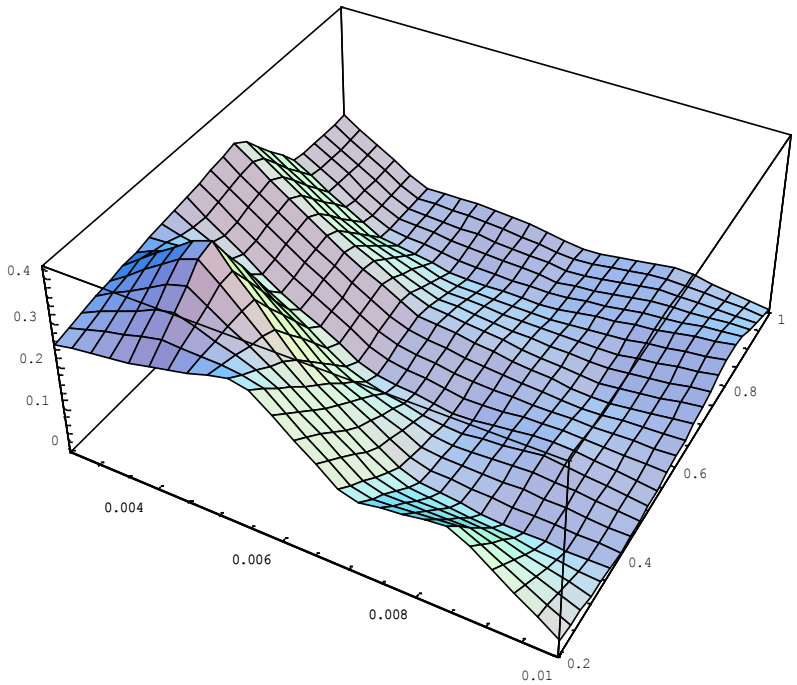

Figure 5.10. Location of the maximum pressure on the surface of the inner shell (radians).

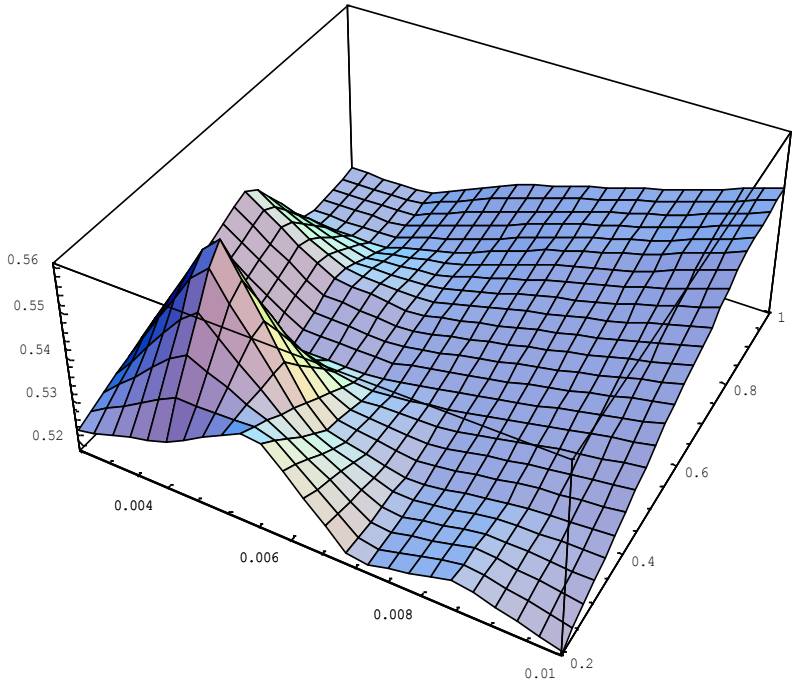

Figure 5.11. Timing of the maximum pressure on the surface of the inner shell (dimensionless time).

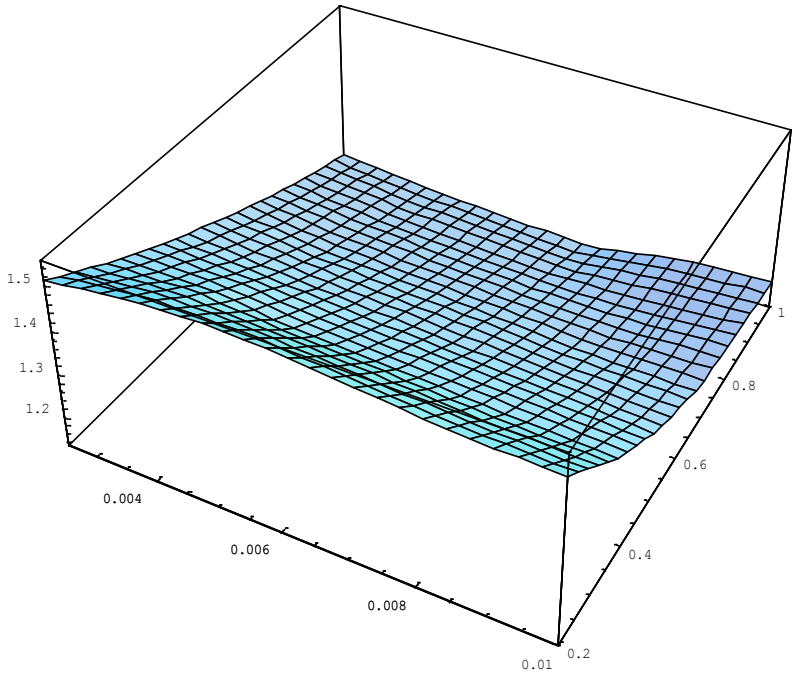

Figure 5.12. Maximum pressure on surface of outer shell (MPa).

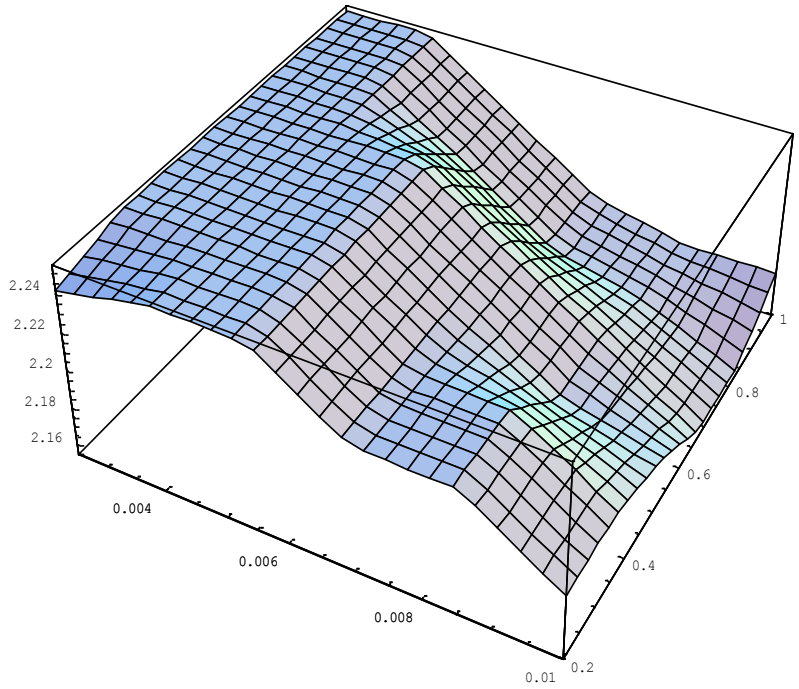

Figure 5.13. Location of the maximum pressure on the surface of the outer shell (radians).

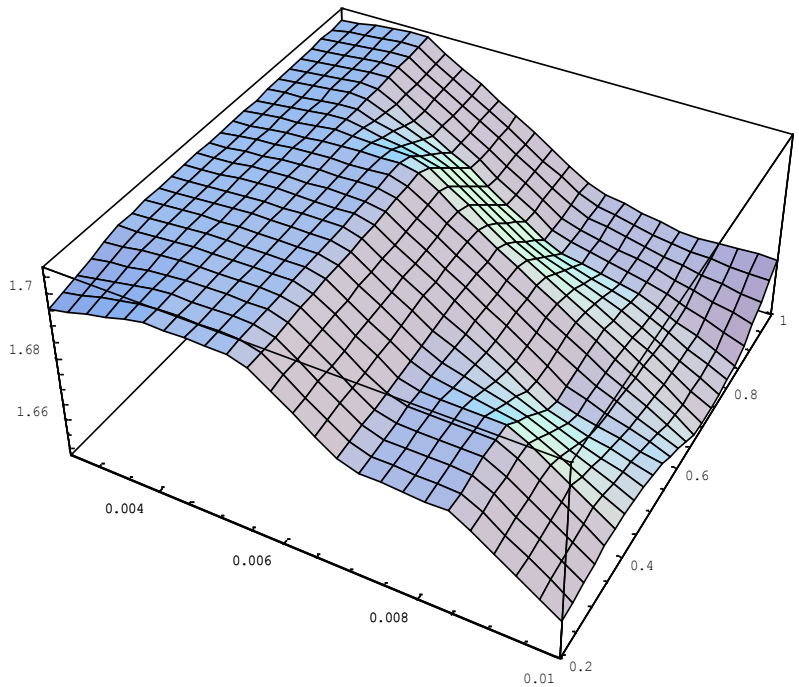

Figure 5.14. Timing of the maximum pressure on the surface of the outer shell (dimensionless time).

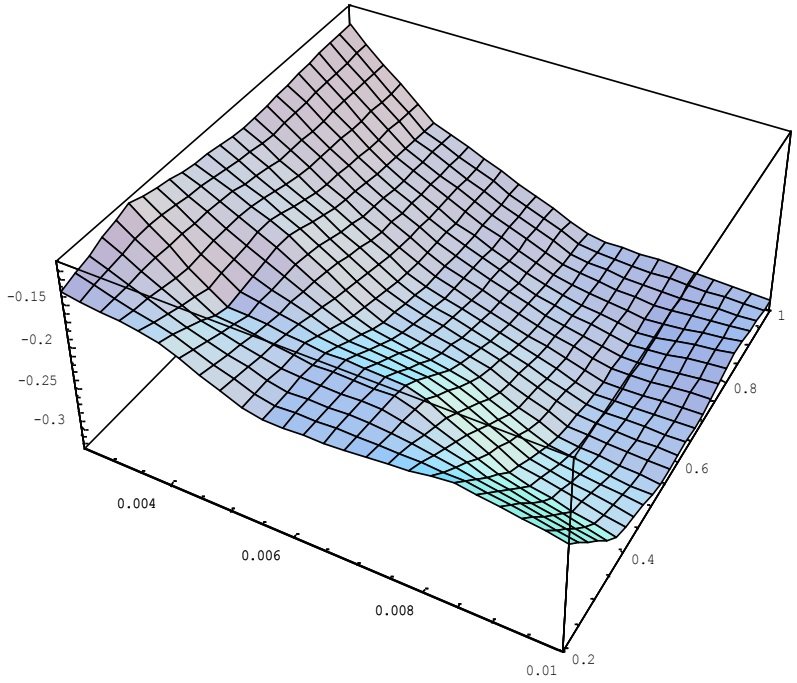

Figure 5.15. Minimum pressure on surface of inner shell (MPa).

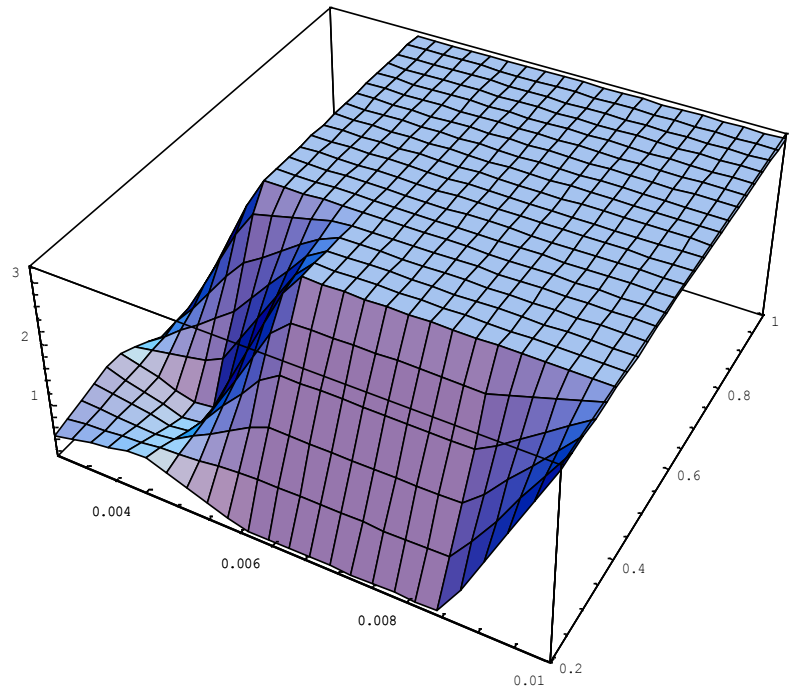

Figure 5.16. Location of the minimum pressure on the surface of the inner shell (radians).

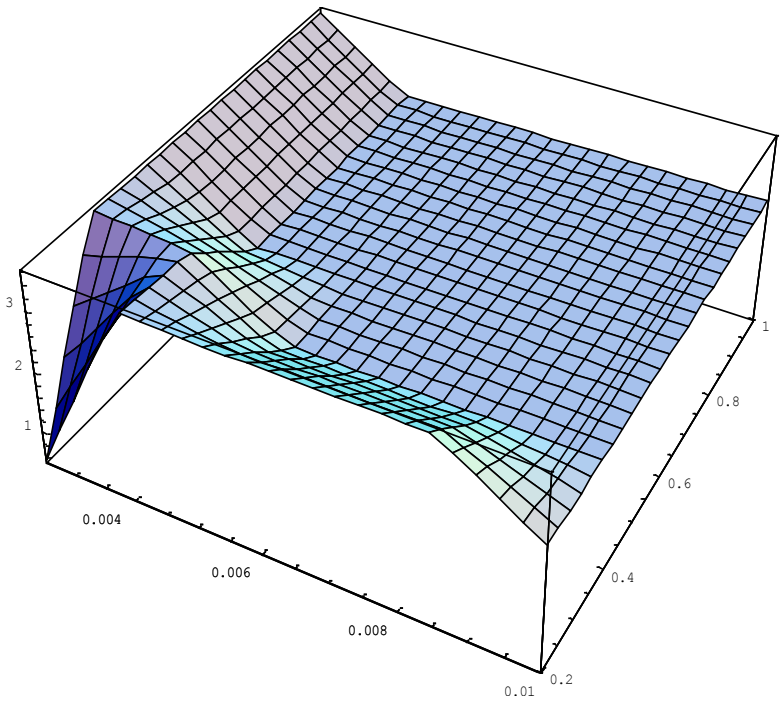

Figure 5.17. Timing of the minimum pressure on the surface of the inner shell (dimensionless time).

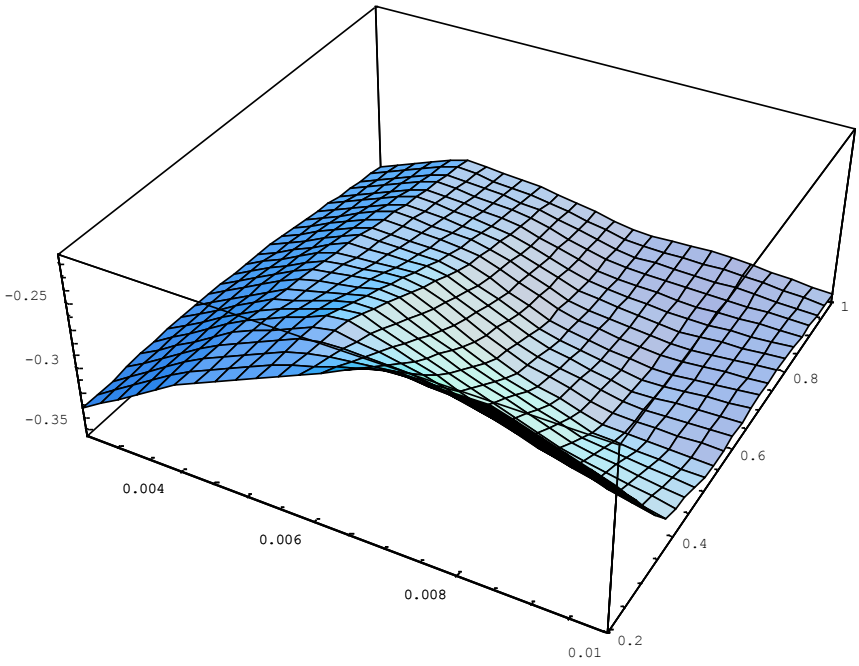

Figure 5.18. Minimum pressure on surface of outer shell (MPa).

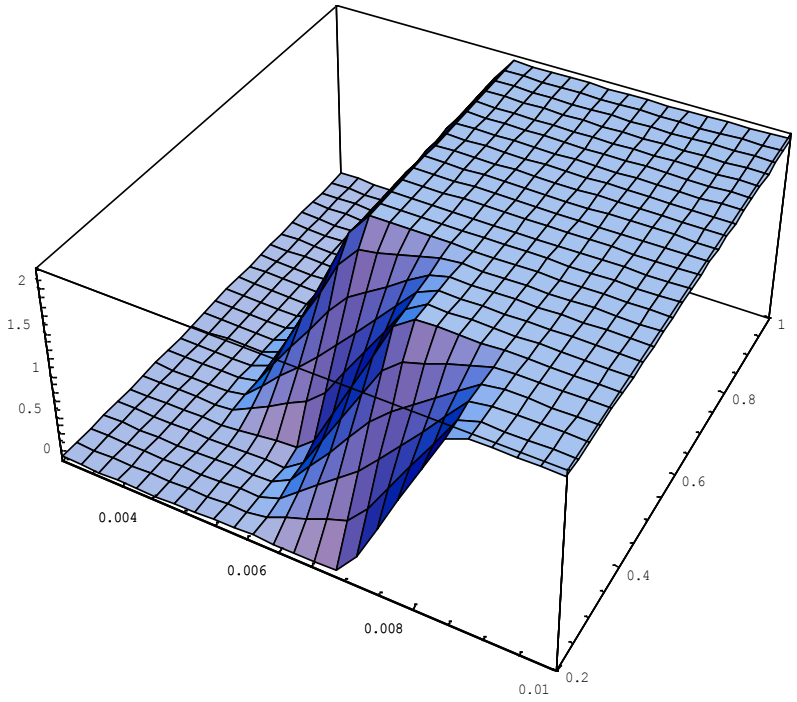

Figure 5.19. Location of the minimum pressure on the surface of the outer shell (radians).

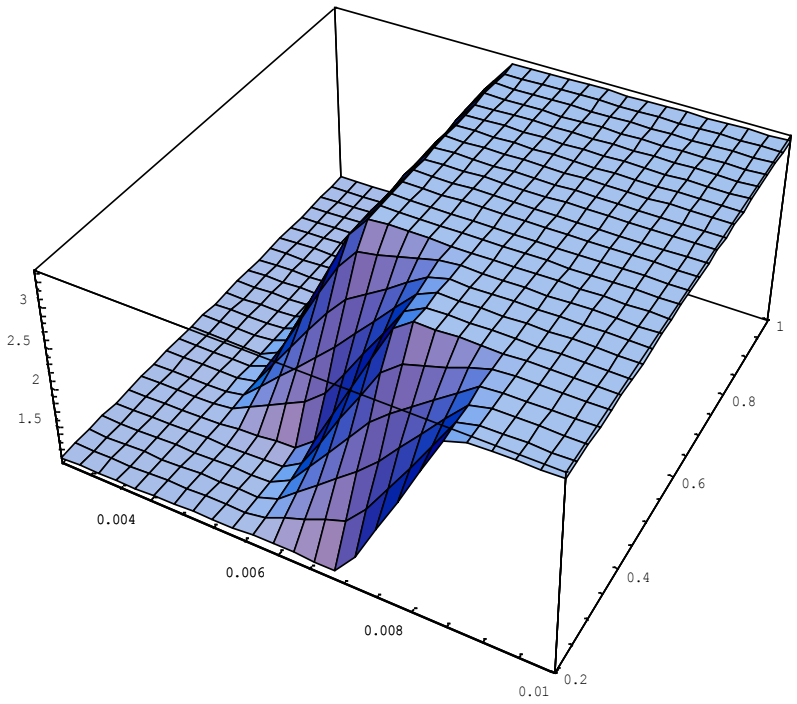

Figure 5.20. Timing of the minimum pressure on the surface of the outer shell (dimensionless time).

Now that one set of parameters have been considered, we can use this analysis as a basis for when we vary other parameters such as the internal shell radius, the outer shell material and the inter-hull fluid. We can run all combination of scenarios and discuss the subtle differences in each variation. The three cases we will consider for the purposes of this thesis are the following: Changing the inter-hull fluid from seawater to diesel fuel, changing the external hull material from steel to a composite metal and changing the internal shell radius from 50% to 90% the radius of the external shell, (effectively reducing the inner hull space). We will then compare the differences when making one parameter change and its influence on the peak values considered, and then a final analysis with all the parameters changed to see if there are any new observations not noticed when adjusting one variable at a time.

5.3 INTER-HULL FLUID DIESEL

We consider the interior shell with radius a = 0.50m and exterior shell with a radius of r_o = 1.00m, both made of steel c_1 = c_2 = 5000 kg/m^3, ρ_1 = ρ_2 = 7800 kg/m^3, and ν_1 = ν_2 = 0.3, submerged in water, c_e = 1400 m/s and ρ_e = 1000 kg/m^3, and with deisel filling the inter-shell space, c_i = 1250 m/s and ρ_i = 880 kg/m^3.

When analyzing the differences when replacing the internal fluid with diesel fuel the following noticeable differences occurred. Regarding the stresses, the only noticeable change was that the maximum stress in the outer shell had slightly higher values across all thicknesses of approximately 6%, but timing and location remained identical and normal displacements saw no noticeable variations at all. Regarding the pressures, there was a slight reduction on peak pressures on the surface of the inner shell with a minor delay in timing of their occurrences. Similarly, there were no noticeable differences for the minimum pressures either. There is, however, a change in the maximum pressures experienced on the surface of the outer shell. First, maximum values in the entire plot are greater than all values in our initial conditions with some new maximums being 12% greater. Furthermore, we no longer see a consistent decrease in maximum pressures when the shell thicknesses increase, nor is there as much influence of one shell's thickness on the other, with the possibility that the outer shell thickness might influence the system more when the inner shell is thicker.

5.4 COMPOSITE OUTER SHELL

We consider the interior shell with radius a = 0.50m and exterior shell with a radius of r_o = 1.00m, with the inner shell made of steel c_1 = 5000kg/m^3, ρ_1 = 7800kg/m^3, and ν_1 = 0.3, the outer shell made of a composite material c_2 = 3430kg/m^3, ρ_2 = 1800kg/m^3, and ν_2 = 0.15, submerged in water, c_e = 1400 m/s and ρ_e = 1000 kg/m^3, and with water filling the inter-shell space, c_i = 1400 m/s and ρ_i = 1000 kg/m^3.

Regarding the stresses, it is no surprise that there is no change to the stress in the inner shell values. However, the outer shell sees an order of magnitude decrease in maximum stresses experienced in the shell with maximum values of 164 as opposed to 1600, occurring at the tail point. Furthermore, there was no change when either thickness varied. This could be due to the properties of the shell material itself. Once again, we see no difference in the normal displacement of the shells. We do however, have an increase of 20-40% in the maximum pressure on the surface of the inner shell and matching the time and location as our initial situation, so we do see the external shell properties affecting the pressure on the surface of the inner shell. On the outer shell, we see a similar range of pressure values but when they occur has now changed with regards to the original case. We now see the maximum values are dependant more so upon the thickness of the inner shell as opposed to the outer shell, and we observe an increase in pressure as either shell becomes thicker which is in opposition to all the other cases. Looking at the negative pressure, we see that the values of concern all now occur at the head point of the shell with insignificant changes in the minimum values. However, one point of interest is that which both shells are at their thinnest. When this occurs there appears to be a doubling of the negative pressures experienced at both shell. This may be a unique scenario and further investigation may be of interest and may be the result of a superposition of to negative pressures at the head point, similar to what we see for peak values of the stress strain state.

5.5 INNER RADIUS 90%

We consider the interior shell with radius a = 0.90m and exterior shell with a radius of r_o = 1.00m, both made of steel c_1 = c_2 = 5000 kg/m^3, ρ_1 = ρ_2 = 7800 kg/m^3, and ν_1 = ν_2

= 0.3, submerged in water, c_e = 1400 m/s and ρ_e = 1000 kg/m^3, and with water filling the inter-shell space, c_i = 1400 m/s and ρ_i = 1000 kg/m^3.

There appears to be a unique influence when expanding the internal radius. The stresses in the inner shell do not change but the stress in the outer shell experience about a 33% increase in value, with these values now occurring exclusively at the tail point. We see a 33% greater normal displacement in both shells as well, with the outer shell now being displaced the exact amount as the inner shell. This seems reasonable as the shell surfaces are now in closer proximity to one another and behave more as a single shell with regards to displacements. The maximum pressures on the inner shell are not affected by the shell's increase in size and the same is true for the outer shell. However, they are now occurring at the front of the shell. Minimum pressures behave the same way, with the values at the inner shell remaining constant but occurring closer to the head point as opposed to at the tail point and almost at the earliest times during the interaction as opposed to later on in the original case. The minimum pressures on the outer shell, however, see a 33% increase in value, now occurring exclusively at the head point and much earlier in the interaction. We see that the internal radius does have an effect on the outer shell, but tends to have a greater effect on the overall timing of maximum value. This is expected because reducing the inter-hull space the inner shell is impacted earlier and the fields created interact earlier with the outer shell as a result, almost "speeding up" the process.

5.6 COMPOSITE OUTER SHELL / INTER-HULL RADIUS 90%

Lastly, we will see if analysing two parameter changes simultaneously will create unique results or will they create results that could be considered an amalgamation of the two cases where only one parameter change was analysed. The two parameters that were considered were the outer shell material (a composite outer shell) combined with the inner radius (at 90% the outer radius). Such an analysis can help determine which parameters may have a greater influence on specific results of interest.

We consider the interior shell with radius a = 0.90m and exterior shell with a radius of r_o = 1.00m, with the inner shell made of steel c_1 = 5000kg/m^3, ρ_1 = 7800kg/m^3, and ν_1 = 0.3, the outer shell made of a composite material c_2 = 3430kg/m^3, ρ_2 = 1800kg/m^3, and

ν_2 = 0.15, submerged in water, c_e = 1400 m/s and ρ_e = 1000 kg/m^3, and with water filling the inter-shell space, c_i = 1400 m/s and ρ_i = 1000 kg/m^3.

We observe both an amalgamation in some aspects and a unique case in other aspects. As done in our original scenario analysis (Chapter 5.2) plots have been provided below for comparable analysis if the current scenario. The value, timing and location of the maximum stress in both the inner and outer shells (Figures 5.21, 5.22, 5.23 and figures 5.24, 5.25, and 5.26, respectively); the normal displacements of the inner and outer shells (Figures 5.27 and 5.28, respectively); value, timing and location of maximum pressure experienced on the surface of both the inner and outer shell surfaces (Figures 5.29, 5.30, 5.31 and figures 5.32, 5.33, and 5.34, respectively); and value, timing and location of minimum pressure experienced on the surface of both the inner and outer shells (Figures 5.35, 5.36, 5.37 and figures 5.38, 5.9, and 5.40, respectively). The plots are arranged so the x-axis, y-axis and z-axis are the inner shell thickness, outer shell thickness and value of interest, respectively. Regarding the stress, the inner shell values stay the same as in all other cases, with identical locations of occurrence. Timing of these occurrences vary depending on the thickness of the inner shell only, with an appearance of a linear reduction in time of occurrence as the shell thickness increases up to 0.5% and then the time of occurrence remains constant. The stress in the outer shell sees the same affect, with a full magnitude decrease as seen in the composite case, and with a slight increase as seen from the 90% internal radius scenario. In comparison of the two shells, we could suggest that the shell material itself has a much larger effect on the stress than the radius, while we still observe the inner shell thickness continuing to have a greater effect on the stress in both shells than the outer thickness, as observed in our original analysis.

The normal displacements see an identical effect as in the scenario when we just considered a 90% internal radius. This seems to confirm that, at least currently, the internal shell radius has the only noticeable effect on the displacement of both shells.

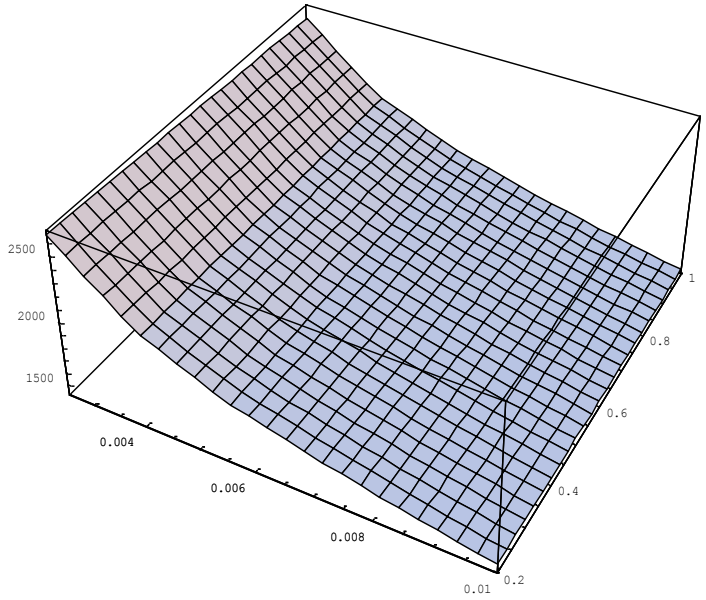

Figure 5.21. Maximum stress in inner shell (MPa).

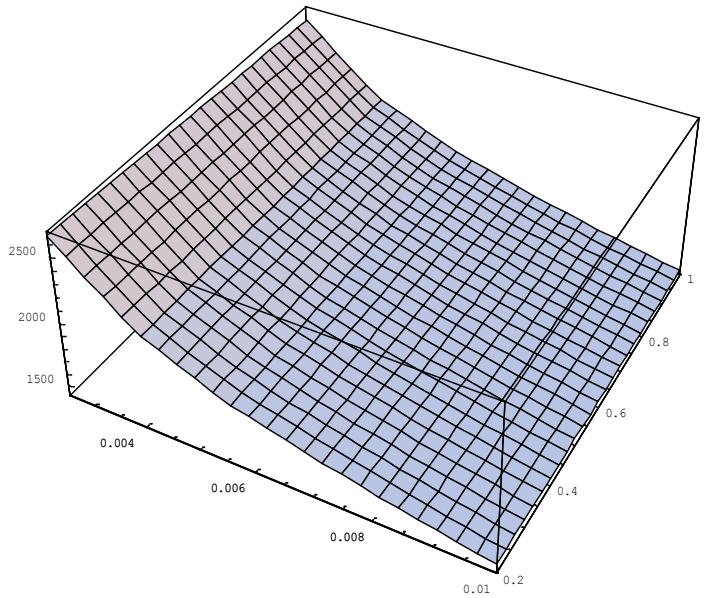

Figure 5.22. Location of maximum stress in inner shell (radians).

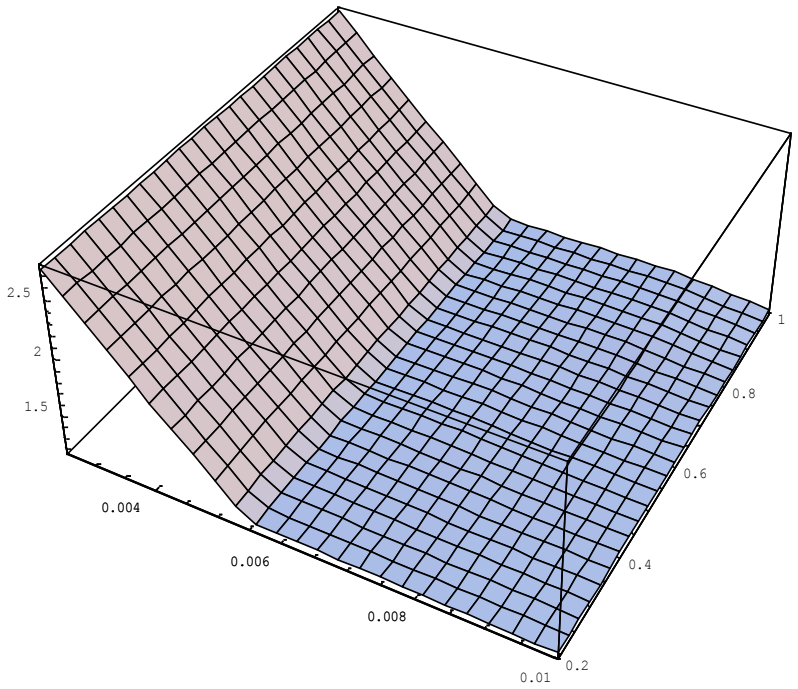

Figure 5.23. Timing of maximum stress in inner shell (dimensionless time).

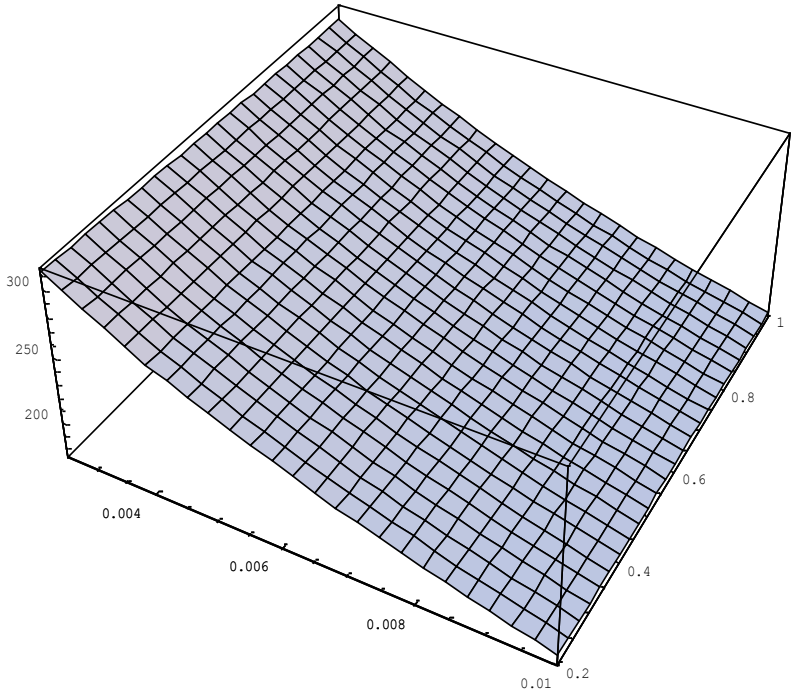

Figure 5.24. Maximum stress in outer shell (MPa).

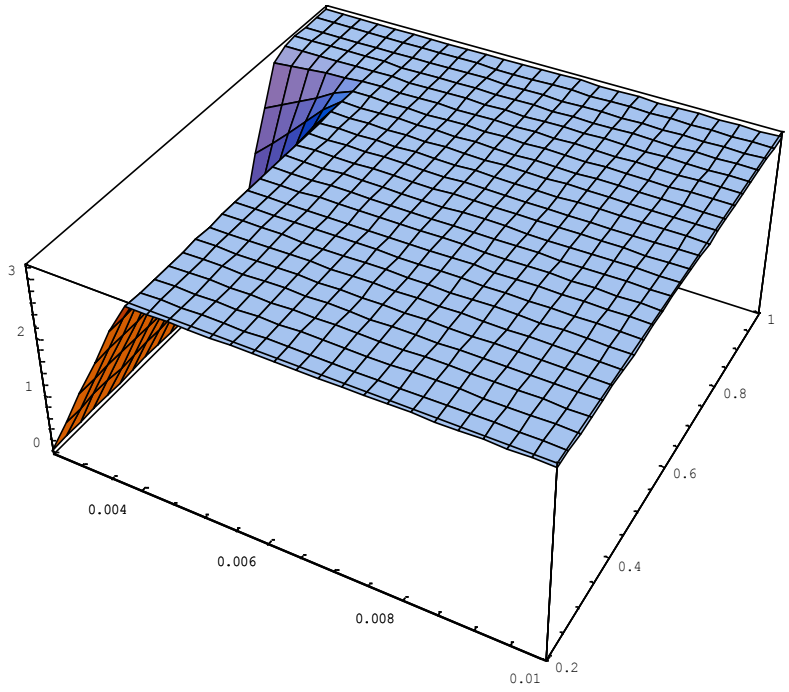

Figure 5.25. Location of maximum stress in outer shell (radians).

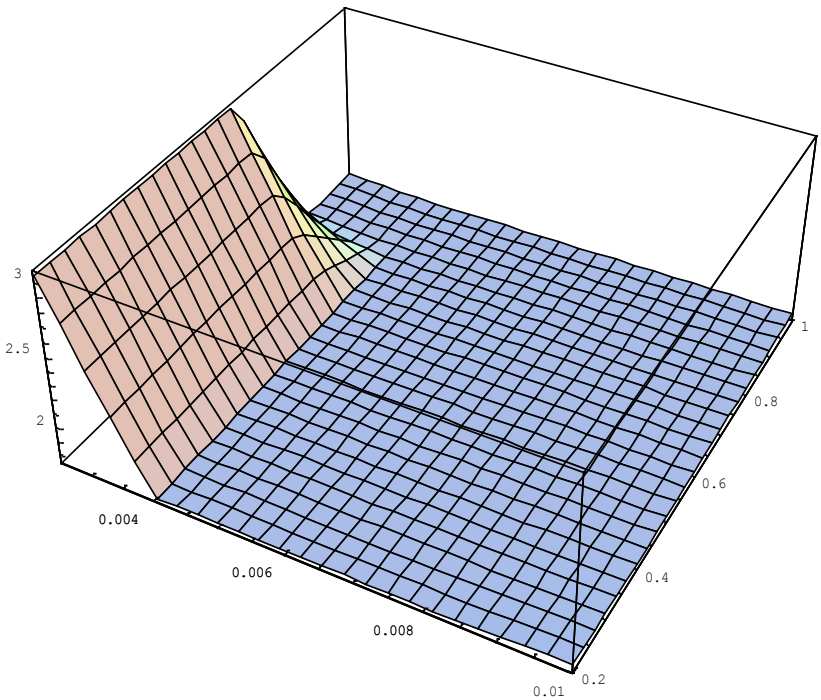

Figure 5.26. Timing of maximum stress in outer shell (dimensionless time).

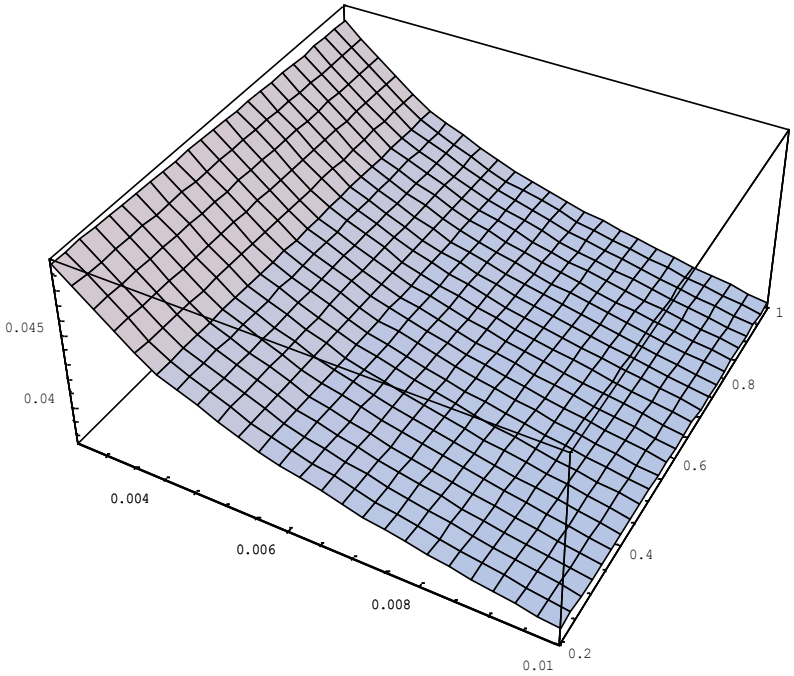

Figure 5.27. Maximum normal displacement in inner shell (normalised to r_0).

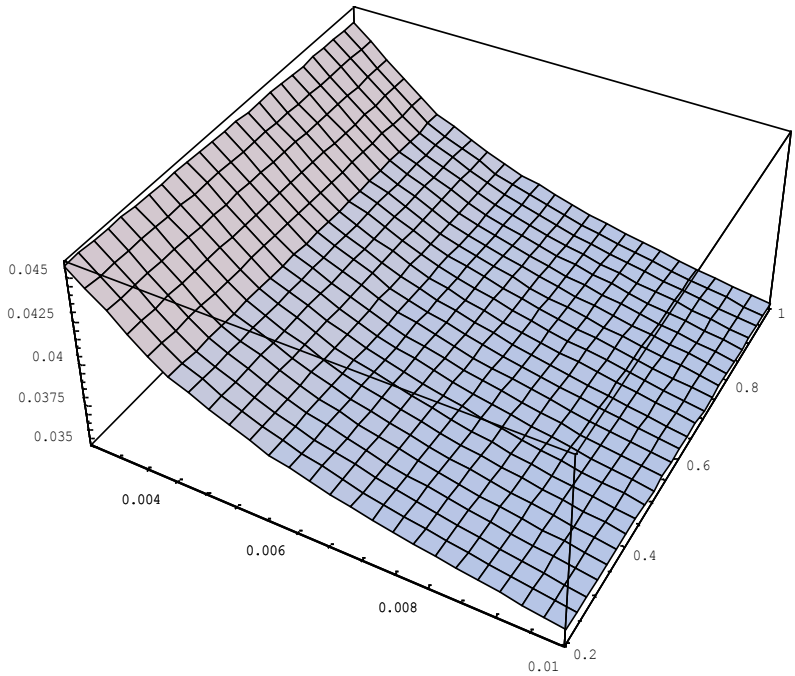

Figure 5.28. Maximum normal displacement in outer shell (normalised to r_0).

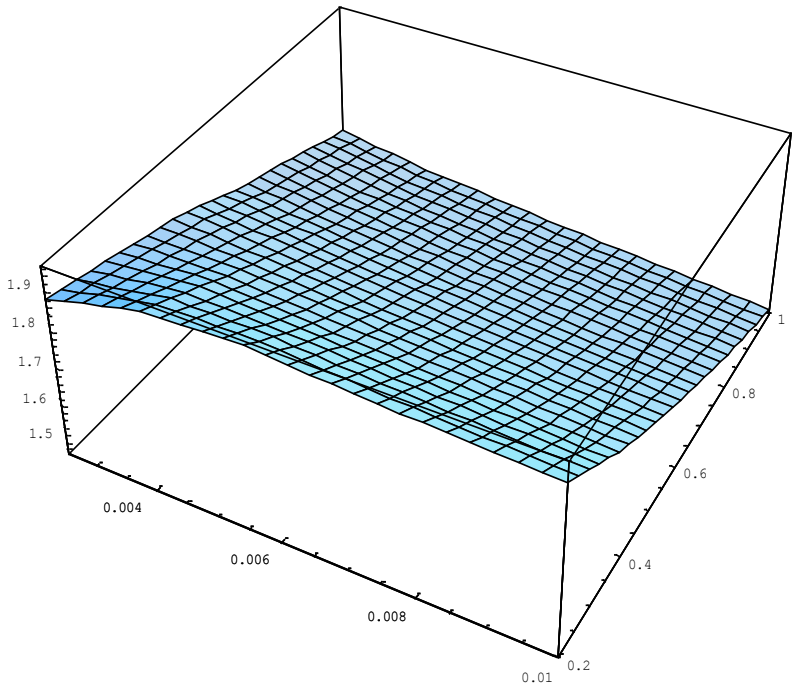

Figure 5.29. Maximum pressure on surface of inner shell (MPa).

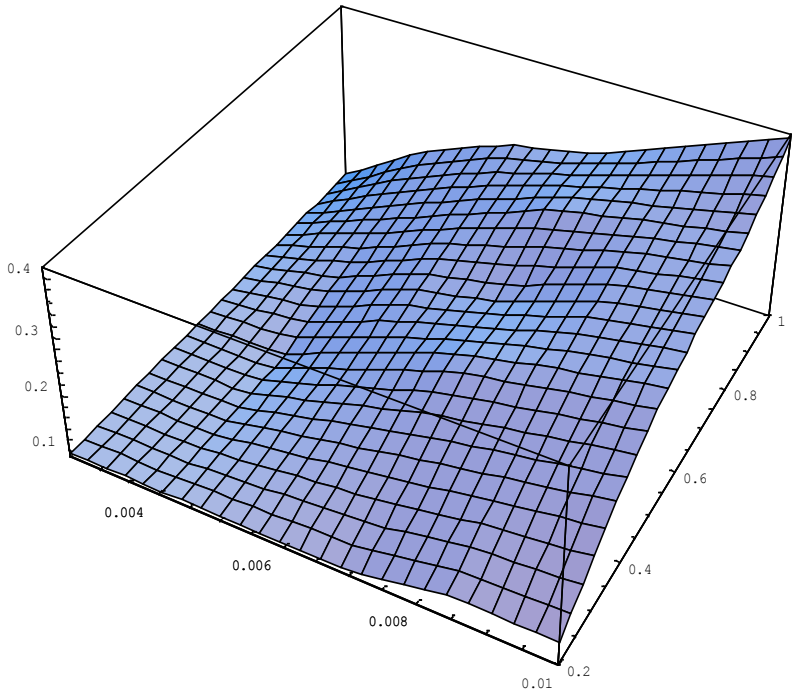

Figure 5.30. Location of the maximum pressure on the surface of the inner shell (radians).

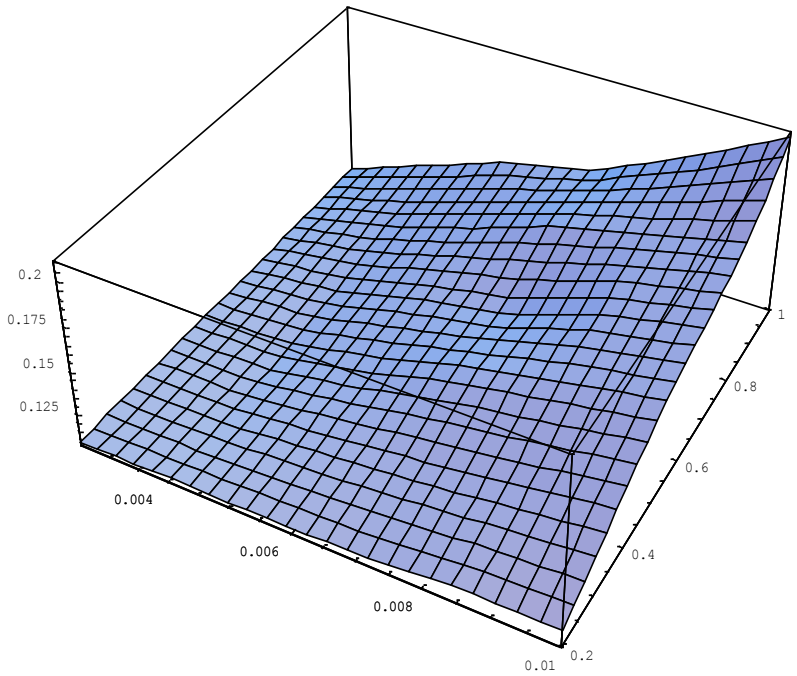

Figure 5.31. Timing of the maximum pressure on the surface of the inner shell (dimensionless time).

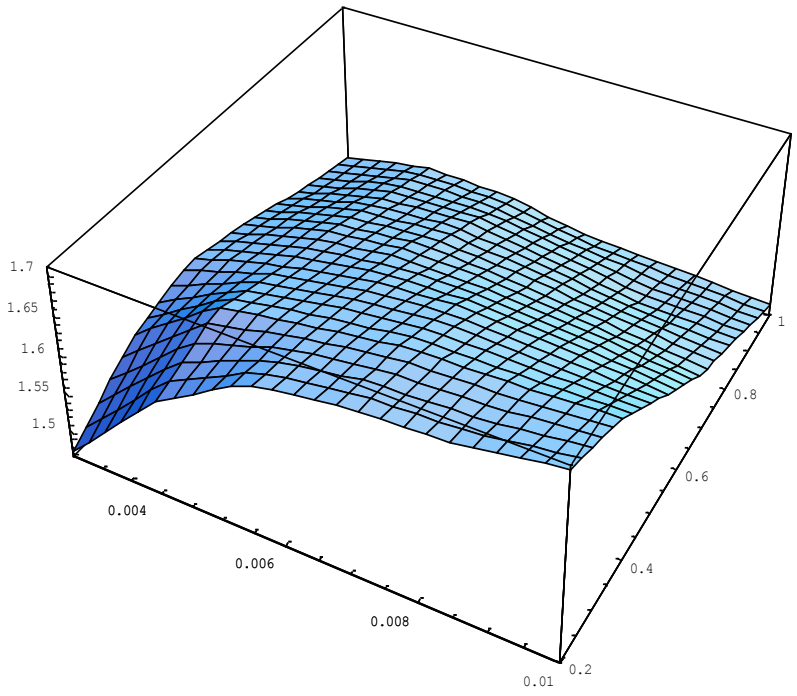

Figure 5.32. Maximum pressure on surface of outer shell (MPa).

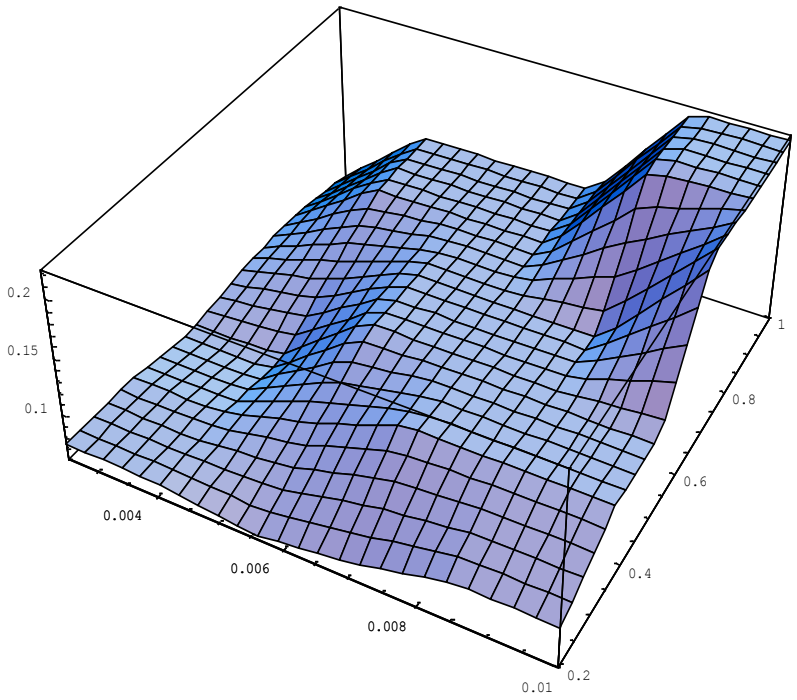

Figure 5.33. Location of the maximum pressure on the surface of the outer shell (radians).

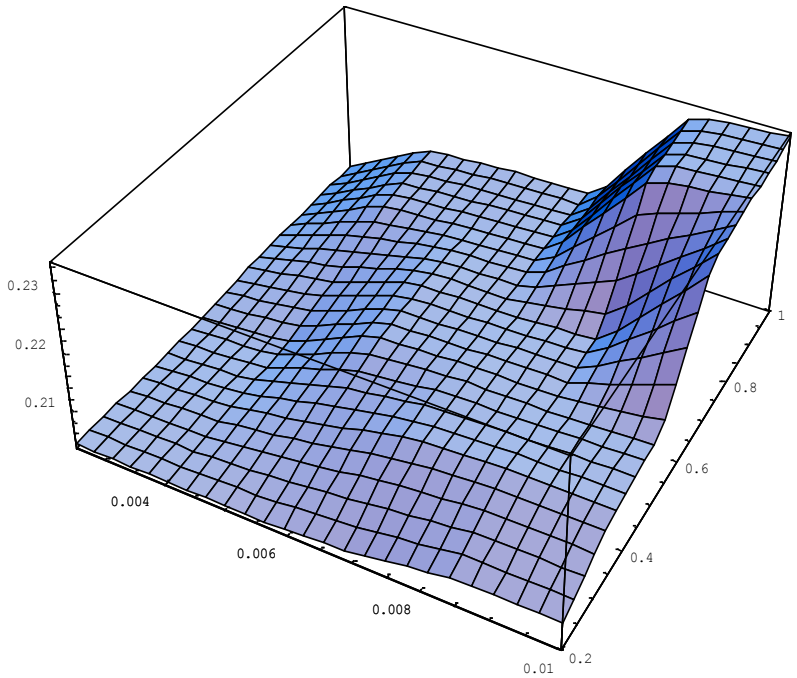

Figure 5.34. Timing of the maximum pressure on the surface of the outer shell (dimensionless time).

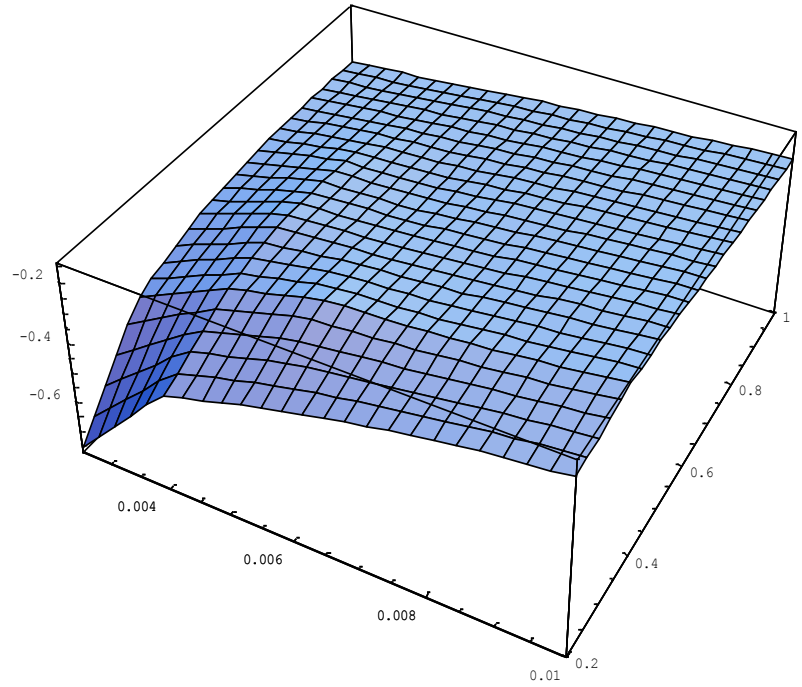

Figure 5.35. Minimum pressure on surface of inner shell (MPa).

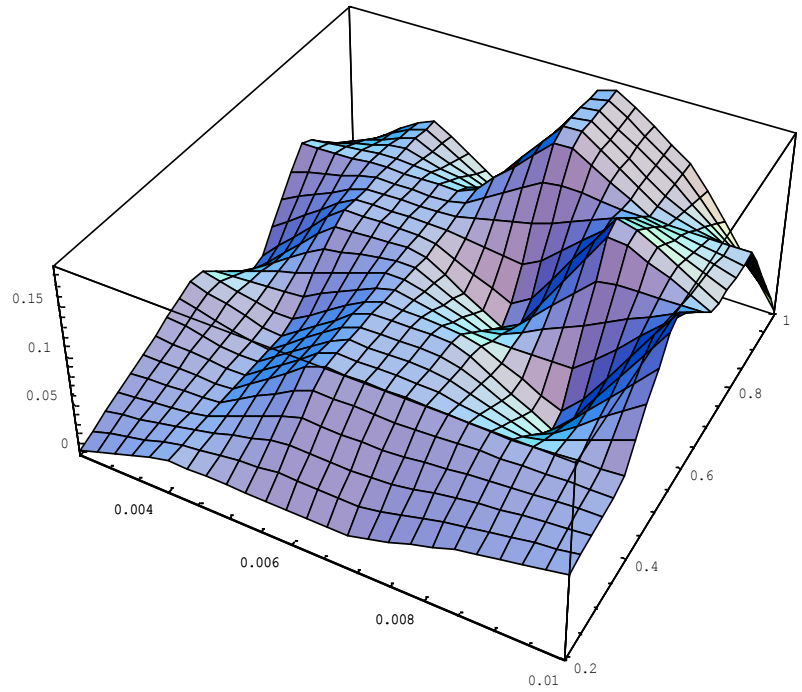

Figure 5.36. Location of the minimum pressure on the surface of the inner shell (radians).

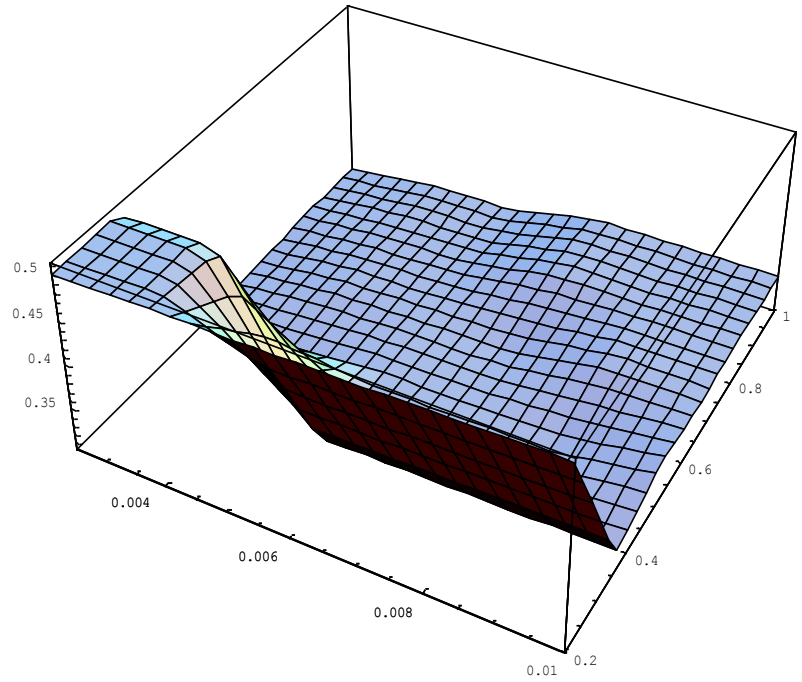

Figure 5.37. Timing of the minimum pressure on the surface of the inner shell (dimensionless time).

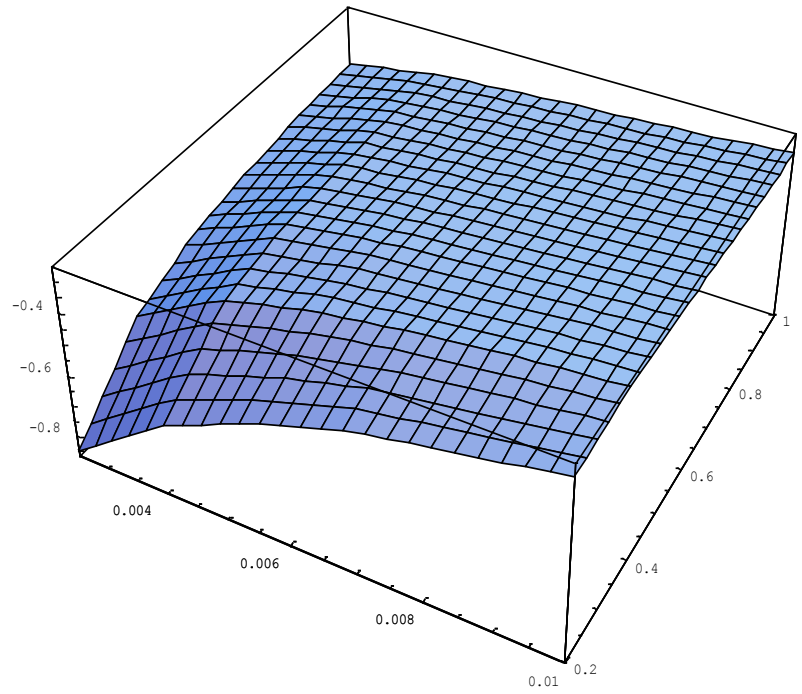

Figure 5.38. Minimum pressure on surface of outer shell (MPa).

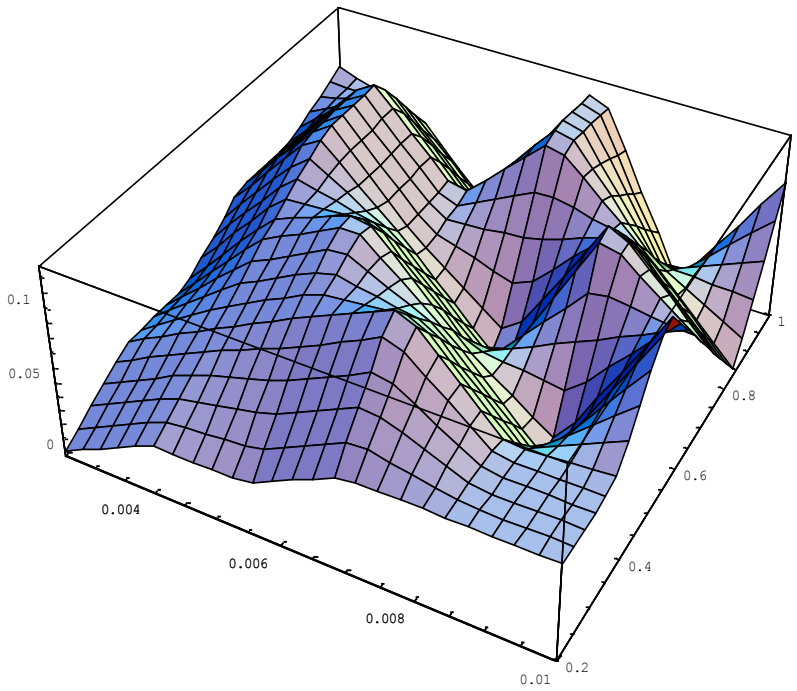

Figure 5.39. Location of the minimum pressure on the surface of the outer shell (radians).

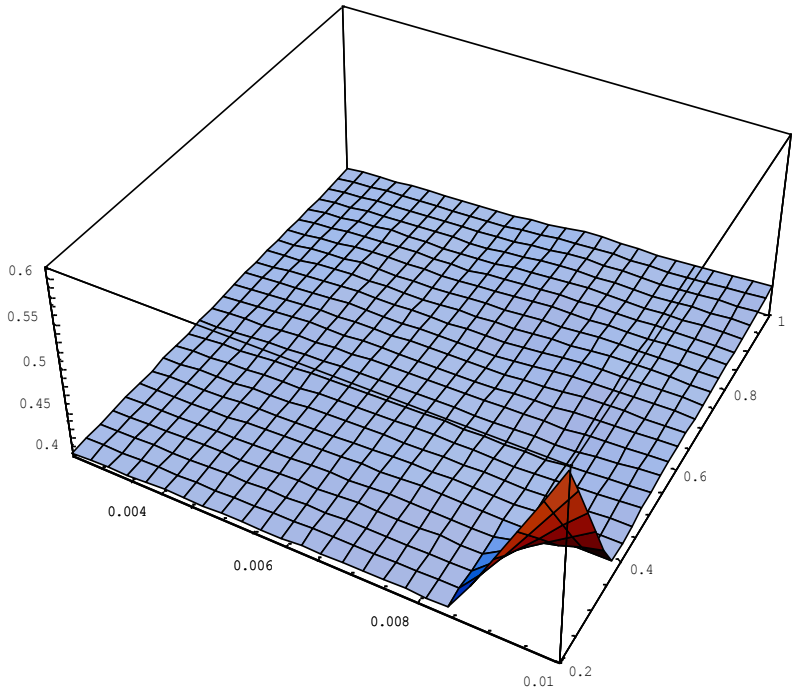

Figure 5.40. Timing of the minimum pressure on the surface of the outer shell (dimensionless time).

The maximum pressure on the surface of the inner shell is unique entirely to these specific parameters, where the location is similar and effected to the extent of the composite-only scenario, but the timing more closely resembles the effects seen from having the internal radius of 90% the external radius. However, the maximum values obtained are the largest seen in comparison to all other scenarios considered. Even if they are not much larger than for the composite only case, we can see that all parameters are having an effect on the pressures in this case. The same can also be said for the maximum pressures on the surface of the outer shell, with all values being equal to or greater than any maximum value seen in all other considered scenarios, even if it is only a 10% maximum increase, with the location and timing resembling that for the 90% only scenario, but with a shape of the graph resembling that seen in our original scenario.

The minimum pressures on the surface of the inner shell closely resemble those of the 90% case including the point of interest when both shells are at their thinnest and we see the doubling of the largest minimum pressure seen yet. What is more interesting is the minimum pressures on the surface of the outer shell; The shape, distribution, timing and location values of the graphs are once again identical to the 90% scenario, however all values have increased, on average, 50%, with the new lowest minimum value being 33% greater than any value seen yet, and it is once again occurring at that unique case of both shells being at the thinnest values.

From the carried out analysis, we can see that there are some qualities and effects that are dependent on only one parameter, while other qualities and effects may show a dependence on multiple parameters.

CHAPTER 6: CONCLUSION

6.1 CURRENT RESULTS

Using a semi-analytical model, based on analytical methods of mathematical physics and finite-difference approximation, the response of two submerged co-axial cylindrical shells with fluid filling the inter-shell space subjected to an external spherical shockwave was analysed. The fluid and structural dynamics was analysed, and the hydrodynamic fields were simulated. We found the interactions had a predominantly wave feature, with multiple waves reflecting off the surfaces of the two shells in the inter-hull space, accompanied by second order waves due to structural effects, and continuous radiation of waves by the external shell.

The structural analysis was then carried out. First, with the normal displacements of each shell, and then 2-dimensional snapshots, clearly demonstrating a shift of the head points down stream for both shells. It was also shown that the inner shell becomes slightly more deformed than the outer shell.

We then analysed the stress state of both shells. This was done through time-history plots, geometrical snapshots and time-space plots, creating three visualizations to simultaneously analyze the entire interaction of the shells. It was shown that both the stress waves circumnavigating the shells and eventually superposing at both the head and tail points, and pressure waves impacting the surface of the shells in the inter-hull space both contributed to the structural dynamics of both shells.

It was also determined that the outer shell and inner shell each behaved similarly to what was seen in the case of a single fluid filled cylindrical shell and the case of an evacuated cylindrical shell, respectively. Furthermore, it was seen that one different feature with the double hulled case is that the tensile stress in the outer shell was seen to be in similar magnitude to the compressive stress. This was seen to be caused by the rebounding pressure waves from the surface of the inner shell and was therefore deemed a unique feature of the double-hull arrangement.

Regarding the maximum and minimum pressures, it was seen that the maximum pressures remained a degree of magnitude higher than the minimum pressures but when considering changing the thicknesses of the shells, the opposite affect was seen

compared to the stresses in the shells in that the outer shell appears to have a greater effect on the pressures experienced at the surface of both shells than vice versa.

Because this thesis was developed for the investigation predominantly focused on how such interaction would affect ships and other marine vehicles, a method was developed to enable the user to carry out extensive parametric studies of the entire system. It was shown in detail how one could select a range of shell thicknesses and visualize how the peak stress, minimum and maximum pressures as well as normal displacement may change along with these varying thicknesses. We found that changes in the inner shell thickness had a greater impact on the stress experienced by the inner shell than that of varying the thickness of the outer shell, which was thought to be of practical importance when considering how to best protect the inner shell from damage. What was also of interest is that varying the thickness of the inner shell was shown to have a more dramatic effect on the outer shell than varying the thickness the outer shell had on itself.

This parametric study went into further detail by evaluating what affects there would be if we changed the material of the outer shell, changed the fluid within the inter-hull space, or increased the radius of the inner shell from 50% to 90% of the radius of the outer shell. It was of interest to see if specific phenomena were dependent upon one parameter, or multiple parameters. It was shown that certain parameters had a greater influence on certain aspects and qualities, the most noticeable being that the shell materials themselves had the greatest influence on the maximum stress in the respective shells, and that the radius of the inner shell (effectively reducing the inter-shell space) had the largest effect on the normal displacements of both shells as well as the timing of maximum values of interest and where they occur on the shells. What was of interest was that even though there would appear to be some consistent effects as one parameter changes, this did not always appear to be the case, especially when evaluating the maximum and minimum pressures. It appears that each unique combination of parameters will create its own unique set of results, even though some aspects will remain constant depending on what parameters are changed, other aspects will change. As was the case when a composite outer shell greatly reduced the peak stresses in the outer

shell with no effect on the inner shell stress, but at the same time increases the maximum and minimum pressures experienced at both shells.

What the author wants to address is that just because there appears to be a trend when adjusting one parameter. It cannot be assumed that an identical trend will be observed when adjusting the same parameters if other parameters are different as well. It is, therefore, best to run the simulations of interest and draw conclusions once the data has been collected.

6.2 FUTURE RESEARCH

The following research was carried out in two-dimensions and was at the early stages with regards to this specific configuration and the respective applied problem. From a practical standpoint, this thesis is meant to lay the foundation for expanding the effort into three-dimensions to enable better understanding of what will happen in real-life situations involving the systems in question.

BIBLIOGRAPHY

Ahyi, A. C., Pernod, P., Gatti, O., Latard, V., Merlen, A. and Ueberall, H. 1988. Experimental Demonstration of the Pseudo-Rayleigh Wave. The Journal of Acoustical Society of America, 104, 5, 2727-2732.

Amabili, M., Pellicano, F. and Paidoussis, M. P. 1998. Nonlinear Vibrations of Simply Supported, Circular Cylindrical Shells, Coupled to Quiescent Fluid. Journal of Fluids and Structures, 12(7), 883-918.

Andrew, B. W. J. and A. L. J. 2000. Fluid-Structure Interaction Mechanisms for Close-in Explosions. Shock and Vibration, 7(5), 265-275.

Apazidis, N. 2003. Focusing of Strong Shocks in an Elliptic Cavity. Shock Waves, 13(2), 91-102.

Bao, X. L., Raju, P. K. and Uberall, H. 1999. Circumferential Waves on an Immersed, Fluid-Filled Elastic Cylindrical Shell. The Journal of the Acoustical Society of America, 106, 2292.

Brett, J. M. and Yiannakopolous, G. 2008. A Study of Explosive Effects in Close Proximity to a Submerged Cylinder. International Journal of Impact Engineering, 35(4), 206-225.

Brevart, B. and Fuller, C. 1994. Radial Impulsive Excitation of Infinite Fluid-Filled Elastic Cylindrical Shells. Journal of Sound and Vibration, 177(3), 411-422.

Brevart and Fuller. 1996. Energy Exchange Between the Coupled Media of Impulsively Excited, Fluid-Filled Elastic Cylinders. Journal of Sound and Vibration, 190(5), 763-774.

Caresta, M. and Kessissoglou, N. J. 2009. Structural and Acoustic Responses of a Fluid-Loaded Cylindrical Hull with Structural Discontinuities. Applied Acoustics, 70(7), 954-963.

Chambers, G., Sandusky, H., Zerilli, F., Rye, K., Tussing, R. and Forbes, J. 2001. Pressure Measurements on a Deforming Surface in Response to an Underwater Explosion in a Water-Filled Aluminum Tube. Shock and Vibration, 8(1), 1–7.

Cohen, S. and Donald, G. H. 1965. Scattering of a Plane Acoustical Wave by a Spherical Obstacle. The Journal of the Acoustical Society of America, 38, 827.

Djellouli, R., Farhat, C., Macedo, A. and Tezaur, R. 2000. Finite Element Solution of Two-Dimensional Acoustic Scattering Problems Using Arbitrarily Shaped Convex Artificial Boundaries. Journal of Computational Acoustics, 8(1), 81-99.

Drikakis, D. Ofengeim, D. Timofeev, E. and Voionovich, P. 1997. Computation of Non-Stationary Shockwave/Cylinder Interaction Using Adaptive-Grid Methods. Journal of Fluids and Structures, 11, 665–691.

Geers, T. L. 1969. Excitation of an Elastic Cylindrical Shell by a Transient Acoustic Wave. Journal of Applied Mechanics, 36(3), 459.

Geers, T. L. 1972. Scattering of a Transient Acoustic Wave by an Elastic Cylindrical Shell. Journal of the Acoustical Society of America, 51, 1640.

Giltrud, M. and Naval Surface Weapons Center Silver Spring MD. 1980. The Numerical Prediction of the Dynamic Response of a Cylindrical Shell in an Acoustic Medium.

Hasegawa, T., Hino, Y., Annou, A., Noda, H., Kato, M., and Inoue, N. 1993. Acoustic Radiation Pressure Acting on Spherical and Cylindrical Shells. The Journal of the Acoustical Society of America, 93, 154.

Haywood, J. H. 1958. Response of an Elastic Cylindrical Shell to a Pressure Pulse. Quarterly Journal of Mechanics and Applied Mathematics, 11, 129–141.

Holba, C. 2010. Exxon Valdez Oil Spill, FAQs, Links, and Unique Resources at ARLIS. Alaska Resources Library and Information services.

Hornung, H. 1987. Regular and Mach Reflections of Shock Waves. Annual Revue of Fluid Mechanics, 18(11), 33-58.

Huang, H. and Wang, Y. F. 1970. Transient Interactions of Spherical Acoustic Waves and a Cylindrical Elastic Shell. Journal of the Acoustical Society of America, 48(1B), 228-235.

Huang, H. 1975. Scattering of Spherical Pressure Pulses by a Hard Cylinder. Journal of the Acoustical Society of America, 58, 310–317.

Huang, H. 1979. Transient Response of Two Fluid-Coupled Cylindrical Elastic Shells to an Incident Pressure Pulse. Journal of Applied Mechanics, 46(3), 513.

Hung, C. F., Lin, B. J., Hwang-Fuu, J. J. and Hsu, P. Y. 2009. Dynamic Response of Cylindrical Shell Structures Subjected to Underwater Explosion. Ocean Engineering, 36(8), 564-577.

Iakovlev, S. 2006. External Shock Loading on a Submerged Fluid-Filled Cylindrical Shell. Journal of Fluids and Structures, 22(8), 997-1028.

Iakovlev, S. 2007. Submerged Fluid-Filled Cylindrical Shell Subjected to a Shock Wave: Fluid-Structure Interaction Effects. Journal of Fluids and Structures, 23(1), 117-142.

Iakovlev, S. 2008a. Interaction Between a Submerged Evacuated Cylindrical Shell and a Shock Wave Part I: Diffraction-Radiation Analysis. Journal of Fluids and Structures, 24(7), 1077-1097.

Iakovlev, S. 2008b. Interaction Between a Submerged Evacuated Cylindrical Shell and a Shock Wave Part II: Numerical Aspects of the Solution. Journal of Fluids and Structures, 24(7), 1098-1119.

Iakovlev, S. 2009. Interaction Between an External Shock Wave and a Cylindrical Shell Filled with and Submerged into Different Fluids. Journal of Sound and Vibration, 322(1), 401-437.

Iakovlev, S., Gaudet, J., Dooley, G. and MacDonald, B. 2010. Hydrodynamic Fields Induced by the Shock Response of a Fluid-Filled Submerged Cylindrical Shell Containing a Rigid Co-Axial Core. Journal of Sound and Vibration, 329(16), 3359-3381.

Iakovlev, S., Santos, H. A. F. A., Williston, K., Murray, R., and Mitchell, M. 2013. Non-Stationary Radiation by a Cylindrical Shell: Numerical Modeling Using the Reissner-Mindlin Theory. Journal of Fluids and Structures, 36, 50-69.

Iakovlev, S., Furey, C., Pyke D., and Lefieux, A. 2015. Shock Response of a System of Two Submerged Co-Axial Cylindrical Shells Coupled by the Inter-Shell Fluid. Journal of Fluids and Structures, 55, 1-24.

Izumi, K., Aso, S. and Nishida, M. 1994. Experimental and Computational Studies Focusing Processes of Shock Waves Reflected from Parabolic Reflectors. Shock waves, 3, 213-222.

Lam, K. Y., Zhang, Z. J., Gong, S. W. and Chan, E. S. 1997. The Transient Response of a Two-Layered Elastic Cylindrical Shell Impinged by an Underwater Shock Wave. Composites Part B, 29(6), 673-686.

Latard, V., Merlen, A., Preobazhenski, V. and Ahyi, A. C. 1999. Acoustic Scattering of Impulsive Geometrical Waves by a Glass Sphere in Water. Applied Physics Letters, 74(13), 1919-1921.

Lee, K. and Seong, W. 2009. Time-Domain Kirchhoff Model for Acoustic Scattering from an Impedance Polygon Facet. The Journal of the Acoustical Society of America, 126(1), 14-21.

Liang, C. 2001. A Study of Transient Responses of a Submerged Spherical Shell Under Shock Waves. Ocean Engineering, 28(1), 71-94.

Lie, S. T. and Yu, G. 2002. Multi-Domain Fluid-Structure Interaction Analysis with a Stable Time Domain BEM/FEM Coupling Procedure. Engineering Computations, 19(1), 6-21.

Mair, H. U. 1996, a. Preliminary Compilation of Underwater Explosion Benchmarks. Proceedings of the 67th Shock and Vibration Symposium, Volume I, SAVIAC, 361-379.

Mair, H. U. 1999, b. Benchmarks for Submerged Structure Response to Underwater Explosion. Shock and Vibration, 6, 169–181.

Mair, H. U. 1999. Review: Hydrocodes for Structural Response to Underwater Explosions. Shock and Vibration, 6, 81–96.

Mayer, L., et. Al. 2013. An Ecosystem Servicing Approach to Assessing the Impacts of the Deep Water Horizon Oil Spill in the Gulf of Mexico. National Academy of Sciences, National Academy of Engineering, Institute of Medicine, National Research Council.

Neubauer, W. 1969. Pulsed Circumferential Waves on Aluminium Cylinders in Water. The Journal of the Acoustical Society of America, 45, 1134.

Neubauer, W. G. 1970. Observation of Waves Radiated from Circular Cylinders Caused by an Incident Pulse. The Journal of the Acoustical Society of America, 48, 1135.

Oakley, J. G., Puranik, B. P., Anderson, M. H., Peterson, R. R. Bonazza, R., Weaver, R. P. and Gittings, M. L. 1999. An Investigation of Shock-Cylinder Interaction. Proceedings of the 22nd International Symposium on Shock waves, Imperial College, London.

Ofengeim, D. and Drikakis, D. 1997. Simulation of Blast Wave Propagation Over a Cylinder. Shock Waves, 7, 305–317.

Pavlov, V. A. 1995. Diffraction of a Strong Shock Wave on a Cylinder with a Time-Varying Radius. Journal of Applied Mechanics and Technical Physics, 36(6), 806.

Park, L. K., Kim, J. C., An, C. W. and Cho, D. S. 2003. Measurement of Naval Ship Responses to Underwater Explosion Shock Loadings. Shock and Vibration, 10(5), 365-377.

Peralta, L. A. and Raynor, S. 1964. Initial Response of a Fluid-Filled Elastic, Circular, Cylindrical Shell to a Shock Wave in Acoustic Medium. Journal of the Acoustical Society of America, 36, 476-488.

Sandusky, H., Chambers, P., Zerilli, F., Fabini, L. and Gottwald, W. 1999. Dynamic Measurements of Plastic Deformation in a Water-Filled Aluminum Tube in Response to Detonation of a Small Explosives Charge. Shock and Vibration, 6, 125–132.

Schedin, S., Gren, P. O. and Wahlin, A. 1997. Shock Waves in an Elliptical Cavity with Varying Height. Shock Waves, 7, 343–350.

Shin, Y. S. and Santiago, L. D. 1998. Surface Ship Shock Modeling and Simulation: Two-Dimensional Analysis. Shock and Vibration, 5(2), 129-137.

Sommerfeld, M. and Muller, H.M. 1988. Experimental and Numerical Studies of Shock Wave Focusing in Water. Experiments in Fluids, 6, 209–216.

Sorokin, S. V. and Terentiev, A. V. 2006. Flow-Induced Vibrations of an Elastic Cylindrical Shell Conveying a Compressible Fluid. Journal of Sound and Vibration, 296, 777-796.

Sprague, M. A. and Geers, T. L. 1999. Response of Empty and Fluid-Filled, Submerged Spherical Shells to Plane and Spherical, Step-Exponential Acoustic Waves. Shock and Vibration, 6(3), 147-157.

Sturtevant, B. and V. A. Kulkarny. 1976. The Focusing of Weak Shock Waves. Journal of Fluid Mechanics, 73, 651–671.

Sun, M. and Takayama, K. 1996. A Holographic Interferometry Study of Shock Wave Focusing in a Circular Reflector. Shock waves, 6, 323–336.

Sun, M. 1999. Conservative Smoothing on an Adaptive Quadrilateral Grid. Journal of Computational Physics, 150(1), 143-180.

Sun, M., Yada, K., Jagadeesh, G., Onodera, O., Ogawa, T. and Takayama, K. 2003. A Study of Shock Wave Interaction with a Rotating Cylinder. Shock Waves, 12, 479-486.

Van, A. J. E., Meijer, G. J. and Lemmen, P. P. M. 1998. Underwater Shock Response Analysis of a Floating Vessel. Shock and Vibration, 5(1), 53-59.

Wang, G., Arita, K. and Liu, D. 2000. Behavior of a Double Hull in a Variety of Stranding or Collision Scenarios. Marine Structures, 13(3), 147-187.

Williams, E. G. 1988. Experimental Investigation of the Wave Propagation on a Point-Driven, Submerged Capped Cylinder Using K-Space Analysis. The Journal of the Acoustical Society of America, 87, 513.

Yang, J. Y., Liu, Y. E. N. and Lomax, H. 1987. Computation of Shock Wave Reflection by Circular Cylinders. AIAA Journal, 25(5), 683-689.

Yao, X., Guo, J., Feng, L. and Zhang, A. 2009. Comparability Research on Impulsive Response of Double Stiffened Cylindrical Shells Subjected to Underwater Explosion. International Journal of Impact Engineering, 36(5), 754-762.

Yoshikawa, S., Williams, F. G. and Washburn, K. B. 1994. Vibration of Two Concentric Submerged Cylindrical Shells Coupled by the Entrained Fluid. The Journal of the Acoustical Society of America, 95(6), 3273.

Zhang, P. 1993. Excitation of a Fluid-Filled, Submerged Spherical Shell by a Transient Acoustic Wave. The Journal of the Acoustical Society of America, 93(2), 696.

Zhang, X. M., Liu, G. R. and Lam, K. Y. 2001. Coupled Vibration Analysis of Fluid-Filled Cylindrical Shells Using the Wave Propagation Approach. Applied Acoustics, 62(3), 229-243.